UNIVERSIDADE FEDERAL DE PERNAMBUCO
CENTRO DE TECNOLOGIA E GEOCIÊNCIAS
DEPARTAMENTO DE ENGENHARIA MECÂNICA
PROGRAMA DE PÓS-GRADUAÇÃO EM ENGENHARIA MECÂNICA

RAFAEL ALBERTO DE ARAUJO SILVA

SHELL AND TUBE HEAT EXCHANGER WITH HELICAL BAFFLES AND GRAPHENE NANOFLUID: a CFD analysis of its performance and characteristics

Recife
2022

RAFAEL ALBERTO DE ARAUJO SILVA

SHELL AND TUBE HEAT EXCHANGER WITH HELICAL BAFFLES AND GRAPHENE NANOFLUID: a CFD analysis of its performance and characteristics

Dissertation presented to the Graduate Program in Mechanical Engineering of the Universidade Federal de Pernambuco, as partial Mechanical Engineering requirement for the delivery of the Master's degree in Engineering.

Area of concentration: Energy.

Advisor: Prof. Dr. Jorge Recarte Henríquez Guerrero.

Co-advisor: Prof. Dr. José Ângelo Peixoto da Costa.

Recife

2022

Catalogação na fonte:
Bibliotecária Sandra Maria Neri Santiago, CRB-4 / 1267

S586s Silva, Rafael Alberto de.
Shell and tube heat exchanger with helical baffles and graphene nanofluid: a CFD analysis of its performance and characteristics / Rafael Alberto de Araujo Silva. – 2022.
110 f.: il., figs., tabs.

Orientador: Prof. Dr. Jorge Recarte Henríquez Guerrero.
Coorientador: Prof. Dr. José Ângelo Peixoto da Costa.
Dissertação (Mestrado) – Universidade Federal de Pernambuco. CTG. Programa de Pós-Graduação em Engenharia Mecânica. Recife, 2022.
Inclui referências, apêndices e anexos.

1. Engenharia mecânica. 2. Trocador de calor de casco e tubo. 3. Nanofluidos. 4. Nanopartículas de grafeno. 5. Chicanas helicoidais. 6. Análise CFD. 7. Geometria do trocador de calor. I. Guerrero, Jorge Recarte Henríquez Guerrero (Orientador). II. Costa, José Ângelo Peixoto da (Coorientador). III. Título.

UFPE

621 CDD (22. ed.) BCTG/2022-287

RAFAEL ALBERTO DE ARAUJO SILVA

SHELL AND TUBE HEAT EXCHANGER WITH HELICAL BAFFLES AND GRAPHENE NANOFLUID: a CFD analysis of its performance and characteristics

Dissertation presented to the Graduate Program in Mechanical Engineering of the Universidade Federal de Pernambuco, Centro de Tecnologia e Geociências, as partial Mechanical Engineering requirement for the delivery of the Master's degree in Engineering. Area of concentration: Energy.

Aprovada em: 31/01/2022.

BANCA EXAMINADORA

_____

Prof. Dr. Jorge Recarte Henríquez Guerrero (Orientador)
Universidade Federal de Pernambuco

_____

Prof. Dr. José Ângelo Peixoto da Costa (Coorientador)
Instituto Federal de Pernambuco

_____

Prof. Dr. José Carlos Charamba Dutra (Examinador Interno)
Universidade Federal de Pernambuco

_____

Prof. Dr. Kamal Abdel Radi Ismail (Examinador Externo)
Universidade Estadual de Campinas

ACKNOWLEDGMENTS

Back in 2018, when I have left the intern program which I was enrolled, and started this MSc program, I was kind of disoriented, still getting back to what I knew and lived at the university. The structure was completely different from what I was living in the company and I felt like I was going back in time. The turnout happened when I started to study with Professor Angelo and Professor Jorge. Professor Angelo and his simplicity, his unique way to talk to someone he's just knew is astonishing. I remember when he started to teach us in ANSYS software, the classes were late and most of the class were there before work, in other words, everyone was exhausted. His way of teaching made everyone feel embraced and with the feeling that in the end, it will work out, no matter how hard it is. This was the first inspiration that I had to start thinking about CFD. Since I was in the undergraduate program, Professor Jorge was always a reference for being one of the "top squad" from the mechanical department. As I did not have the chance to study with him, I thought as how challenge this would be: study with one of the most loved and feared lecturers of the department? (Yes professor, you can laugh about this quote). Having no other thoughts, I took the challenge and started to study combustion, probably one of the best disciplines I have studied in my entire student career. Professor Jorge and his way of teaching, of inspiring anyone who talks to him was unique to me. The challenging essays and the comments were a really tipping point in my life.

I'm surely could be writing another dissertation just talking about how these two individuals helped me in my personal choices, but for a quick word: THANK YOU!

I wish to thank all my friends, from work, from the university and even from college, you have been incredible with me, helping me become a better professional and person. I used to say that somehow even being an only child, I've got many brothers and sisters, and for this, I cannot thank them enough.

Another huge thanks which I must endorse is for CAPES, which has financially made this work possible, especially during the pandemic.

There's no way to finish this work without thanking my entire family, which supported me even when the darkest moments have come. They did not hesitate to get me up and back on tracks. I just want to end this saying that I deeply love all of you.

ABSTRACT

Heat exchangers are a heavily used equipment in both industry and daily lives. The most famous example of an industrial application for heat transfer is the shell and tube heat exchanger, being a classic model used even nowadays. This type of heat exchanger varies in size, in tubes profile, quantities, fluid direction and in its geometry, especially in the baffles and its varieties, which can help to increase thermal efficiency and to reduce pumping costs. The field of study of heat exchangers is not new to science, but when the baffle geometry is changed for a determined application, the performance can vary widely. On the other hand, nanofluids are still a new field of research. Nanofluids can be defined as a blend of a nanoparticles, fluid and other chemicals to stabilize the moisture. The literature has reviewed nanofluids as a promising way to improve heat transfer in the same heat exchanger. This present study has the aim to investigate and compare three different heat exchanger's baffle geometry and three graphene based nanofluids for the optimal heat transfer performance and overall equipment performance. The study was conducted through Ansys CFX software with nine different inputs for each geometry. The geometries studied were continuous helical (CH) with the setups of 360º and 1080º; segmented helical (SH) baffles, both for the same sized heat exchanger with a counterflow configuration. The cold fluid inputs were (0.051 kg/s, 0.1kg/s and 0.2kg/s) at 25ºC. The hot fluid inputs were (60ºC, 50ºC and 40ºC) for 0.05kg/s. The nanofluid was made based in Graphene nanoparticle (GNP) and water, and were only allocated in the hot domain, with its total weight (wt.) concentrations as (0.0125%, 0.025% and 0.05%). The results have shown that for overall equipment performance, the SH configuration has shown the best results for any given hot inlet temperature, and the result is amplified when the hot inlet temperature is low. On the other hand, when the best thermal performance is to be achieved, the 1080CH baffle configuration has performed better than any other, showing a very relevant finding about continuous baffles for the inputs presented in this work. For all different inputs, the 360CH shown the worst overall equipment performance. The study also has shown that the best performance working fluid was the 0.025% wt. graphene, which has shown to be the tipping point for higher nanofluid concentration.

Keywords: shell-and-tube heat exchanger; nanofluids; graphene nanoparticles; helical baffles; CFD analysis; heat exchanger design.

RESUMO

Os trocadores de calor são equipamentos muito utilizados na indústria e no cotidiano. O exemplo mais famoso de aplicação industrial para transferência de calor é o trocador de calor de casco e tubo, um modelo clássico utilizado até hoje. Este tipo de trocador de calor varia em tamanho, no perfil e quantidade de tubos, na direção e sentido dos fluidos e em sua geometria, principalmente nas chicanas e suas variedades, o que pode ajudar a aumentar a eficiência global. O área de estudo de trocadores de calor não é nova para a ciência, mas quando a geometria do defletor é alterada para uma determinada aplicação, o desempenho pode mudar bastante. Por outro lado, os nanofluidos ainda são um novo campo de pesquisa. Nanofluidos podem ser definidos como uma mistura de nanopartículas, fluido e estabilizantes. A literatura tem revisado os nanofluidos como uma forma promissora de melhorar a transferência de calor. O presente estudo tem como objetivo investigar e comparar três diferentes geometrias de chicanas de trocadores de calor e três nanofluidos à base de grafeno para encontrar o melhor desempenho do equipamento. Foi utilizado o software Ansys CFX com nove entradas diferentes para cada geometria: helicoidais contínuas (HC) com arranjos de 360º e 1080º; chicanas helicoidais segmentados (HS), todos com configuração de contrafluxo. As entradas de fluido frio foram (0.051 kg/s, 0.1kg/s e 0.2kg/s) a 25ºC. As entradas de fluido quente foram (60ºC, 50ºC e 40ºC) para 0.05kg/s. O nanofluido foi feito à base de nanopartícula de grafeno (GNP) e água, e foram alocados apenas no domínio quente, com suas concentrações de peso total percentual de (0.0125%, 0.025% e 0.05%). Os resultados mostraram que, para o desempenho geral do equipamento, a configuração SH mostrou os melhores resultados para qualquer temperatura de entrada quente, e o resultado é amplificado quando a temperatura de entrada quente é baixa. Por outro lado, quando se deseja obter o melhor desempenho térmico, a configuração do defletor 1080CH tem um desempenho melhor do que qualquer outra, mostrando um achado muito relevante sobre defletores contínuos para as configurações de entrada apresentadas neste trabalho. Para todas as entradas diferentes, o trocador com chicanas do tipo 360HC mostrou o pior desempenho geral do equipamento. O estudo também mostrou que o fluido de trabalho de melhor desempenho foi de 0.25% em peso percentual de grafeno, que tem se mostrado o ponto de inflexão para maior concentração de nanofluidos.

Palavras-chave: trocador de calor de casco e tubo; nanofluidos; nanopartículas de grafeno; chicanas helicoidais; análise CFD; geometria do trocador de calor.

LIST OF FIGURES

LIST OF TABLES

LIST OF SYMBOLS

k	Thermal conductivity [W/mK];
g	Gravitational accelerarion [m/s^2];
T_∞	Ambient temperature [^{o}C];
U_∞	Ambient fluid velocity [m/s];
ρ	Fluid density [kg/m^3];
C_P	Specific heat [J/kgK];
U	Fluid velocity [m/s];
D	Diameter of the tube [m];
ν	Kinematic viscosity [m^2/s];
μ	Dynamic viscosity [kg/ms];
C_f	Friction coefficient [dimensionless];
V'^2	Upstream velocity [m/s];
U_{mean}	Mean fluid velocity [m/s];
ΔP_{lenght}	Pressure drop in a tube's length [Pa];
h_L	Head loss [m];
$\dot{W}_{pump}$	Pumping work [W];
$\dot{m}$	Mass flow [kg/s];
q	Quantity of heat [J];
C_{hot}	Heat capacity rate of hot fluid [W/K];
C_{cold}	Heat capacity rate of cold fluid [W/K];
ΔT_{lm}	Logarithmic mean temperature difference [K];
A_f	Flow passage area [m^2];
D_H	Hydraulic diameter [m];
Q	Fluid flow [m^3/s];
k_{eff}	Effective thermal conductivity [W/mK];
φ	Particle concentration [ppm];
E	Entransy dissipation [dimensionless];
e	Baffle overlap proportion [%].

TABLE OF CONTENTS

1 INTRODUCTION

Heat exchangers are very popular equipment, widely used not just by the industry, but to maintain daily routine on modern cities. Due to its importance, they can be seen coupled with most of machinery such as chemical engineering process, power plants, process industries, air conditioning and food industry. But even in devices such as mobile phones, tablets, computers and other electronics, heat exchangers are used to avoid overheating and possible component failure. The most commonly used and classic example of a heat exchanger is the shell and tube configuration, which is extensively studied in experimental and numerical applications, usually called Computational Fluid Dynamics (CFD) simulations [1].

The goal of heat exchangers is to transfer thermal energy between fluids (water, nanofluids, gases, oil…) through heat conduction and convection. In its classical application, two fluids are necessary. The heated one is carried out and conducted through pipes which are emerged in a cooling fluid. Both are pumped to different reservoirs and they are not mixed in the process. To enhance heat transfer, some mechanisms can be applied such as a large equipment [2]. The classic configuration consists of circular tubes, a shell and baffles, these exchangers are created to have a very flexible design, considering its maintainability, performance and reliability, as they can be used in many different applications, including those with elevated pressure [3].

To be efficient as possible, heat exchangers must have a high heat transfer coefficient, high mass flow (in the cold fluid) and a very low pressure drop. To improve heat transfer, the literature shows that counter flow configuration performs better compared to parallel. The baffles also, play a main role in this part, as they are responsible for most of the turbulence due to its format. The turbulence is caused to enhance heat transfer between fluids, but it can also increase pumping losses, decreasing the overall efficiency of the equipment. To achieve a higher heat transfer without the pressure drop, baffles with different shapes were proposed and extensively studied in shell and tube heat exchangers [2].

Segmented baffles were found to create most of the pressure drop when compared to other geometries such as “flower” and helical baffle configuration. The drop is mainly caused by velocity jets and fluid recirculation, being crucial due to heat

exchanger operating costs. In industrial applications, cooling high powered engines is very challenging. Even if it is possible to introduce very large heat exchangers, it can quickly become costly. Trying to achieve a higher efficiency using the same equipment, scientists have tried to improve the design, changed construction materials, working temperatures and other configurations to optimize heat exchangers [4].

Another possible solution to increase heat transfer was introduced by Maxwell when he added small particles, usually made of metal oxides, carbon nanotubes and carbides, to improve heat transfer in a fluid. The main problem of these new fluid is the suspension of larger particles, which can be seen as responsible for clogging pipelines and erosion in pumps` propellers. The nanofluid, a blend between a fluid and very small particles (named nanoparticles) have been studied by scientists with the aim to achieve a better combination of a very high thermal conductivity material with a proper fluid [5].

The fluid is also characterized for its lower pumping losses if compared to bigger particle additives such as milli and micro sized. Characteristics such as lower erosion and viscosity due to its smaller particles makes it even more interesting in a global heat exchanger efficiency analysis. [6]. The literature shows that nanofluids have a much higher thermal conductivity than usual operating fluids such as water or engine oil, and some authors even suggests that nanofluids can be used in car transmission systems, drilling, and even as transformer oil [7]. The number of nanoparticles is also another factor that improves heat transfer due to its higher thermal conductivity compared to regular fluids. The Reynolds number also plays a crucial role in thermal exchangers, determining the type of its flow. Usually a turbulent flow is better to transfer heat. This happens mainly because of increased particle mixing, collision between particles and heat exchanger walls', and a higher convection. Nanofluid can be made with single or multiple materials, called mono and hybrid, respectively [8].

Recent studies have pointed out that graphene nanoplatelet is significantly better compared to other nanomaterials. With a higher thermal conductivity, researchers have found that at room temperature and lower weight concentrations, the heat transfer coefficient in a shell and tube heat exchanger have increased by 35% compared with deionized water. On the other hand, graphene is expensive to obtain, being necessary to make it in alternative ways, such as from regular cooking oil [9]. Through the recent years, CFD is becoming more popular due to the high cost of experimental studies and

the decreasing price of standard personal computers, which usually carry very powerful processors. This tool became commonly used to study fluid flow, heat transfer and chemical reactions associated with the system. It can predict how fluid will behave in distinctive environments and mechanical applications. Using the Navier-Stokes equation, iteratively the Computer Aided Engineering (CAE) software can solve equations for conservation of momentum, mass and energy for the analysed system. The interesting part is that same methods used in traditional fluids can be used to the nanofluids, as the literature suggests [10]. Single phase models are very popular for numerical studies for its simplicity. In the homogenous fluid, nanoparticles are distributed in the fluid and the assumption of the model is that liquid and solid particles are in chemical and thermal equilibrium [11].

1.1 MOTIVATION: WHY CHOOSE FOR GRAPHENE, CFD AND HELICAL BAFFLES?

Through the recent years, the energy field has become more popular over the media. The debate about climate change is now a reality between not just the scientists, but has become a target for multinational companies, which are under a huge amount of pressure to reduce energy consumption and change oil dependency. The year of 2021 has shown the potential of how a post-pandemic world economy can be hurt when a surge in energy price comes. This effects only aggravates the urgency of a less energy-consuming society.

Through the last years, researchers have been trying to achieve higher heat transfer from traditional fluids by adding nanoparticles and modifying heat exchanger`s design. The CFD approach is an inexpensive way to understand and to achieve the best configuration a heat exchanger has. In addition to that, the processing power of personal computers have increased widely, making possible to study some models from home.

Yet to be considered a recent field, graphene nanofluids have been studied in different configuration heat exchangers. But when the internal flow design has helical baffles, the literature is still scarce. The behaviour of graphene nanoplatelets associated with different baffle geometry is promising to achieve a higher equipment efficiency.

1.2 RESEARCH AIM

The aim of this study is to evaluate global heat exchanger performance through a parametric analysis via CFD to find the best efficiency in a shell and tube heat exchanger with complex helicoidal baffles running a water-graphene nanofluid with a variable concentration as working fluid.

1.3 RESEARCH OBJECTIVES

- Make a literature review about the state of art in the subject of helical baffle heat exchangers and its performance running nanofluids;
- Define heat exchanger and baffle optimal design;
- Develop and comprehend the elements of computational fluid dynamics based in the heat exchanger design;
- Validate mesh and numerical model;
- Develop a parametric analysis to achieve the best configuration for each baffle design, fluid input and nanofluid concentration.

1.4 STRUCTURE

The work is divided into six chapters, including the current chapter dedicated to the introduction. In this chapter the study is contextualized, and its objectives are presented. In chapter 2, the theoretical framework of the study presents the solid knowledge acquired through. This section will describe heat transfer mechanism, fluid flow inside tubes and discuss about heat exchangers. In chapter 3, the literature review outlines the results of a background analysis performed prior to the design activities. It synthesizes the answer for the first research objective into a coherent discussion. The numerical and mathematical modelling is presented in chapter 4, which discusses the strategy used to validate the chosen designs and to proof the acceptance of the results compared to previous experimental setup. In this chapter, the geometry, governing equations, mesh criteria, boundary conditions, methodology proof will be discussed, and the background to validate it. The fifth topic shows the results and discussion, where not

only the most important results are shown, but we also interpret and explains it in a comparison between different heat exchanger input setup. The chapter 6 the conclusion is presented, finishing this dissertation and suggesting paths that are worth of future research.

2 THEORETICAL FRAMEWORK OF THE STUDY

In this section, all accumulated knowledge in the field of heat transfer related to heat exchangers will be discussed in order to give the reader a brief reminder of what is in the field.

2.1 A BRIEF INTRODUCTION TO HEAT TRANSFER

There are three different mechanisms of heat transfer: conduction, convection and radiation. Both conduction and radiation rely only in a temperature difference to conduct heat. Convection is different because it also relies on mechanical mass transport, changing how it behaves depending on the environment, but also on temperature difference. In this paper, the focus will be on conduction and convection, since radiation is negligible for the analysis. If the reader needs more background on the subject to understand this paper, it is recommended to read classic heat transfer books, which can be seen in references section.

2.1.1 Conduction

Heat is conducted through a solid body whenever a temperature gradient exists between distinct points, heat will always flow from the highest to the lowest temperature region. The rate of heat transfer depends also on a physical property called thermal conductivity *k*, which can determine the amount of heat that is flowing per a unit of area when the gradient is unity. Therefore, we can define the rate of heat transfer by conduction (also referred as Fourier's law) by the following equation:

$$\dot{q}_x = -kA\frac{dT}{dx} \tag{1}$$

The Fourier's law shows that the rate of heat conduction on a homogenous medium is proportional to the area times the temperature gradient. The minus sign is to guarantee that heat is transferred from the hottest to the coolest point, hence if the temperature decreases within the positive x axis, temperature gradient will be also negative, showing the direction of the heat transfer according to Equation 1. Fourier's law can also be

considered in a multidimensional analysis, meaning that the vector of heat flux can be expressed as a sum of heat contributions of all three dimensions. Considering an isothermal surface and a point P which have a normal line *n*, the conduction vector can be expressed as below:

$$\dot{q}_n = -kA\frac{\partial T}{\partial n} = -\left(kA_x\frac{\partial T}{\partial x} + kA_y\frac{\partial T}{\partial y} + kA_z\frac{\partial T}{\partial z}\right)$$

The corresponding areas are normal to each direction x, y and z respectively. It is also important to remember that the materials which will be studied in this research are isotropic materials, which means that their properties are constant in all directions, hence *k* will be always constant.

To obtain the general heat conduction equation, we must consider an unitary volume element (from Figure 1). Its dimensions are Δx, Δy, Δz, density is ρ, and specific heat is *c*. The energy balance can be expressed as:

$$q_x + q_y + q_z - q_{x+\Delta x} - q_{y+\Delta y} - q_{z+\Delta z} + \dot{E}_{gen,element} = \frac{\Delta E_{element}}{\Delta T}$$

Figure 1 – Multidimensional heat conduction through a volume element

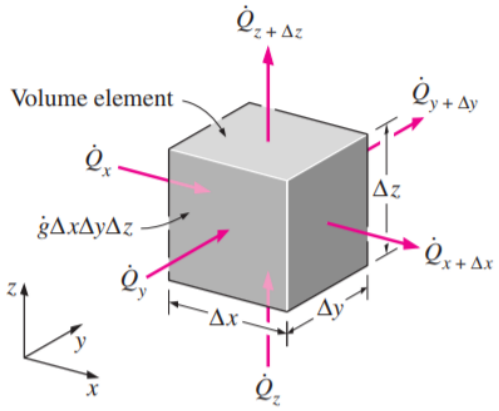

Source: Çengel [12]

After some mathematical simplifications and rearrangements, the final expression can be seen below:

$$\frac{\partial^2 T}{\partial x^2} + \frac{\partial^2 T}{\partial y^2} + \frac{\partial^2 T}{\partial z^2} + \frac{\dot{e_{gen}}}{k} = \frac{1}{\alpha}\frac{\partial T}{\partial t} \qquad (2)$$

Equation 2 also known as Fourier-Biot equation represents the general equation of heat conduction in cartesian coordinates considering the thermal conductivity will not change. The property $\alpha = \rho/C_p$ is known as thermal diffusivity. The elements on the right-side represents the conductivity in the element in all three directions in addition of the generated heat. The left-side represents the rate of change of the energy element. Equation 2 can also be expressed in cylindrical and spherical coordinates. For this study, we will be limited to cylindrical coordinates, which will be enough for this approach. Considering:

$$x = r\,cos\emptyset, y = r\,sin\emptyset\ and\ z = z$$

After some mathematical techniques, we can obtain the equation below:

$$\frac{\partial^2 T}{\partial r^2} + \frac{1}{r}\frac{\partial T}{\partial \emptyset} + \frac{1}{r^2}\frac{\partial^2 T}{\partial \emptyset^2} + \frac{\partial^2 T}{\partial z^2} + \frac{\dot{q}}{k} = \frac{1}{\alpha}\frac{\partial T}{\partial t} \qquad (3)$$

2.1.2 Convection

To understand convection, we must remember a few properties of how fluids behave near a surface. In Figure 2, the fluid velocity profile u(y) is zero at the surface, and gradually increases as it distances from it, until it will behave like the ambient fluid velocity U_∞. The temperature profile is maximum at surface T(y). It will decrease with distance, until it reaches room temperature T_∞. The convection phenomena can be understood as two different events happening at the same time: conduction between microscopic molecules, also called diffusion; and the macroscopic motion of fluid parcels (fluid motion), known as advection, which are generated by an external force: pressure difference and density gradient.

Figure 2 – Convection phenomena

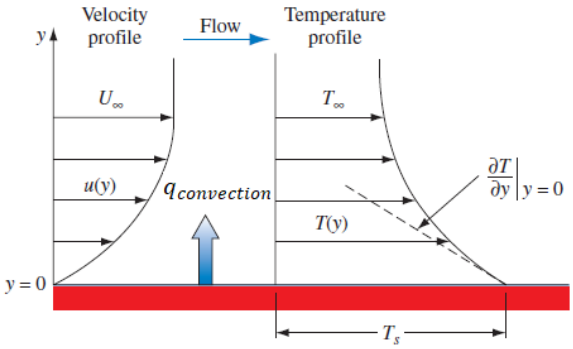

Source: Kreith et al. [13]

In Figure 2, it can be imagined that air is taking heat from the hot surface. But if the fluid is changed to water, the phenomenon will happen fast. This is due to fluid properties: dynamic viscosity μ, heat conductivity *k*, density ρ, specific heat c_P. The fluid velocity *U* also plays an important role in convection, which will also depend on solid rugosity, geometry and flow type (laminar or turbulent). Newton observed that even in a very complicated phenomenon such as convection, the rate of heat transfer by convection is proportional to the temperature difference:

$$\dot{q}_{convection} = h(T_{surface} - T_\infty) \qquad (4)$$

The above equation is also known as Newton's law of cooling. The convection coefficient can be understood as the rate of heat transfer between a solid surface and a surrounding fluid, per unit of area and temperature difference. The no-slip boundary condition also known as no velocity-offset boundary condition, assumes that the speed of the fluid layer in direct contact with the boundary is exactly the same to the velocity of this boundary. For this condition, there is an absence of relative movement between the boundary and this fluid layer, therefore there is no slip. Discontinuity in velocity is an assumption for this condition. This condition is essential to develop fluid velocity profile. A consequence of a no-slip condition is crucial to aircrafts: drag. The no-slip condition implies that heat is conducted through a solid body, until it reaches its surface. There, it starts to be transferred by convection. Equation 5 below shows how heat convection coefficient can be calculated when temperature distribution inside the fluid is known.

$$\dot{q}_{convection} = \dot{q}_{conduction}$$

$$h\left(T_{surface} - T_{\infty}\right) = -kA\left(\frac{\partial T}{\partial y}\right)_{y=0}$$

$$h = \frac{-k_{fluid}A\left(\frac{\partial T}{\partial y}\right)_{y=0}}{\left(T_{surface} - T_{\infty}\right)} \quad (5)$$

The equation 5 shows that to determine h, the temperature gradient must be understood.

The Nusselt number comprehends the relation between viscous and inertial forces, showing how effective is convection A higher Nusselt number represents that heat transfer is dominant by convection rather than by conduction. Represents the heat transferred between fluid layers as convective heat related to pure conduction, so it is dimensionless. Its numerical form can be seen in Equation 6.

$$\frac{\dot{q}_{convection}}{\dot{q}_{conduction}} = \frac{h\,\Delta T}{\frac{k\,\Delta T}{L}}$$

$$Nu = \frac{hL}{k} \quad (6)$$

Another parameter which is also fundamental is Fluid flow. It can determine how convection will happen. Viscosity is the measure of fluid adherence, it happens between the movement of fluid layers, the slowest tries to “brake” the faster layer, this resistance is called viscosity. To simplify fluid analysis, viscous and inviscid flow regions are determined. Viscous regions are those near solid surfaces, when viscous forces are significant to fluid flow. As fluid flow develops, the viscous forces become negligible compared to pressure and inertial forces.

Laminar flow is characterized when the fluid layers are absent of random fluid fluctuation quantities, in other words, velocity, pressure, temperature and density remains almost constant in a certain limit. This flow is smooth and orderly. On the other hand, when these fluctuations happen constantly, fluid flow is characterized as turbulent. In a

pipe-flow, this chaotic flow can increase heat transfer, but it also can increase pumping power. As it is shown in fluid dynamic literature, the dimensionless parameter to classify fluid flow is determined by a value called Reynold's number. It represents the relation between inertial and viscous forces, determining the transition between laminar to turbulent flow. Reynold's number can be calculated in Equation 7 below.

$$Re = \frac{\rho u D}{\mu} = \frac{u D}{\nu} \tag{7}$$

Velocity and thermal boundary layers are important concepts to background this work. The velocity boundary layer is the region which the viscous forces and shear stress are felt. This recall the concept of the viscous and inviscid flow region, which the boundary layer region is affected by viscous and inertial forces. The thermal boundary layer is very similar; it can be understood as the area which the surface temperature influences the adjacent layers, when this influence is negligible, it is the thermal boundary layer thickness, which is increased in flow direction, since the effects of heat transfer are felt in larger distances from the surface. It can be noticed that the both of velocity and thermal boundary layers will be developed simultaneously in most cases, being defined by the shape of the body and fluid velocity, these concepts have a strong influence on how convection will happen. The Prandtl number is a dimensionless parameter to measure the contribution of velocity and thermal layer to heat transfer. Its definition is the ratio of diffusivity of momentum and heat, as can be seen in Equation 8.

$$Pr = \frac{\nu}{\alpha} = \frac{\mu C_p}{k} \tag{8}$$

The surface shear stress happens when the fluid layer in contact with the solid surface tries to drag the above layer, causing friction force. Shear stress is then defined by the ratio of friction force by unit area. Therefore, for a parallel flow of a Newtonian fluid shear stress is proportional to the gradient of velocity in the direction perpendicular to the flow, that is seen in Equation 9.

$$\tau_{s,y} = \left(\mu \frac{\partial u}{\partial y}\right)_{y=0} \tag{9}$$

In Newtonian fluids, which shear stress and strain-rate are proportional, this is the behaviour that characterizes the Newtonian fluid. The strain-rate is then represented by the velocity gradient. The constant of proportionality μ is called dynamic viscosity. In some practical approaches, the fluid velocity profile it is not known. For this scenery, shear stress can be calculated through the upstream velocity of the fluid and the friction coefficient C_f, which can be seen in Equation 10, also known as Darcy Friction Factor. The Darcy equation is theoretical which predicts the frictional energy loss in a pipe based on the velocity of the fluid and the friction resistance. Usually, it is utilized for calculation of head loss caused by friction in a turbulent flow. The coefficient is important for heat transfer applications, and its factor C_f is selected from a chart known as Moody diagram, which relates friction factor to Reynolds number and the relative roughness of a pipe.

$$\tau_s = C_f \frac{\rho V'^2}{2} \tag{10}$$

2.1.3 Fluid flow inside tubes

A very important insight in a heat exchanger is how fluid will flow inside its tube. Parameters discussed in previous chapters of this paper such as turbulence, Prandtl number, Reynold's number, fluid viscosity and Nusselt's number are crucial to determine heat exchanger's efficiency. For continuous operation, pumping losses overflown a higher thermal efficiency, then the above parameters play a very important role in a global analysis. At the entrance region, due to the no-slip condition, fluid particles near the tube surface are brought to rest. This effect slows other fluid layers as result of friction, but the fluid flow remains constant. As a result, the fluid is be developed over the tube, with its parabolic velocity profile in its final region, which can be seen in Figure 3; the parabola is the hydrodynamically developed region, which the velocity profile does not change. The flow region which shear viscous stress is felt, is the boundary layer. The region which the temperature develops is called thermal entrance region, which can be seen in Figure 4. After that, the temperature profile starts to develop until temperature or heat flux is still changing, but on

thermally developed region it is constant and follows a dimensionless profile $\frac{T_{surface}-T(r)}{T_{surface}-T_{mean}}$. The region which both hydrodynamically and thermally regions are developed is called fully developed flow, which will be our region of interest in this study. In this region, the friction and convection coefficients stay constant

Figure 3 – Hydrodynamic Boundary Layer

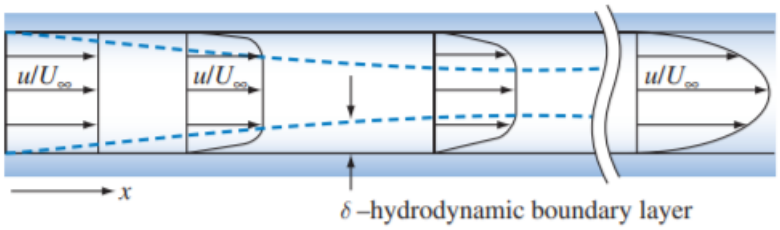

Source: Kreith et al. [13]

Figure 4 – Thermal Boundary Layer

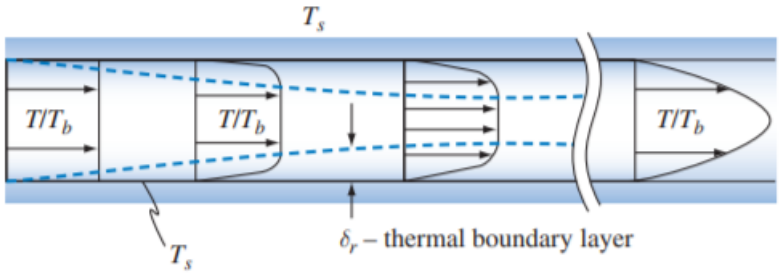

Source: Kreith et al. [13]

2.1.4 Pressure drop

In a fully established flow, the effects of Reynolds' will determine how the heat exchange will happen. In a laminar flow (Re<2100), there's an absence of eddy motion causing most of thermal exchange to happen by conduction, which will be dependent on fluid thermal conductivity, which is generally highly associated with fluid thermal viscosity. Since the goal of this study is nanofluids and water, the conductivity is low, and the eddy motion can determine how well the heat exchanger will perform. A higher Reynolds' number is also associated with a significant increase in Prandtl's number, as

can be seen in Figure 5. The mixing motion increases significantly the heat transfer, but also increases frictional pressure drop, as can be seen in Equation 11.

Figure 5 – Fluid flow (air) in a long-heated tube

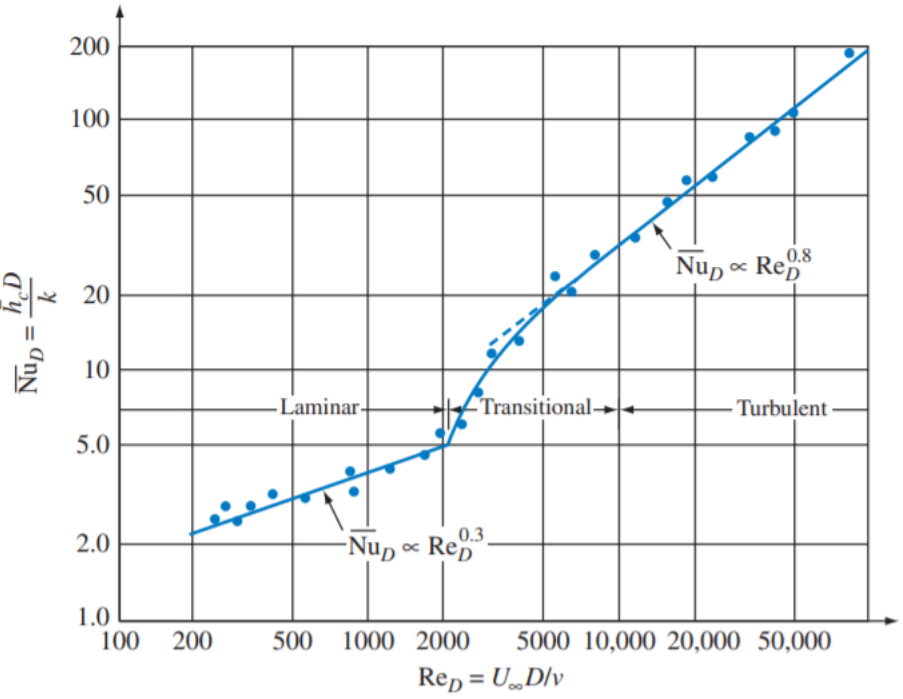

Source: Kreith et al. [13]

$$\Delta P_{lenght} = f \frac{L}{D} \frac{\rho U_m^2}{2} \tag{11}$$

Equation 11 shows the effect of pressure drop exclusively by viscosity effects. On the other hand, the head loss effect also relates the pumping power necessary to overcome height elevations due to internal friction inside the tube, which also considers curves, valves and diffusors. The head loss is the reduction in total head (potential, velocity and pressure head), it can be obtained by dividing Equation 11 by ρg. Once it is known, pumping power can also be determined.

$$h_L = \frac{\Delta P_{lenght}}{\rho g} \tag{12}$$

$$\dot{W}_{pump} = \dot{m} g h_L \tag{13}$$

2.2 HEAT EXCHANGERS

The general definition of a heat exchanger is a device which energy is transferred in format of heat. The classic application happens between fluids, but solid-fluid heat exchangers are also very usual. The fluids can vary widely depending on application. The most common heat exchanger is the “Shell and Tube” configuration - being classified as a recuperator: heat is transferred by conduction and convection, each fluid is separated by a wall.

Figure 6 – Recuperator type: shell and tube

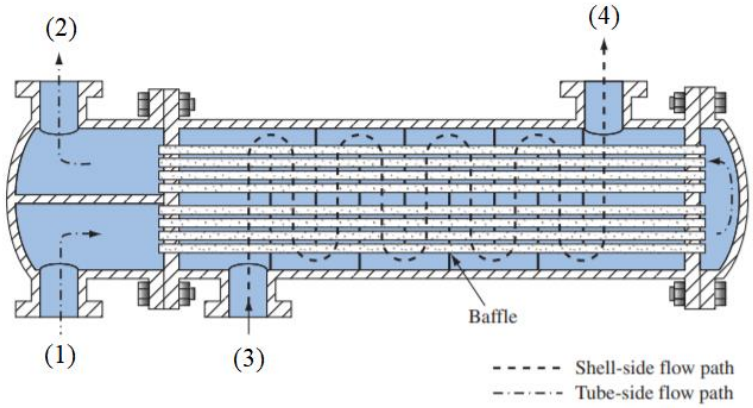

Source: Kreith et al. [13]

Figure 6 illustrates the process which cold fluid enters in (1), and exits warmer in (2). On the other hand, the hot fluid flows the path of the inside-tubes in (3) and exits colder in (4). Baffles are added to create turbulence and increase heat exchange through eddy-motion. They can ensure flow passes through all the tubes in each session. The classic baffle arrangement is this semi-circumference shown in figure 6, but other schemes are also used such as segmental and helical baffles. It can also be noticed in this arrangement that fluid is flowing in counterflow. The parallel flow is also another option in heat exchangers, but it has a lower heat transfer coefficient. This classic heat exchanger arrangement is limited to very clean fluids, and small temperatures differences between cold and hot fluids, due to thermal expansion between the body’s structures and tubes.

The prime concern for designing a heat exchanger is its heat transfer coefficient, which will be influenced on baffle configuration, flow direction, and building material. The geometry will also show how problematic the leakage between tubes and baffles’

hole can be, lowering the average heat transfer coefficient. Size and weight can also be another concern. In automotive application, overweighed heat exchangers can increase vehicle's fuel consumption, on the other hand, a very large heat exchanger may be too much for a car's hood. This kind of application require what can be called "compact heat exchanger", which the most iconic example is human lungs.

2.2.1 Overall heat transfer coefficient

Usually, the first task evaluating the design of a heat exchanger is to calculate the overall heat transfer coefficient between working fluids. This coefficient is a general form of the Newton's law of cooling covering all heat transfer mechanisms in the process, known as "U".

$$q = UA\Delta T \tag{14}$$

2.2.2 Logarithmic mean temperature difference (LMTD)

Inside a heat exchanger, fluid temperature will vary along the flow. This interferes directly in the overall heat transfer coefficient, even for a constant thermal resistance material, the rate of heat flow will change along the path. As it was discussed in the previous sections, this change is also related with flow direction. Figure 7 and 8 shows how temperature changes along the path in parallel and counter-flow respectively.

Figure 7 – Parallel flow heat exchanger

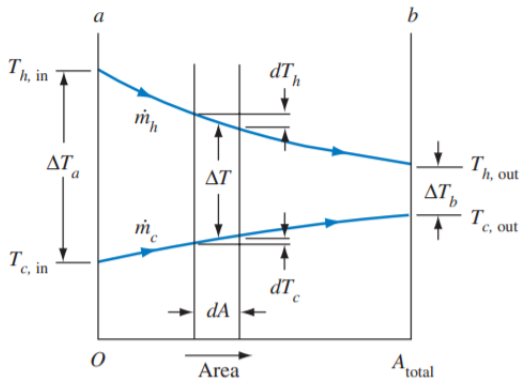

Source: Kreith et al. [13]

Figure 8 – Counter-flow heat exchanger

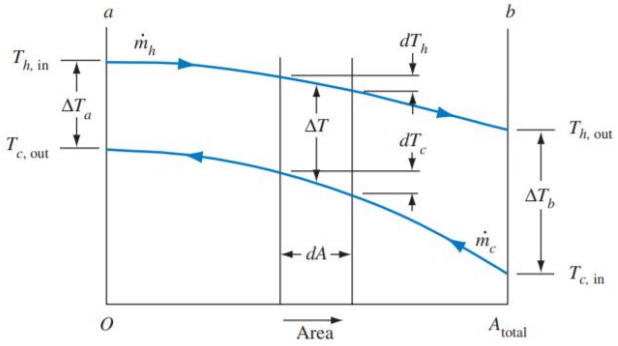

Source: Kreith et al. [13]

In a parallel flow heat exchanger, it can be observed that fluid temperature difference decreases exponentially, with the cold fluid never exceeding the hot fluid's temperature. Assuming steady state, constant fluid properties, and insulated surface of the heat exchanger, the energy balance in each fluid can be shown in Equation 15. We can conclude that the heat loss in any section of the heat exchanger is transferred to cold fluid in that part, and C_{hot} and C_{cold} can be integrated along the path of the heat exchanger

$$dq_{hot} = -\dot{m}_{hot} c_{p,hot} dT_{hot} = C_{hot} dT_{hot}$$

$$dq_{cold} = -\dot{m}_{cold} c_{p,cold} dT_{cold} = C_{cold} dT_{cold} \quad (15)$$

After combining Equation 15 in 14 and some mathematical arrangements, we can conclude that the mean temperature difference is a logarithmic mean temperature difference, consequently, it can be written as Equation 16.

$$q = U\ A\ \Delta T_{lm} \quad (16)$$

It is also wise to mention that ΔT_{lm} will change according to flow patterns, if it is counter-flow or parallel, which can be seen in the referenced books in this paper. Equation 17 shows the counter-flow criteria.

$$\Delta T_1 = \left(T_{hot,in} - T_{cold,out}\right)$$

$$\Delta T_2 = \left(T_{hot,out} - T_{cold,in}\right)$$

$$\Delta T_{lm} = \frac{(\Delta T_1 - \Delta T_2)}{\ln\left(\Delta T_1 - \Delta T_2\right)} \quad (17)$$

2.2.3 Heat exchanger effectiveness

Differently from the LMTD method, which the outlet hot fluid temperature is required, the Effectiveness method measures how well the heat exchanger will perform compared to the maximum possible rate of heat transfer. Another important concept to introduce when talking about effectiveness is the heat capacitance, which is defined by the product of the mass flow by specific heat of the fluid. The numerator is the product of the lowest heat capacitance (cold of hot fluid) by the temperature difference of the hot fluid inlet and the cold fluid outlet, which can be seen in Equation 18.

$$C_r = \frac{(\dot{m}c_p)_{min}}{(\dot{m}c_p)_{max}} \quad (18)$$

The denominator is the ideal case, which happens when the cold fluid outlet temperature is equal to hot fluid's outlet, in other words, the heat exchanger is considered of infinite heat transfer area and in a counter-flow configuration. If only the inlet temperatures are known, it will be a tedious process to analyse a heat exchanger by an iterative process within the LMTD method, this is the main reason why the effectiveness method can be very useful. The equation form of the effectiveness method can be seen in Equation 19.

$$\varepsilon = \frac{\dot{q}_{real}}{\dot{q}_{max}} \quad (19)$$

By definition, effectiveness is a dimensionless number varying between 0 to 1. It is easy to relate effectiveness to a relation of fluids' heat capacity, which is a ratio called Number of Transfer Units (NTU). The NTU is very important in heat exchanger design,

being related with the effectiveness as a function, also known as Effectiveness-NUT or e-NTU method. For this study, this method will be used.

$$NUT = \frac{UA}{C_{min}} = \frac{1}{1 - C_r}\, ln\left(\frac{1 - \varepsilon\, C_r}{1 - \varepsilon}\right) \tag{20}$$

2.2.4 Performance criteria

Several techniques can be used to enhance heat transfer. These changes can be geometrical, such as changing hydraulic diameter, increasing the length of the flow passage and flow arrangement. Other changes can also be pointed out, such as increasing Nusselt's number (which is a function of Reynolds and Prandtl) can make convection more efficient, but on the other hand, it can affect pressure drop, decreasing overall performance.

In this study, the heat exchanger design will be shell and tube. Flow arrangement is counter-flow, this was chosen because counter-flow arrangement requires less surface area for the same inlet and outlet temperature than the parallel configuration. The outer cask of the heat exchanger will not be modified, but on the other hand, the baffles will be a subject of interest. The baffles works as a flow-directing or obstructing structure to create a more turbulent flow and enhance heat transfer, being an integral part of the heat exchanger, they also help to support tubes. In this work, we will discuss about segmented and helical baffles. It is also important to mention that baffles do not work as fins, which are used to enhance heat transfer area, baffles are a way to increase residence time of the cold fluid and to prevent stagnant sections. The Chilton-Colburn factor *j*, a dimensionless number which analogy related heat, momentum and mass. It is an important parameter to measure the differences in heat exchanger configuration, since its geometry will be changed.

$$j = \frac{h\, A_f}{c_p\, \dot{m}}\, P_r{}^{2/3} \tag{21}$$

The pressure drop, which is the difference between the inlet and outlet's pressure is also another important design factor to lower frictional losses in the heat exchanger. The Fanning friction factor can be seen in Equation 22, its an element of calculation of pressure loss due to friction in a tube, and the level of turbulence within the flow.

$$f = \frac{\tau_s}{(\frac{1}{2}\rho u_m^2)} \tag{22}$$

where u_m is the mean flow velocity in the channel.

3 LITERATURE REVIEW

Through the Maxwell's idea of suspending small particles in a fluid aiming a higher thermal conductivity, which can be understood in Figure 9, Choi and Eastman [14] have conducted the first study of nanofluid in 1995, in an effort to fight the main limitation of heat transfer fluids: its thermal properties. The concluding remark of the study was the potential of the nanofluids in order to reduce energy consumption through lower pumping energy compared to regular working fluids. Due to its higher thermal exchange characteristics, the nanofluids can achieve the desired heat transfer with much lower effort. Researchers have also pointed out that even for nanofluids, pumping power must be highly increased to improve overall heat transfer. For instance, to increase heat exchange in a factor of 2, pumping energy needs to be 10 times higher [14].

Figure 9 – Graphic comparison of thermal conductivity
for different liquid and solid materials.

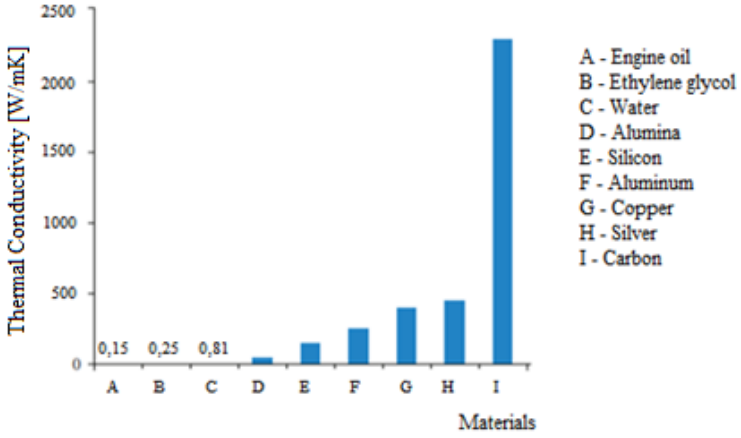

Source: Wong and Castillo [15]

Although with a huge development challenge, nanofluids have been extensively studied in the past two decades. Appearing in multiple combination of metal oxides, carbides, nitrides and general metals, there are two widely known methods for nanofluids synthesis. The most popular is the *two-step method,* which relates to the production of dry nanoparticles, either by physical or chemical means (grinding, inert-gas condensation, microemulsions, pyrolysis, thermal spraying, chemical vapour deposition), and the dispersion with the base fluid. The huge advantage of this methodology is its simplicity,

combined with inert-gas-condensation, the *two*-step method can be promising for producing large quantities of nanopowder. But on the other hand, inner particle agglomeration stimulates a distance dependant force also known as Van der Waals forces, it is an inevitable drawback. In the *single-step* method, the nanofluid is both made and dispersed at the same time, this happens by chemical techniques. Since the nanoparticles are placed in base fluid in the moment they are made, oxidation is reduced. This synthesis can be made with higher advanced methods such as laser ablation and submerged arc nanoparticles [15].

Effective thermal conductivity, k_{eff}, is the most used parameter to compare different nanofluids in its thermal capabilities. It is influenced by base fluid, nanoparticle concentration, stabilization technique, size (d_p), shape, thermal conductivity, and working temperature and measurement method. The concentration (φ) is usually the most controversial topic in nanofluids research. Studies have shown that concentration has a tipping point, higher than that, it will deteriorate nanofluid's performance. Fluid's working temperature is another important factor. Due to Brownian motion (collision between nanoparticles), at a higher temperature, the collision happens more frequently, leading to a better heat exchange and showing that at higher temperature application nanofluids can be more effective. In order to produce a high quality nanofluid, additive selection, sonication time and frequency are critical to avoid clustering. Although with these many characteristics, nanofluids are extremely dependant on nanoparticle size. Although most of studies have shown that nanoparticles smaller than 100nm should perform better in a nanofluid, especially when the working temperature is high, there's a huge controversy in experiments, showing the lack of standardization of measurement techniques, lack of particle shape description, and general information in experiments. [16]

As can be seen in Figure 9, the interest in carbon due to its properties leaded to the study of its allotropes. Graphene, a recent discovered carbon allotrope has a two-dimensional crystalline structure, in a format of a honeycomb. With a large usability, graphene is interesting in the heat transfer field due to its high thermal conductivity. Graphene oxide-deionized water (GO-DI) nanofluid and Graphene nanoparticle-deionized water (GNP-DI) were experimented not just as a heat transfer fluid, but also as a lubricant, being very dependent on concentration, as it was stated by [16]. The study

was conducted in a bearing of a grinding disk, also varying time of operation, load and frequency. Results have shown that GO-DI nanofluid friction coefficient and abrasion loss were significant lower compared to deionized water, with the nanoparticles interacting between lower and upper surface, adding more slippage between surfaces. The friction reduction caused by the nanofluid have shown its good tribological properties, giving space for GO-DI to be used as a coolant. [17]

An experiment was conducted in circular tubes with porous graphene synthesized. The nanofluid was created with Ter-polymer surfactant and an ultrasonic sonicator to disperse nanoparticles through the fluid, producing a stable nanofluid. The concentrations were lower than 0,1%wt and results have shown an increased thermal conductivity by almost 4%. The study also indicated that this graphene nanofluid increased convective heat transfer coefficient by almost 34% compared to the original working fluid. Another interesting consideration was the increase of the thermal conductivity with the rise of temperature and Reynolds number [18].

The two-step methodology is extremely popular between nanofluid researchers, even used to create graphene nanofluid through graphite foam, from dehydration of sugar. The conducted experiment created graphene nanofluid, which was dispersed in deionized water, and magnetic agitation, for surfactant Gum Arabic was added, which is curious because of its traditional usability in candy industry. Four different concentrations were created (0,01, 0,05, 0,1 and 0,2%) to analyse heat transfer in a vertical shell and tube heat exchanger. The results have shown that the nanoflakes with the size ranging between 50-140nm with a 0,2% concentration performed better than water base fluid. The heat transfer coefficient improved by almost 30% and the mean thermal efficiency by 14%. The study also concluded that results were limited to a range of temperature and fluid flow, but at the same time, to a point of view of heat exchanger efficiency, they are promising [19].

It is important to mention that graphene itself is a single-atom thick layer of hexagon sp^2 atoms. The different named materials also are made differently and have different properties. It can be said that in most studies the different types of graphene materials are seen in Figure 10. (a) Multi-layer Graphene (MLG), (b) Graphene quantum dots (GQD), (c) Graphene nanoplatelets (GNP), (d) Graphene oxide (GO) and (e) reduced Graphene oxide (rGO). [20]

Figure 10 – Graphene different materials

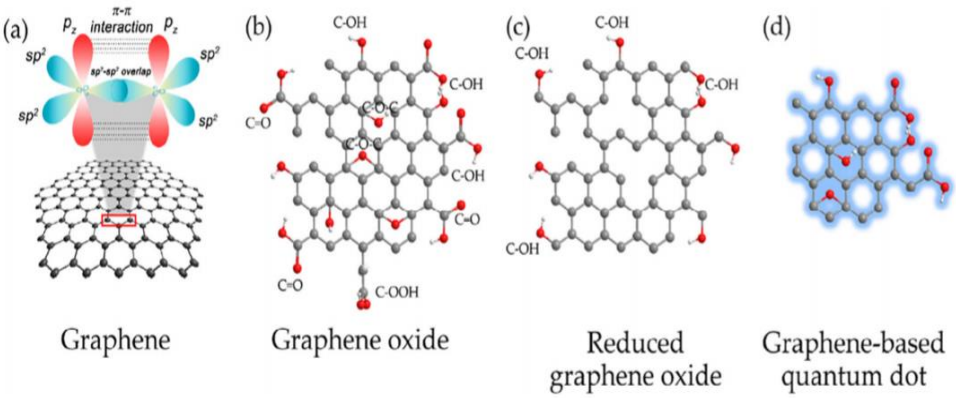

Source: Bahiraei and Heshmatian [20]

Each structure has different and unique characteristics, but in this paper, Graphene Nanoplatelets (GNP) will be discussed further due to its cheap and easier synthesis, allowing experimental research.

Graphene nanoplatelets (GNP) is a 2D structure made of stacks of graphene layers, the number of layers will influence the final nanofluid. A good thing to mention is that the addition of more layers can decrease its thermal conductivity. It is dispersed easier than nanotubes, but on the other hand, nanotubes have a much smaller surface area [20]. GNP is also hydrophobic, meaning that a surfactant should be used to stabilize and disperse the nanofluid. But its reputation as a good conductor, has led researchers to use a 4 to 8nm GNP with high conductivity and surface area to create a nanofluid with H_2O-Ethylene Glycol (H_2O-EG), to use as a coolant in an automotive radiator. The nanofluid was synthesized by non-covalent functionalization method, surfactant was sodium deoxycholate, the mixing process was magnetic agitation and the dispersion was by ultrasonication method. The radiator worked as a cross-flow heat exchanger, with the air cooling the nanofluid which was flowing inside a vertical elliptical tube, with GNP/H_2O-EG concentration varied between 0,1 to 0,5%. The results showed that the nanofluid increased overall heat transfer coefficient by more than 100% at 0,5% concentration. On the other hand, pressure drop was significantly increased by almost 40%, showing a relation directly proportional to concentration, but at the same time, being too insignificant to overcome the benefits of higher thermal exchange [21].

Another study using GNP nanofluid was conducted in an annular tube format, which is very common in heat transfer applications. To understand the behaviour of covalent and non-covalent nanofluids, GNP-SDBS (Sodium dodecylbenzene sulfonate) and GNP-COOH (Carboxylic acid) respectively, were used as working fluid in heat exchangers. The study was conducted both experimentally and numerically, with the results being compared and then, the nanofluid being parametrically studied in the annular tube. The research used a multi-phase approach, to better represent Brownian motion, dispersibility, segmentation and other nanofluid effects which are not fully understood in a single-phase study. Results have shown that suspended GNP particles increased heat transfer properties in general, being directly proportional to concentration. However, the study did not compared results with a single-phase approach, which consumes much less computational power, and could have presented a similar result, considering that in most studies, nanoparticles and base fluid are considered in equilibrium, and the single-phase method is used [22].

An experimental investigation of GNP nanofluid in a microchannel heat exchanger was conducted to analyse total energy expenditure and side effects. With concentration varying from 0,025 to 0,1%, the two-step method was used to disperse GNP into deionized water with nonyl phenol as surfactant. Due to its physical characteristics of a compact heat exchanger, it was expected to achieve a much higher heat transfer coefficient in a microchannel heat exchanger. The results have shown a huge contributor to heat exchanger, which was Brownian motion. This nanoparticle colliding motion was responsible for carrying heat from the hot parts of the microchannel to the cold area, showing that GNPs act as an energy carrier, transporting sensible heat. The pumping power changed with fluid concentration and at higher Reynolds' number, even at laminar flow. Thermophoresis was another important phenomenon to transport heat, associated with Brownian motion. The study concluded that even at higher GNP concentration, the pressure drop was negligible compared to the increased thermal performance over 75% [23].

Shell and tube heat exchangers are widely used in industry, as it was stated in the first sections of this paper. But there is not much literature about nanofluid influences, and when it comes to different geometry heat exchangers, it becomes even harder. Baffle's geometry is extremely important in a heat exchanger, the most common design,

segmental baffles are used due to its ability to create turbulence in a twisting pattern. But on the other hand, dead zones with low heat transfer coefficient and high-pressure drop are created between two adjacent baffles. This can increase vibration and decrease heat exchanger's life due to fatigue. In addition, the fouling factor can increase with time, lowering efficiency [24].

Helical baffles were first proposed by Lutcha and Nemcansky in the 90s with the aim to reduce pressure drop caused by segmental baffles. They have found that this revolutionary design can approach a condition which fluid flows without a back mixing, condition also known as "plug flow". In this condition, the increased velocity gradient also contributed to the augmented heat transfer. Since then, many researchers have been conducting experiments both numerically and experimentally with helical baffles [25].

The main reason for using helical baffles is to create a circular flow pattern. A 4-piece of an ellipse can be imagined, where fluid is leaded inside a circle until it reaches through the next quadrant, the process continues to a complete rotation. A numerical study was conducted in a shell and tube heat exchanger using a two-phase method to investigate the application of nanofluids in a shell and tube heat exchanger with helical baffles. The model was used to simulate forced convection between water and water-Al_2O_3 nanofluid. Helix angle and baffle overlapping were optimized to increase heat transfer and lower pumping power losses. Five different concentrations of the nanofluid were studied with six different helix angles (30, 34, 38, 42, 46 and 50º) and overlapping varying between (0, 0.1, 0.2, 0.3, 0.4, 0.5 and 0.6mm). Results have demonstrated that reducing helix angle and increasing baffle overlapping seems to be the most effective way to achieve a better heat transfer and lower pressure drop. Another conclusion was that higher nanoparticle concentration led to a better thermal efficiency. Researchers have also figured out that overlapping has a gigantic effect on increasing pressure drop, concluding that higher values can only be used when increasing pumping power is no issue [24].

Figure 11 – Helical baffle design

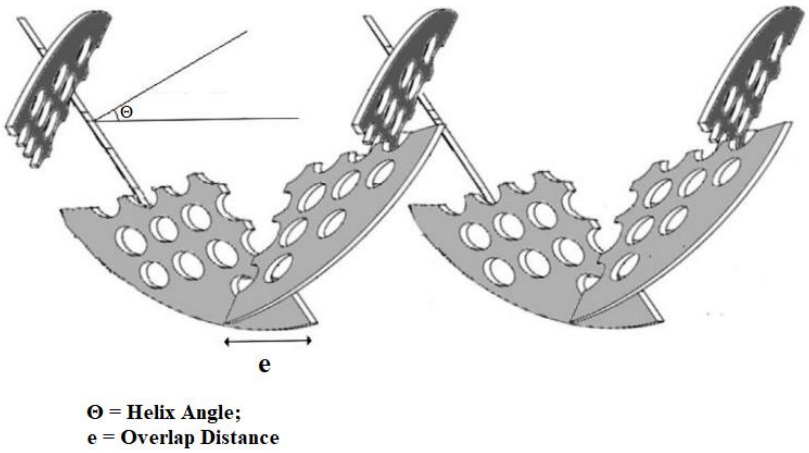

Source: adapted from Bahiraei et al. [24]

In most helical baffle studies, researchers are varying baffle angle and overlap. In 2015 a study was conducted both numerically and experimentally to understand the behaviour of segmented helical baffles compared to continuous helical baffles. The scheme is demonstrated in Figure 12: 20º Trisection circumferential overlap (TCO), 18º Quadrant circumferential overlap (QCO), 18º Quadrant end-to-end overlap (QEE), 18.4º Continuous helical (CH). The study has presented a comparison between these four different configurations with the identical input parameters. It has been found that segmented helical baffles have a higher heat transfer coefficient with the 20ºTCO being the highest. The CH configuration has shown the worst performance in heat transfer, nevertheless it also has shown the lowest friction factor due to the continuous velocity vector, which are not presented in other schemes due to leakage presented in the V-notch zone [26]. Although it has become clear that the segmented helical baffle has advantages in this case, it was still unclear the overall performance of the heat exchanger due to the study limitation.

Figure 12 – Helical segmented x continuous baffles

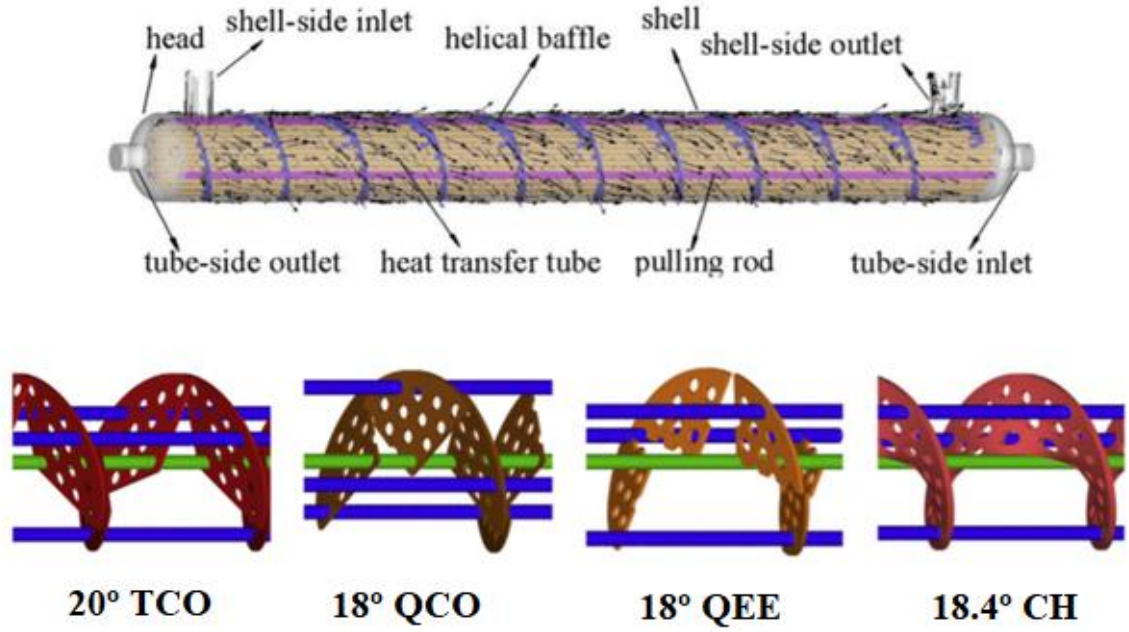

Source: adapted from Dong et al. [26]

A study conducted in ANSYS FLUENT software used continuous and non-continuous helical baffles varying helix angles (20^0, 30^0, 40^0) to understand the fluid behaviour and its effect in a shell and tube heat exchanger. The baffles were designed in a quadrant format. The same thermophysical properties were used to minimize non related effects, fluid flow was different to understand the influence in overall performance. Results have shown that higher helix angle leads to a lower heat transfer, but on the other hand, the pressure drop is lower. The researcher also concluded that the highest heat transfer configuration was the helix angle of 20^0 with overlapping, but the best ratio between heat transfer and pressure drop was found in the 40-degree continuous baffle scheme. The conclusion was that continuous baffles with larger helix angles contributes to a better performance in a heat exchanger with the same helix angle and fluid flow, if compared to overlapped helical baffles [27].

According to [28], which conducted a numerical and experimental investigation in thermal-hydraulic performance of a shell and tube heat exchanger was managed with continuous (CH), quadrant (QH) and sextant helical (SH) baffles to understand overall heat exchanger performance. Overlapping was also another important criterion to

compare baffle configurations, in this case, varying from end-to-end until 50mm overlap scheme. The swirl flow could be achieved only in the continuous baffles, in the other configurations, a pseudo-helical flow was obtained due to fluid leakage in the gaps with V format (QH and SH baffles), but on the other hand, the most homogenous velocity field was found in the SH configuration, which can be seen in Figure 13. The circumferential structure in the SH configuration has solved the problem of leakage. The performance evaluation depicted that the SH has the highest heat transfer coefficient with the lowest pressure drop ratio. This leads this configuration to the best thermohydraulic performance in all configurations. On the contrary, the QH with 50mm overlap and CH configuration having the worst $h/\Delta p$ ratio respectively. The overlap building technique is concluded as beneficial to enhance heat exchange, however, in some configurations overlap is so high that it surpasses pressure drop allowance, leading to a lower heat exchange efficiency, this case can be seen in the QH with 50mm overlap scheme. The author also has made an exergetic analysis comparing each different configuration. The criteria was the *Be* number (Bejan number), which is the ratio of heat transfer generated entropy by total entropy generation rate. In the exergetic analysis, in general, the Bejan number was lowered as Reynolds' number was higher. The findings were that both SH and QH configuration represented the minimum entropy generation with a Reynolds' number lower than 2500, higher than that, the opposite happened [28].

Figure 13 – Sextant helical baffles

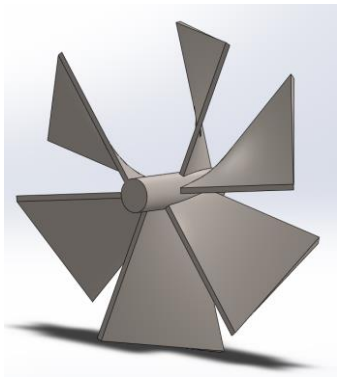

Source: Author (2022).

The study of heat transfer by the view of the second law of thermodynamics is largely important to understand irreversibility in the process and to optimize it. Baffle design modification and its angle have a direct effect on flow resistance on shell side of

a heat exchanger and consequently, on heat transfer properties. An experimental study varying discontinuous helical baffles angle (8, 12, 20, 30 and 40^0) was conducted to modify a shell and tube heat exchanger design. An important design parameter which has been used is the baffle overlap proportion *e*:

$$e = \frac{2l}{D_{in}} * 100\% \tag{23}$$

This proportion is an important project parameter, usually varying from 10% to 50%. When the end-to-end method is applied (continuous baffles, for instance), the ratio is zero.

The concept entransy dissipation was introduced to explain the loss of heat transfer potential in the process and can also be used to measure irreversibility. The concept sums the dissipation caused by flow friction and finite difference temperature and is used as a dimensionless number to evaluate heat exchanger performance, which can be seen in Equation 24.

$$E = \frac{\dot{E}_{\Delta T} + \dot{E}_{\Delta P}}{Q(T_{h,in} - T_{cold,in})} \tag{24}$$

Results have shown that from a point of view of the second law of thermodynamics, the irreversibility grows up with a higher baffle angle. The findings also pointed out that the irreversibility is directly proportional to Reynolds number.

On the other hand, for a heat exchange performance analysis, the correlations between Colburn *j-factor* and Nusselt number have shown that with the increase of baffle angle, the Nu was increased by 33%. This can be explained by the thin boundary layer formed and detached from the tube's wall with the fluid flowing asymmetrically. This effect enhances heat transfer and it is amplified with a higher Re number. Results have also proven that a higher helix angle decreases pressure drop, but at the same time, this reliability is only worth at lower Re number, since the irreversibility starts to grow [29].

With all this research, it is still unclear how helical baffles behave in an environment with a graphene based nanofluid. The next sections of this paper aim to

contribute to the reviewed literature showing the effects of baffle design on a shell and tube heat exchanger with a graphene based nanofluid as working fluid.

4 NUMERICAL AND MATHEMATICAL MODELLING

In this chapter, computational model will be explained: governing equations for continuity, momentum, energy, k and ε. Boundary conditions will also be described. The dimensions of the heat exchanger-based model and its real conditions will be shown with the addition to the Mesh generation, selection criteria, data reduction and model validation.

4.1 THE GEOMETRY

The CAD (Computer aided design) model seen in Figure 16 was built in Solidworks 2019 software, following experimental setup, then exported to Ansys Geometry DesignModeler. The geometry shown in Figure 16 was submitted to a CHT (Conjugate Heat Transfer) analysis, which allows for the simulation between solid and fluid domains by exchanging energy in a format of temperature in the interfaces between them, this kind of analysis is perfect for heat exchangers, in this case, with shell and tube. The model was created in a personal computer with the following specs: processor Intel® Core™ i7-4790k 4.0 GHz, NVIDIA GeForce GTX 970 4Gb SSC, 16Gb Corsair Vengeance 1866Mhz RAM.

Figure 16 – Trimetric view of the original heat exchanger

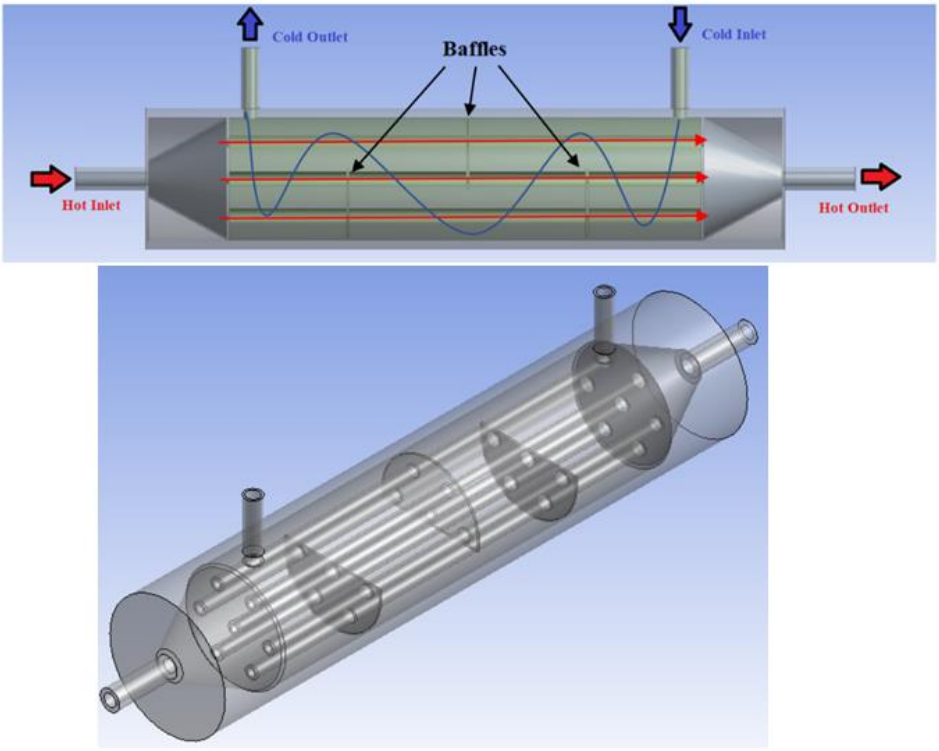

Source: Author (2022).

The geometry itself is a simple shell and tube heat exchanger, with 7 tubes for the hot fluid converging into a conical structure to the outlet. The cold fluid is forced through the alternate segmental baffles. A section view of the geometry can be seen in Figure 17 (a) and (a1), showing flow directions, and baffle type. (b) and (b1), (c) and (c1), (d) and (d1) describes the 360CH, 1080CH and SH geometries respectively.

This first Geometry shows the original heat exchanger in CAD, which will be used to prove the chosen approach via results comparison (experimental *versus* mathematical). Although, the main purpose of this paper is to study geometry differences influence in the behaviour of heat transport with different nanofluids. The following geometries (Figures 18-20) with modified baffles will be the focus of this paper. The continuous helical (CH) geometries were created in three different shapes, varying the baffle angle rotating on its own axis by 360^0 and 1080^0.

Figure 17 – CAD Model – Heat exchangers baffle modification comparison

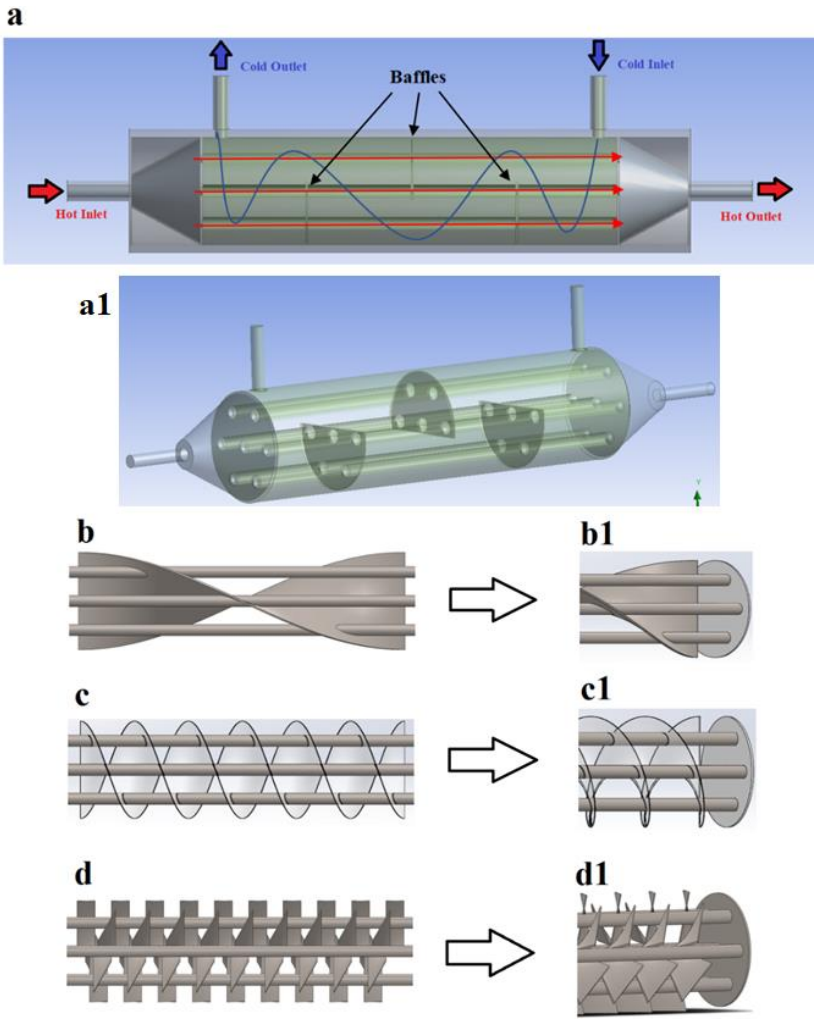

Source: Author (2022).

These types of baffle geometry have shown a very low pressure drop, that's the reason they were chosen to this present work. The last design shown in Figure 20 is the most complex one. The helical spiral is formed by sextant geometry with a helix angle of 40^0. This last geometry was made based on previous studies shown in the literature review chapter.

Table 1 – Geometric parameters of helical baffles

ITEM	360 CH	1080CH	SH
Shape	Continuous	Continuous	Segmented Sextant
Helix Angle (^{0})	43,36	70,56	40
Helix Pitch (mm)	173	57,66	69,01
Overlapped space (mm)	-	-	2,21
Baffle number	1	1	55
Baffle thickness (mm)	0,5	0,5	0,5
Axial overlapped ratio (%)	-	-	8,5

Source: Author (2022).

Figure 18 – Continuous Helical 360º Geometry

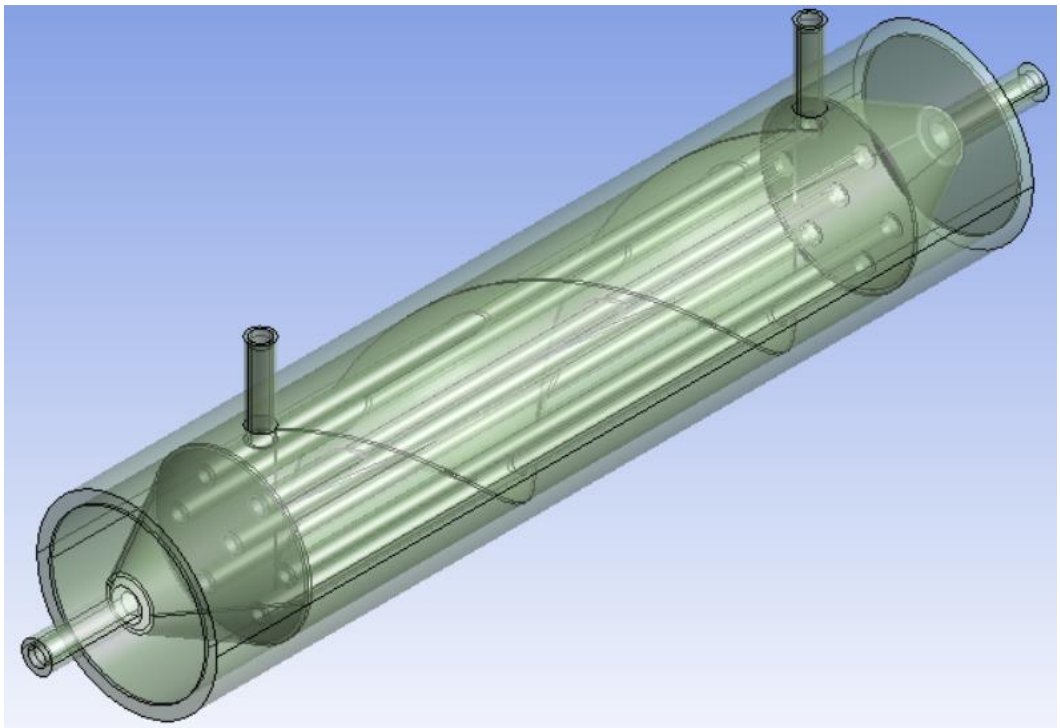

Source: Author (2022).

Figure 19 – Continuous Helical 1080^0 Geometry

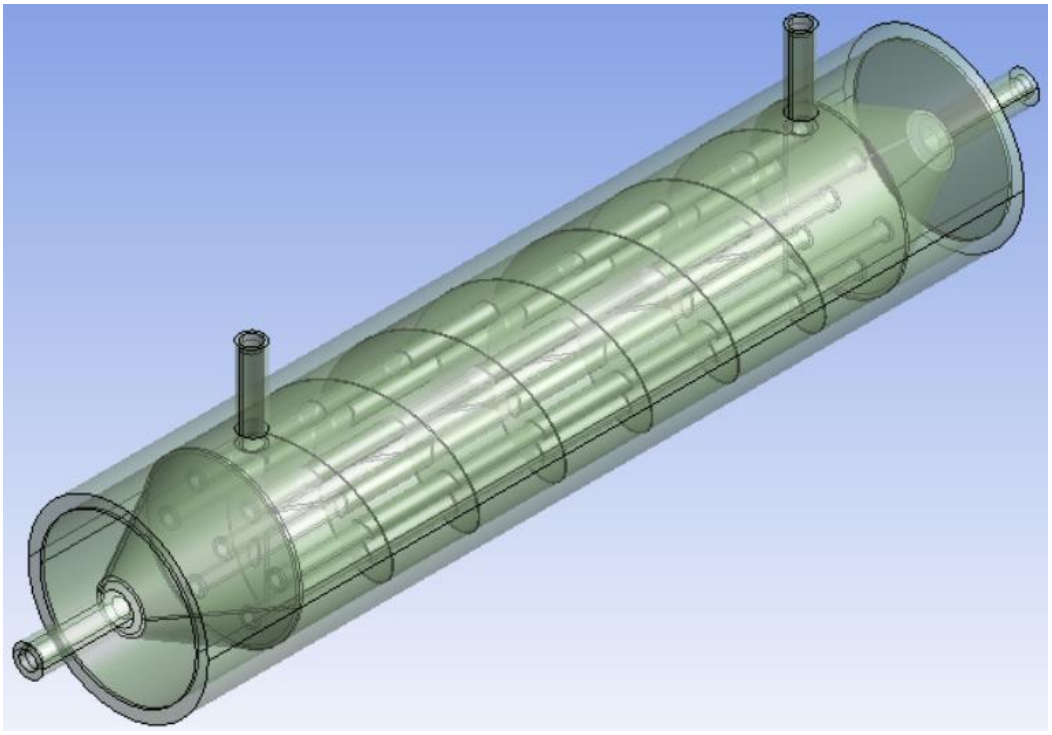

Source: Author (2022).

Figure 20 – Segmented Helical Baffles Geometry

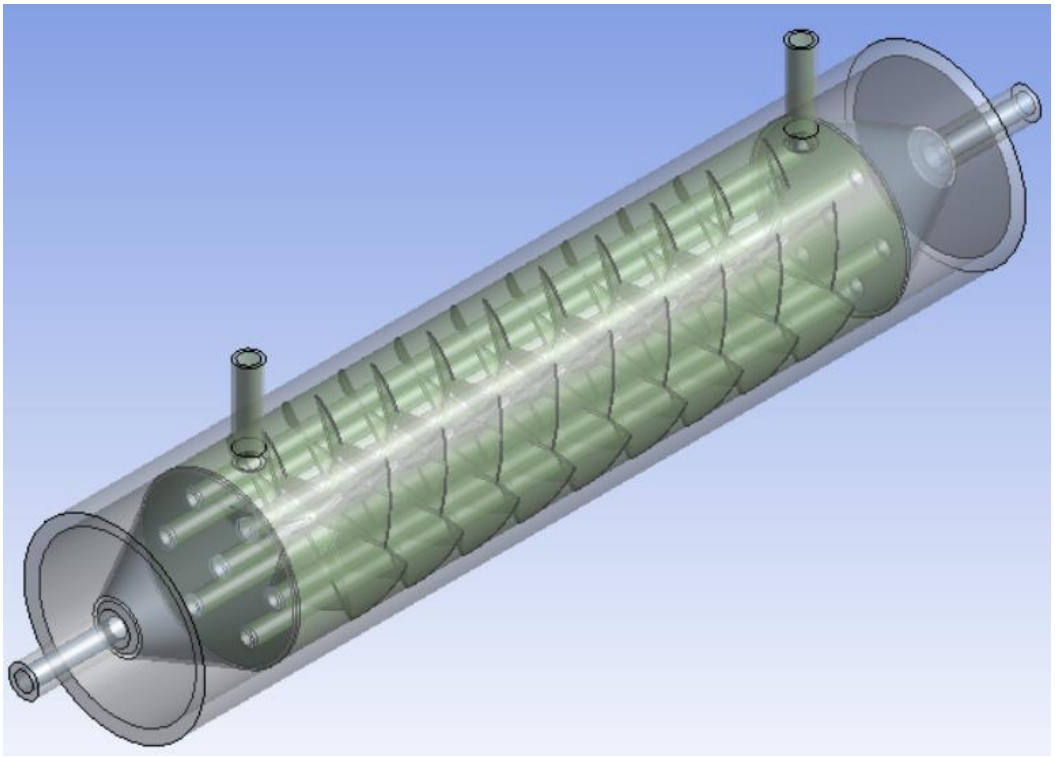

Source: Author (2022).

4.2. GOVERNING EQUATIONS AND BOUNDARY CONDITIONS

The governing equations are the continuity, momentum and the conservation of energy. The solving of each of them is crucial to obtain the desired results. For these equations to work in its entirety, there is a necessity to determine where and how they will be accepted and their limitation. For this, the boundary conditions are set, determining each domain and their characteristics.

4.2.1 Governing equations

Conjugate heat transfer (CHT) analysis involves solving the mass, momentum and energy conservation equations. With the increase in momentum, turbulence is inevitable and a wanted event. Within the solid domain, the conservation of energy equation can account for the transport of heat, due to solid motion, conduction and volumetric heat sources.

The k-epsilon turbulence model is the most common method to simulate turbulent fluid flow characteristics. It is part of the Reynolds-averaged Navier Stokes (RANS) family (which describes all turbulence effects), which modifies the original unsteady Navier Stokes equations into a statistical model representing mean flow quantities only. The two-equation model solves conservation equations in addition to turbulent kinetic energy *k*, which determines energy in turbulence, and the turbulent dissipation rate, known as ϵ. The model is reliable for free-shear flow with small pressure gradients, which applies to this problem. [31]. Turbulence can increase heat transfer and it will be explored in the model. The governing equations for energy k-ε, continuity, and momentum in the computational domain for an incompressible and Newtonian fluid are written as follows.

- Continuity equation

$$\nabla\left(\rho_{eff}\bar{V}\right) = 0 \tag{25}$$

- Momentum equations

$$\nabla\left(\rho_{eff}\overline{VV}\right) = -\nabla\overline{\mathrm{P}} + \mu_{eff}\nabla^2\bar{V} - \rho_{eff}\nabla\left(\overline{v'v'}\right) \tag{26}$$

- Conservation energy

$$\nabla\left(\rho_{eff} C_{p,eff} \overline{V}\overline{T}\right) = \nabla\left(\left(k_{eff} + k_t\right)\nabla\overline{T}\right) \tag{27}$$

In the above equations, components $\overline{V}, \overline{T}$ and $\overline{\mathrm{P}}$ represents the time averaged flow variables, while v' is the velocity fluctuations. The turbulent shear stress is the term $\rho_{eff}\nabla\left(\overline{v'v'}\right)$, k_{eff} is the effective molecular conductivity and k_t represents the turbulent thermal conductivity. To model the flow in the turbulent regime, which is usually determined by Reynolds number, the standard k- ϵ model is represented by the following equations.

- Turbulent kinetic energy

$$\nabla\left(\rho_{eff} kV\right) = \nabla\left[\left(\frac{\mu_t}{\sigma_k}\right)\nabla(k)\right] + G_k - \rho_{eff}\varepsilon \tag{28}$$

- Turbulent energy dissipation

$$\nabla\left(\rho_{eff}\varepsilon V\right) = \nabla\left[\frac{\mu_t}{\sigma_\varepsilon}\nabla\varepsilon\right] + \frac{\varepsilon}{k}\left(C_{1\varepsilon}G_k - C_{2\varepsilon}\rho_{eff}\varepsilon\right) \tag{29}$$

Where, $\mu_{eff} = \mu + \mu_t$, $\mu_t = \frac{\rho_{eff} C_\mu k^2}{\varepsilon}$, $G_k = \mu_t(\nabla V + (\nabla V)^T)$, and μ_{eff} and μ_t stands for effective viscosity and viscosity coefficient for turbulent regime.

After discretization, governing equations are solved by a numerical method. In CFD, the finite volume method is very utilized to do numerical calculation. In this paper, the CFX solver was the chosen software to be implemented, the ANSYS CFX software uses finite volume method. The CFX uses the SIMPLE (Semi-Implicit Method for Pressure Linked Equations), also commonly known as pressure-based solver to show how pressure and velocity couple. The advection scheme used a High-Resolution method, which is the standard for CFX. The Turbulence was solved by First Order method. The number of iterations were set for a starting point until it reaches 2000 or the convergence criterion were reached. The criterion established for convergence was to limit residuals

by RMS (Root mean square) and specify target value. The specified value is that the normalized absolute residuals are less than 10^{-4}. For most engineering problems, this value seems sufficient at least as a start.

4.2.2 Boundary conditions

Water and three different graphene nanofluids are assigned in the heat exchanger. The pure water is always the cold fluid, which is located at the shell-side. The three fluids are found in the tube-side. The medium is steady-flow with turbulence, and the fluids are considered incompressible. In all models depicted in this paper, each fluid properties were unique according to laboratory experimental results obtained by [30], although they seem to vary linearly with temperature. The thermophysical parameters of all experimental fluids and pure water can be seen in Table 2, where the nanoparticle fraction can be seen in the first column "Wt%".

Table 2 – Thermophysical properties of fluids

Wt %	k (W/mK)	ρ (kg/m³)	μ(kg/ms)	Cp (J/kg.k)	T (°C)	Pr
Water	0.62	937.5	0.000891	4120.0	25	5.92
0.0125	0.57	947.1	0.000919	3842.0		6.19
0.025	0.60	964.0	0.000948	3846.1		6.07
0.050	0.63	971.5	0.001008	3854.5		6.16

Source: Adapted from Lima [30].

The hot domain is stands for the hot inlet, outlet and the interface. The heat transfer model is thermal energy. The inlet is kept at static temperature (40ºC, 50ºC and 60ºC) and flow regime is set to be subsonic and the mass flow rate number is 0.051 kg/s. Turbulence model is k-Epsilon with wall function scalable (which resolves the discontinuous transition between wall and boundary layer). The outlet follows the subsonic flow regime, with mass and momentum with an average static pressure of 0 Pa (gauge pressure). The entire domain is non-buoyant, and the motion is stationary. Cold domain has also heat transfer model of thermal energy, turbulence k-Epsilon with scalable

wall function. Inlet is also kept at constant temperature (25ºC) and the fluid flow is set to be subsonic (0.05 kg/s, 0.1 kg/s, 0.2 kg/s). The outlet flow regime is subsonic with a static pressure of 0 Pa (gauge pressure).

The solid domain is composed by Steel contained in ANSYS CFX material library. The solid has a continuous morphology and the heat transfer does occur (it is not isothermal nor adiabatic). The heat transfer is conservative interface flux, the momentum boundary for all solid surfaces is non-slip and the roughness is negligible, being smooth wall.

The counter-flow configuration is used in the heat exchanger with its temperature interface being widely exploited to exchange heat. The turbulence is set to be of medium intensity and eddy viscosity ratio. The outlet pressure is maintained at 0 Pa (gauge) for both fluid flows.

4.3 THE MESH

The mesh generation is crucial to CFD analysis. The mesh quality can determine how close results are from what was expected (usually, a comparison between experimental and numerical results). It is also responsible for the amount of computational time, and could limit the analysis due to its complexity.

4.3.1 Grid generation

The mesh was generated by ANSYS Meshing software, making a 3D grid system for further mathematical modelling. As the mesh must be made in different geometries, the properties of each grid are unique. The first model (which is the copy of the physical heat exchanger) has a much simpler geometry due to its baffle configuration. As the first trial, this geometry was made in Meshing standard configuration, which is quadratic element order, no inflation, tetrahedral elements, and a number of nodes and elements of 3845120 and 2862792 respectively.

Figure 21 – Mesh display: original heat exchanger

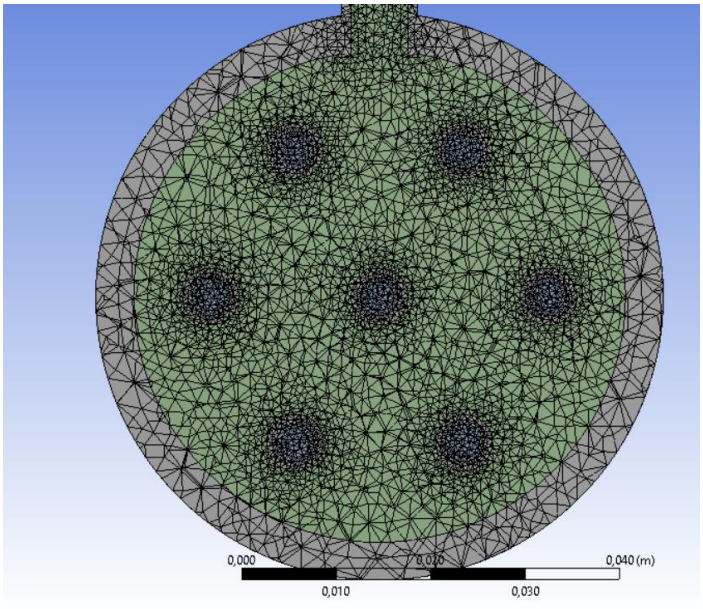

Source: Author (2022).

To compare grid independence and to have certainty that the grid number is both accurate and efficient, a comparison of three different meshes were made: extra refined, refined and simplified. The Table 3 shows the details of each mesh generated for the segmented sextant geometry.

Table 3– Mesh parameters

ITEM	Segmented Sextant		
Grid	Extra refined grid	Refined Grid	Simplified Grid
Elements	1465052	758858	280945
Nodes	21230003	10696546	421325
Element type	Tetrahedron	Tetrahedron	Tetrahedron
Inflation	Yes	Yes	Yes
Element Order	Quadratic	Quadratic	Quadratic
Sizing	Face Sizing / Element Sizing/Patch Conforming	Face Sizing / Element Sizing/Patch Conforming	Face Sizing / Element Sizing/Patch Conforming

Source: Author (2022).

The element type chosen was Tetrahedron due to its possibility to highly detailed structure, such as the helical and segmented helical baffles. The sizing happened in

different faces and volumes; the aim was to increase element number to achieve a higher precision. The inflation was set to have 8 layers around the internal tubes, the maximum thickness was set to be 0.008m.

4.3.2 Mesh analysis

The biggest challenge when generating a mesh is to achieve high-quality and the lowest possible computational time. All parameters shown in Table 4 were obtained by countless trials to generate mesh in very small surfaces such as the segmented baffles. Due to its complicated geometry (the baffles are rotated in two different axis) and thin width, the element sizing and number of elements were some used tools. The extra refined mesh was the first trial to achieve success in convergence. The element number is very high, making the analysis very time consuming.

Figure 22 shows how hot fluid temperature outlet behaved in the simulation. The extra-refined mesh took 08:59:23 to complete the simulation with 1229 iterations to achieve convergence. The refined took 05:16:32 for 1396 iterations and for the last mesh, the simplified took 02:54:35 at 1448 iterations. The “Outlet hot fluid temperature” parameter in Figure 22 depicts the average outlet temperature of each different mesh, in this comparisson with water as working fluid and coolant. For this type of comparison, even a very small values can propagate a large error, and the difference can be considered big, for this reason the Simplified grid was discarted even presenting a percentage difference of 0.43%. The Refined Grid was chosen due to its 0.10% difference in average results compared to the Extra-Refined.

Figure 22 - Grid complexity comparison

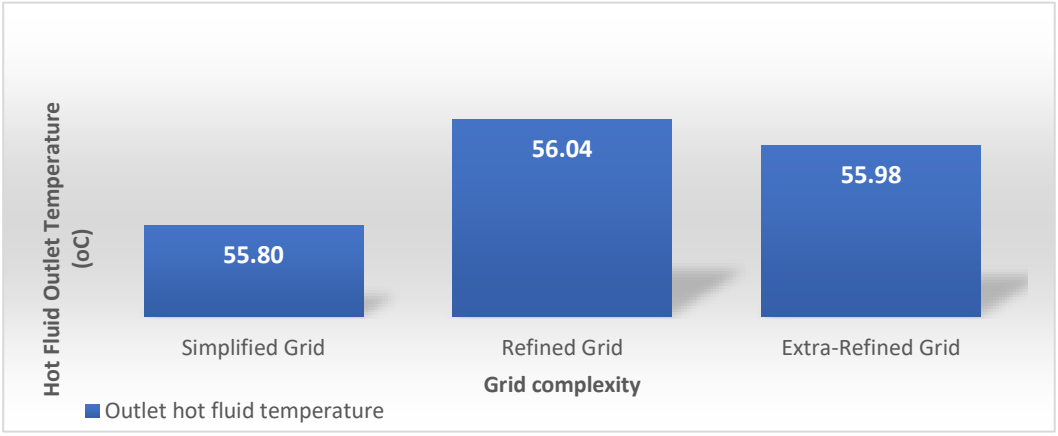

Source: Author (2022).

To understand why this mesh was chosen, we must consider some conditions. To calculate the heat transfer coefficient, a logharitimic function will be utilized and for this reason the error could be devastating. This is the main reason why the Simplified Grid was not chosen, since the difference found in the logharitimic mean temperature difference was 11.67% times the first value obtained by the Refined Grid. The Extra-Refined Grid test for the logharitimic mean temperature difference was 3.67% lower than the Refined Grid. With this results, we can be sure that the best chosen Grid for this simulation is the Refined Grid.

[33] has shown a method to calculate Reynolds number in a helical baffle pattern. The equivalent Diameter (D_e) for the triangular tube alignment, Reynolds number, cross sectional area A_s and baffle spacing e are shown in the following equations:

$$D_e = \frac{4\left(P_t{}^2 - \frac{\pi d_0{}^2}{4}\right)}{\pi d_0} \tag{30}$$

$$R_{e,shell} = \frac{D_e \dot{m}_{hot}}{\mu A_s} \tag{31}$$

$$A_{ss} = 0.639(P_t - d_{outlet})e\sqrt{\frac{CL}{CTP}\frac{A}{d_0 L}} \tag{32}$$

$$A_{scnc} = 0.5e\left[D_{shell} - D_{otl} + \frac{D_{olt} - d_{outlet}}{P_t}(P_t - d_{outlet})\right] \tag{33}$$

Where P_t is the tube pitch, D_e is the shell diameter, A_s is the cross-sectional area of the shell, according to the baffle, A_{ss} stands for the segmental baffles and A_{scnc} for the continuous and noncontinuous and e is the baffle spacing. The Reynolds number, cross sectional area A_s and baffle spacing e are shown.

Wall functions are a set of empirical formulas connecting different variables as velocity, pressure and temperature at the wall to the turbulence boundary layer (near wall). They are applied by using the law of wall for variables near wall region. Depending on the turbulence model, the most common used formulations are: standard wall function, non-equilibrium wall functions and enhanced wall functions. Wall functions make possible to calculate boundary condition away from the wall. These functions are responsible for the need to change the turbulence model to explain viscosity layer near wall region. The standad wall function, which was utilized for the turbulence model k-Epsilon needs a $\boldsymbol{y}^+$ value varying between 15 to 300. Figure 23 shows the walls shear stress comparison for the three different meshes analyzed and its corresponding $\boldsymbol{y}^+$ [34]. For a comparisson criterium, the average Wall Shear Stress was calculated and compared in terms of percentage. For the simplified mesh, $\tau_s = 0.282098$ [Pa], for the refined mesh, $\tau_s = 0.357787$ [Pa], and for the extra-refined mesh, $\tau_s = 0.342431$ [Pa]. The simplified mesh has a 21% divergent result compared to the refined and a 17.61% difference from the extra-refined. This difference is very signficant for a dynamic analysis of the quality of the mesh, which can also be understood as a possibility of unstable results. For the refined mesh, the percentage difference with the extra-refined was 4.48%. The y^+ shows us that most of the flow happens at a low Reynolds number. In the law of the wall region, inertial forces dominate over viscous forces and there is a high presence of turbulent stresses (this is known as the high-Re composite region). If using a low-Re model, the whole turbulent boundary layer will be resolved including the log-law region. However, it possible to use semi-empirical expressions known as wall functions to bridge the viscosity-affected region between the wall and the fully-turbulent region. The main benefit of wall function approach lies in the reduction in mesh resolution and thus reduction in simulation time. However, the shortcoming lies in numerical results deteriorating under subsequent refinement of the grid in wall normal direction [34]. Although the y^+ value seems sufficient for the simplified mesh, when temperature and h are also important, the chosen mesh was the Refined.

Figure 23 – Wall shear stress and y^+ comparison

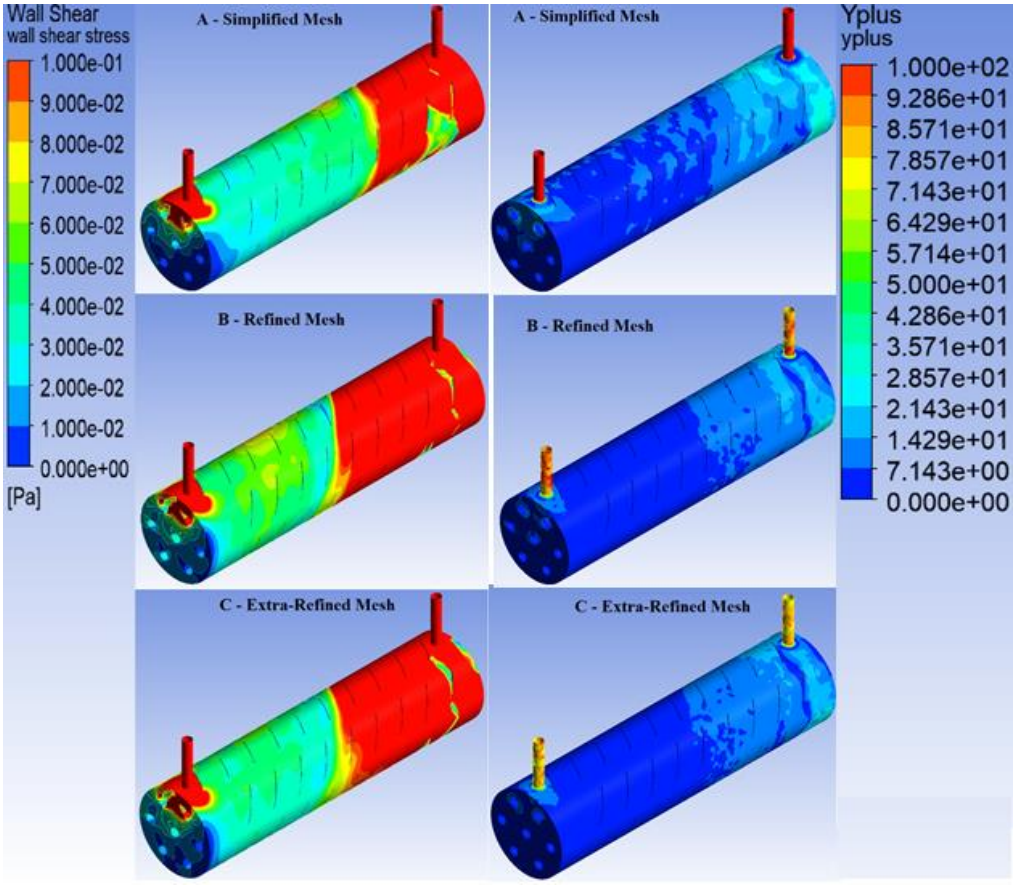

Source: Author (2022).

The Figure 24 shows how detailed is the grid in the CHT analysis. From A, it can be seen two different sections in planes XY represented by red and green axis, and from B, YZ cut represented by green and blue axis (cross section) with whole element representation. It can be seen the inflation layers (8 layers of 0.008m each) around the tubes. Inside each tube, the face sizing was applied to ensure each element had 0.001m. The cold fluid mesh, which is the most important parameter in this study was also controlled to have elements with no bigger than 0.002m. The mesh itself shown quite complex due to the geometry of the heat exchanger.

Figure 24 – Chosen mesh

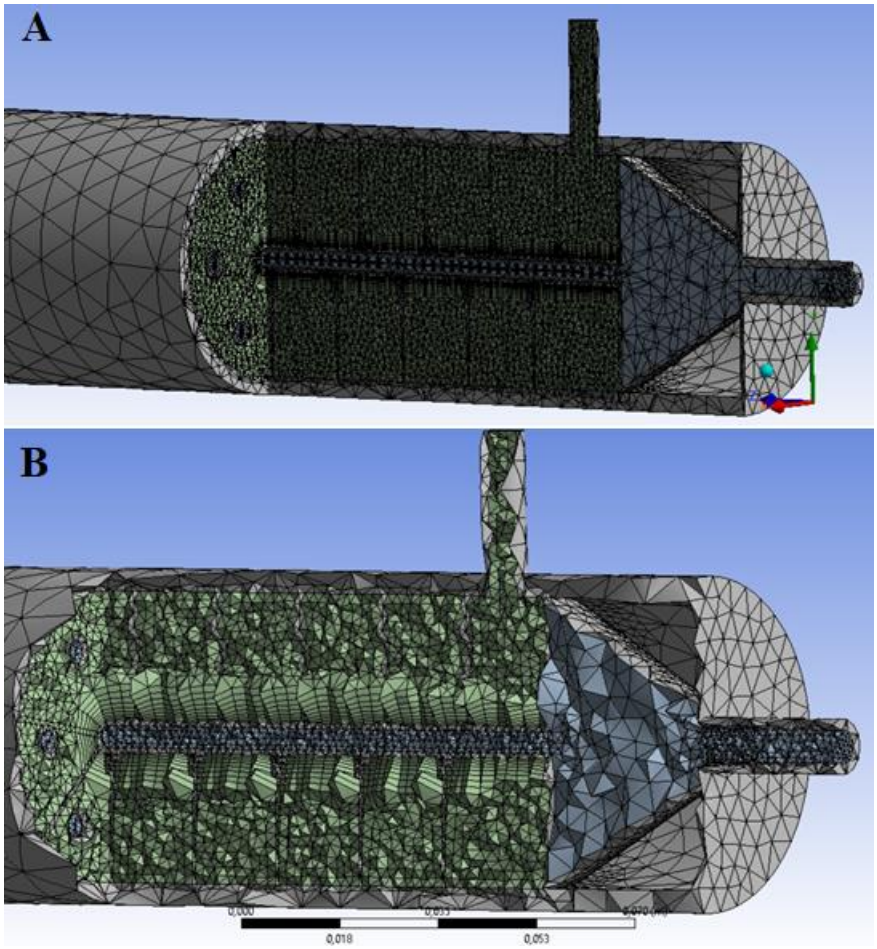

Source: Author (2022).

4.3.3 Methodology proof

Before analysing the results of this current paper, a comprehensive comparison between simulations and experimental work data provided by [31] and [30] was deeply exploited to later prove the methodology followed in this work. To make sure each step was made correctly, the same input values found in [30] and [31] were used in this approach: the cold and hot fluid inlet flow were set to be 0.051 kg/s, the cold fluid temperature (water) was 25ºC, and the hot fluid temperature (water) was 60ºC. It can be noticed that both these input values are found in experimental and in the mathematical model. The study made by [30] was based on two different heat exchangers with different nanofluids which were described in Table 2.

The author also has chosen to build a finite volume approach as a mean to validate data obtained by experimental results. The geometry was identical to the heat exchanger, the criteria used to prove the methodology was a parametrical comparison between outlet temperature, Re, Nu to different temperatures and nanofluid concentration.

Table 4 – Methodology proof

	[30] Experimental Analysis		**[30] CFD Analysis**		**STHE (CFD)**		**Difference [%]**	
	Inlet	Outlet	Inlet	Outlet	Inlet	Outlet	Experimental	CFD
Cold fluid temperature [ºC]	28.20	32.09	28.20	31.13	28.20	31.53	1.75	1.28
Hot fluid temperature [ºC]	58.46	55.07	58.46	56.04	58.46	55.35	0.51	1.23

Source: Author (2022).

Table 4 shows the comparison between models of the heat exchanger. The current algorithm used in this paper has shown even a closer result to the experimental work conducted by [30]. The current model presented in this paper has shown more precision if compared to the results achieved by [30] simulation. Although the difference between both CFD models were small, the mesh developed in this current work was more refined (inflation, smaller element size played a crucial rule in this higher number of elements). This small difference in the results occurs because of the simplification attached to the CFX solver and the mathematical model.

With the proof of the above model, many geometric changes can be made to study how the heat exchanger will behave under determined conditions. For the purpose of this work, the geometry will be changed to understand the differences in heat transfer between different baffles, fluid flow and temperature.

5 RESULTS AND DISCUSSION

In this section the detailed results obtained from the numerical analysis will be presented and discussed. The shell-side pressure drop will be the first section, followed by the thermal analysis.

5.1 SHELL-SIDE FLOW RESISTANCE CHARACTERISTICS

Figure 25 shows the effect of the higher fluid flow over head loss. The different baffle scheme and volume flow resulted in a significant head loss difference. As expected, higher fluid flows cause more turbulence and an increase in pressure drop. The Reynolds number plays an important role in this analysis, varying between 422 to 6840, indicating laminar, turbulent and transient regimes. It is clear that the Segmented Helical baffle configuration has shown the best results with the lowest pressure drop in any fluid flow configuration. It must also be pointed out that at lower cold fluid flow, the pressure drop change is small compared to what can be seen at medium and higher volume flow. The SH has a Reynolds number of 1427 for the 0.051kg/s flow, 2798 for the 0.1kg/s and 5596 for the highest flow (0.2kg/s).

Figure 25 – Shell-side head loss effect

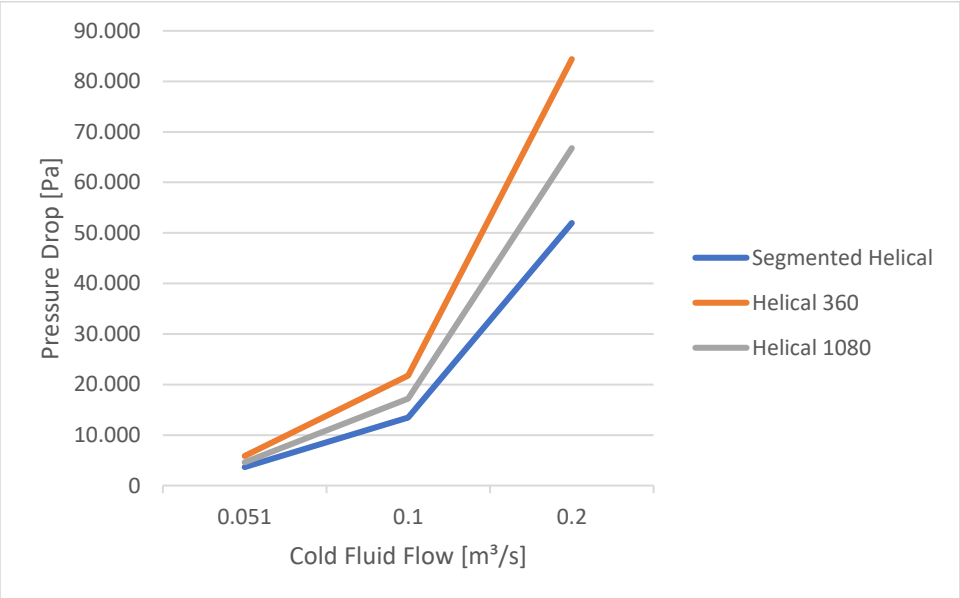

Source: Author (2022).

Nevertheless, the 1080 CH configuration has shown a lower pressure drop compared to the 360 CH. For the 1080CH, the Reynolds number varies from 422, 828 and 1657 respectively for the 0.051, 0.1 and 0.2 kg/s flow. The 360CH has 1250, 2452, 4904 Reynolds number respectively for the same flow from the 1080CH scenario. The 360CH result was firstly unexpected due to the lower complexity of the baffle, this simplicity was presumed to achieve a lower amount of eddy motion and a significant reduction in pressure drop, but actually the opposite occurred.

The 360 CH configuration can be seen in Figure 26. It must be remembered that the cold fluid flow starts from the right side of the heat exchanger (inlet – red velocity streamlines) to the left (outlet – blue and green velocity streamlines), where the velocity profile is shown. The profile depicts where the eddies start to be formed, especially in the first part of the baffle as soon as they reach the second quadrant. The higher velocity streamline at the beginning of the flow was expected due to the high flow versus the tube inlet size. As the helix path starts to be formed, it can be seen the fluid path flowing mostly from one side of the continuous baffle design. The highlighted squared area shows divergent fluid behaviour, which could be indicated by the “gap” contained in the baffle design. In the squared area, turbulence is strong and the continuous path can barely be seen. The following figures were taken with the highest cold fluid flow of 0.2 kg/s.

Figure 26 – Fluid velocity profile 360 CH

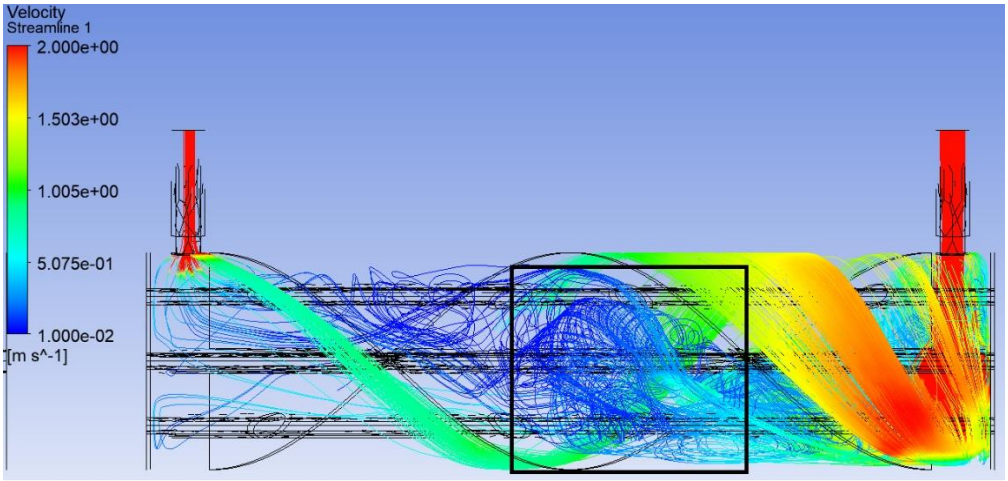

Source: Author (2022).

It is very intriguing to compare streamlines between 360CH, 1080 CH and SH configurations. It can be clear that in the 360CH the average velocity is much lower compared to 1080CH, but higher than SH configuration, this can be concluded by the pressure drop, since the outlet tubes do not change its geometry.

At first, velocity streamlines are clear at the beginning, but as fluid flows, turbulent effects can be seen. The vortex created inside the 360 CH is huge and most of the streamlines do not follow a straight pathway, leading to a higher pressure drop. As cold fluid starts to swirl, most of its energy is lost through the geometry at the beginning of the baffles. As it can be concluded, the counterflow starts to appear by the first 90º angle of the continuous baffle, it also can be seen that just a small part of the original flow with higher velocity is maintained and leaves the heat exchanger at the outlet. As helix pitch is huge, the triangle between baffle and tubes (triangular zone) is not well formed, but a higher velocity current can be seen in the light blue lines. Irregular dark blue lines display velocity decrease, turbulence and backflow phenomenon due to the pressure difference between upwind side and backwind side of the baffles.

In the 1080CH geometry, seen in Figure 27, the velocity field follow a different pattern of the 360CH configuration. The streamline has a more defined path, showing a constant value for velocity, which can be seen from its colour. Lines are clearer and velocity seems more constant compared to the first geometry, indicating a possible lower pumping loss. It can also be seen a circular flow pattern, which can be understood as a result of the higher helix angle, contributing to more baffle segments and also leading to a higher free flow area. On behalf of velocity, the lines shown a light blue colour, which on average, represent a higher velocity compared to the 360CH configuration. As the quantity of lines is the same for all geometries,

Flow is particularly different from what was seen in the 360CH design. At the intake, most of the cold fluid flow behaves exactly the same as the 360CH, due to the same inlet geometry. The effect can be seen as the abruptly change of flow direction (causing a higher average velocity at the inlet, the highest of the three configurations, 0.72m/s) which happens as it enters into the baffles. As fluid starts to follow the helix path, the velocity is drastically decreased and kept almost constant for the rest of the flow. The change in fluid velocity in addition to backflow in the helix region is important to achieve a higher heat transfer. The evidence seen in Figure 27 suggests that pressure drop

happened after the fluid reaches the first swirl of the helix. After that, most of flow seems almost laminar through the entirety of the heat exchanger.

Figure 27 – Fluid velocity profile 1080 CH

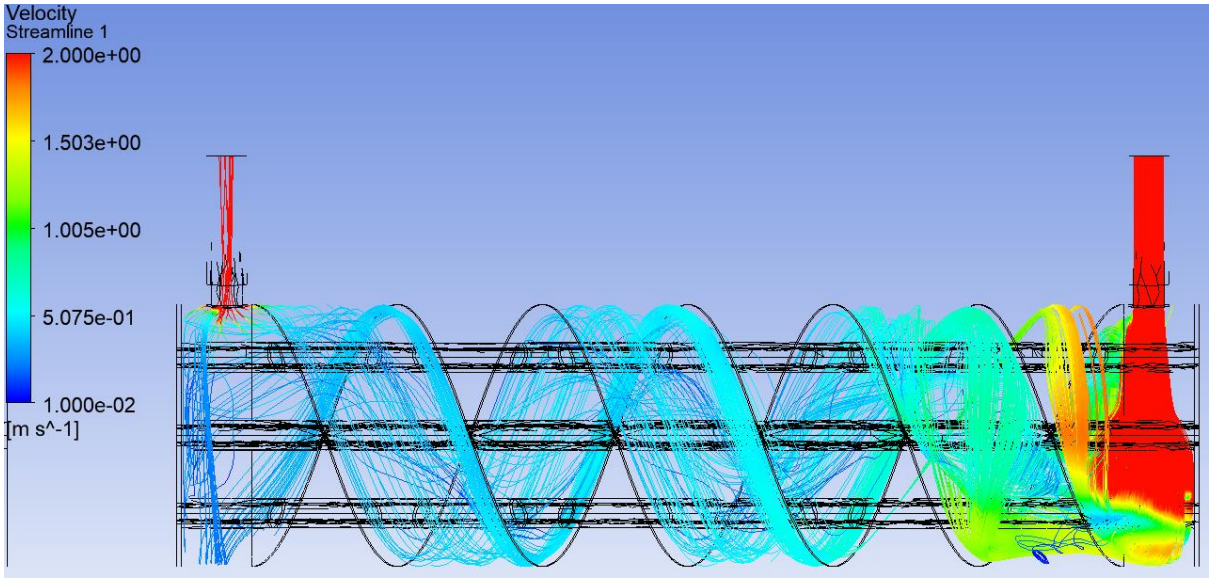

Source: Author (2022).

In SH configuration fluid flow behave is quite different, as can be seen in Figure 28. At the beginning, turbulence is high due to change in flow direction, following a similar pattern to what was seen at both continuous configurations, but for this scenario, the streamlines show a significant better flow distribution (can be seen from the smaller number of red lines, meaning less velocity loss). As flow starts to develop through the baffle design, velocity vectors are seen in most of the heat exchanger area, showing a better distributed flow through the entire heat exchanger. The overlap between baffles creates additional direction to the path, but on the other hand, it also leads to turbulence. Even though, fluid flow is smoother for the SH. The evidence suggests that this path was created also due to the increased number of baffles and an optimal overlap distance. Counter flow can also be seen, but do not play the majority of the flow, as can be understood from the lower pressure drop found at this scenario. The lowest pressure drop is explained by the better flow distribution mostly at the entrance, but also through the flow path. On the other hand, it should be noticed that the lowest velocity profile, which is, the average fluid velocity is the lowest in this scenario.

Figure 28 – Fluid velocity profile SH configuration

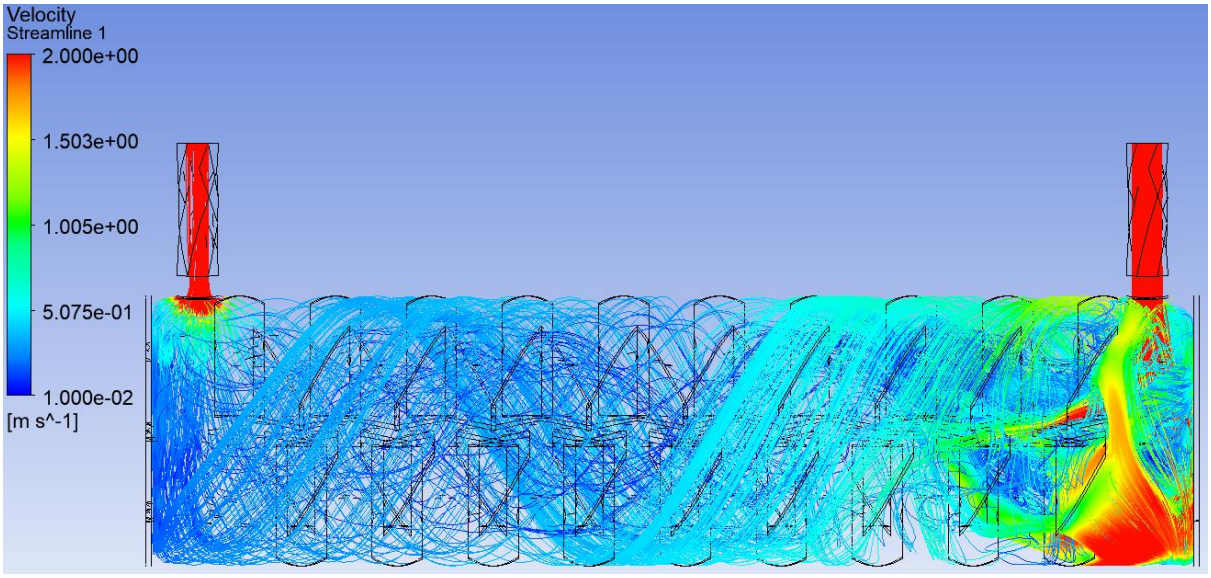

Source: Author (2022).

It is also convenient to point out that smaller helix angle (smaller than 40º) leads to a higher pressure drop. At a given volume flow rate, the pressure drop of larger helix angles is lower than that of small helix angles. The reason why this phenomenon happens is explained as follows. Small helix angle leads to a shorter helical pitch and a smaller free flow area at the shell centreline, which can be clearly observed in Figures 26-28. A larger helix angle creates a larger triangular zone, enhancing heat transfer in the area, but increasing pressure drop at the adjacent baffles. The leakage in the triangular zone will bring fluid to the next stage instead of flowing helically around, this creates turbulence and overall lower heat transfer coefficient. It can also be pointed out that no short-circuit flow was found in this study, probably due to no leakage CH geometry and the high number of baffles in the SH configuration.

The free flow area is another very important parameter which shows how well heat transfer occurs. The 360CH has a 0.08017m² free flow area, 1080CH responds for 0.09123m². The larger flow area came in the SH configuration, 0.10175m. The velocity vectors seen in Figures 29, 30 and 31 show fluid direction in a shell-side cross-section, Figure 29 and 30 were both taken by half of the heat exchanger, Figure 31 shows 5 sections of the flow in a contour-style figure. The sections were taken with a difference of 20mm each, from inlet to outlet.

Figure 29 depicts 360CH and 1080CH configuration. The flow from the 360CH did not develop equally between the two sides of the continuous helical path, causing the velocity vectors to be stronger at one side of the heat exchanger, while it can see a very low velocity at the other. An additional information is that no leakage can be found between baffles, indicating an assumption of a strict assembly, which was set on the geometry.

Figure 29 – 360CH and 1080CH velocity vectors in a cross-section view

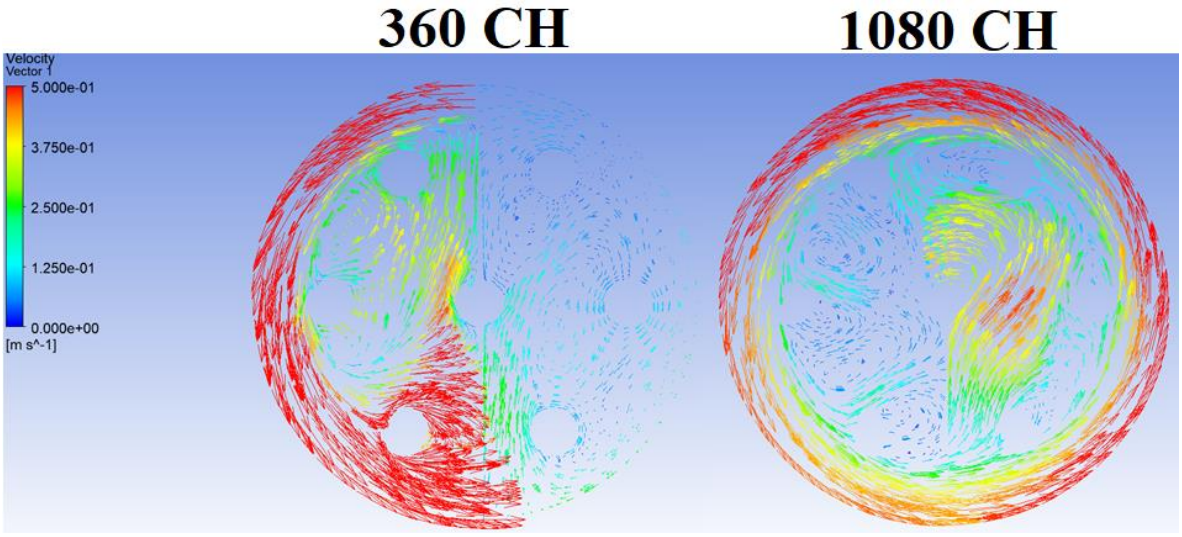

Source: Author (2022).

The 1080CH path is clear in addition to the eddy formation, especially next to the heat tubes. Fluid flow distribution is better in this case, but on the other hand, velocity vectors have a lower velocity compared to the first scenario, which can be translated as a lower Reynolds number, indicating a less turbulent regime. Figure 30 shows how well-developed fluid flow is in SH configuration. The velocity vectors are clearly distributed. The formation of eddies is much lower compared to the other cases, showing why this last heat exchanger design has performed better in pumping losses.

Figure 30 – SH velocity vectors in a cross-section view

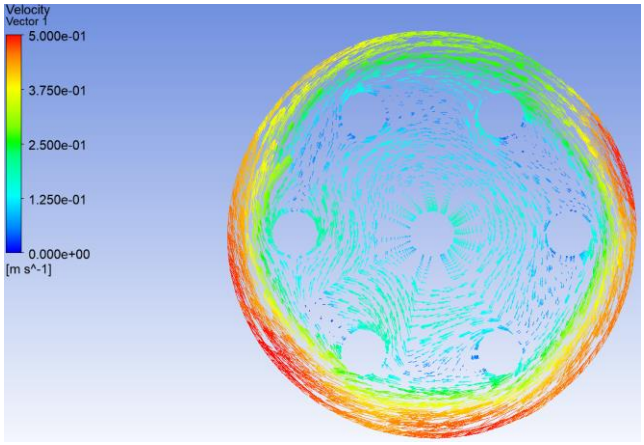

Source: Author (2022).

Figure 31 – Shell side velocity contours comparison in a cross-section view

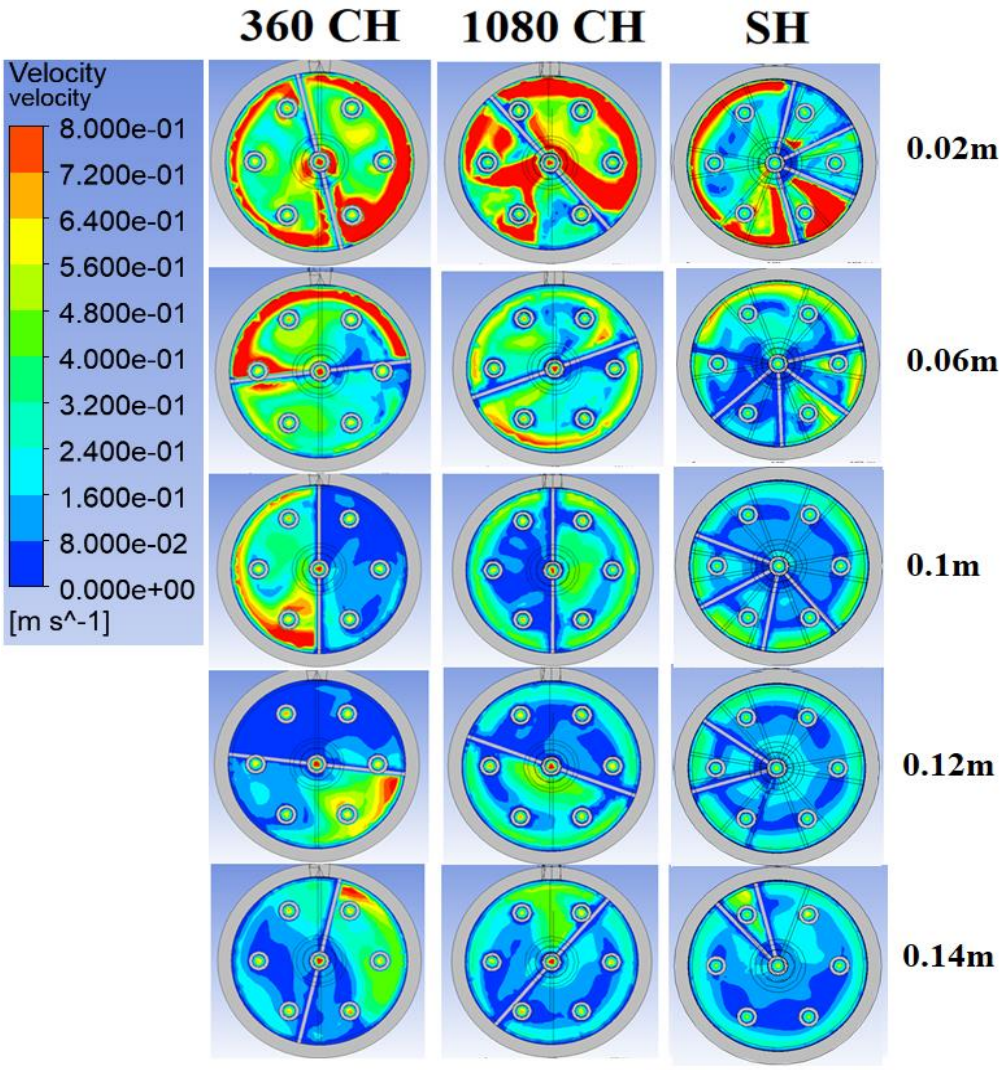

Source: Author (2022).

In Figure 31, it can be seen the velocity contours for the two different domains of the heat exchanger (cold and hot domain). The Inlet of all three configurations show a high velocity profile caused by the change of fluid direction and the start of the baffles. The fluid achieves a helix path at 0.06m distance. Evidence seen from figure shows a distorted velocity contour for the 360CH, where the variation is high. For the 1080CH, the distribution is better, showing a high velocity contour for almost the entire geometry. For the SH, most of the velocity is almost at the shell, probably a consequence of a larger free flow area near the shell due to the baffle geometry.

5.2 HEAT TRANSFER CHARACTERISTICS

Overall heat transfer coefficient, heat transfer rate, and temperature distribution are important heat exchanger parameters to achieve the objective of each different application. In this section, they will be extensively explained.

5.2.1 Data reduction

The heat transfer rate of the shell-side and tube-side can be determined as follows:

$$Q_{shell} = \dot{m}_{cold} C_{p,cold} \left(T_{cold,inlet} - T_{cold,outlet}\right) \quad (34)$$

$$Q_{tube} = \dot{m}_{hot} C_{p,hot} \left(T_{hot,inlet} - T_{hot,outlet}\right) \quad (35)$$

Where $\dot{m}$ denotes the mass flow rate in both conditions (shell and tubes). The shell-side heat transfer coefficient, total heat transfer area, can be seen as follows in Equations 36-40. The A_o is the heat exchanger area based on the outer diameter of the tubes multiplied by its number, in this case, 7.

The logarithmic mean temperature of the shell ΔT_{lm} can be determined by Equation 38, and because this is a counter-flow pattern with only a single shell, the correction factor for the logarithmic mean temperature difference is 1.

$$h_{shell} = \frac{Q_{shell}}{A_o \, \Delta T_{lm}} \tag{36}$$

$$A_o = n\pi d_0 l \tag{37}$$

$$\Delta T_{lm} = \frac{\Delta T_{max} - \Delta T_{min}}{\ln\left(\frac{\Delta t_{max}}{\Delta T_{min}}\right)} \tag{38}$$

$$\Delta T_{max} = T_{shell,in} - T_{wall} \tag{39}$$

$$\Delta T_{min} = T_{shell,out} - T_{wall} \tag{40}$$

Even though as the 360CH, 1080CH and SH configuration were all simulated in the same conditions and with high accuracy convergence history (1e-04), heat flux on the shell-side differs from the tube-side. The heat transfer rate from the tube side is slightly bigger than in the shell-side.

This seems to be a subtle deviation from the chosen turbulence model, as a result of the low y^+ and k and ε model. In this scenario, to get a higher accuracy simulation result, the heat transfer rate considered is from the tube-side, which have nanofluids. This consideration is particular to this simulation, since the outlet temperature is the most important parameter for this work.

Heat transfer from both sides will be calculated as described by Equation 30. Following Equation 31 heat transfer coefficient, and the conclusion taken by the CFX deviation, it can be concluded that both overall heat transfer coefficient and local heat transfer coefficient will be exactly the same for this simulation.

The following data will be described in different cases according Table 5 which can be seen below:

Table 5 – Parametric Data Inputs

	Cold fluid temperature (ºC)	Cold fluid flow rate (kg/s)	Hot fluid temperature (ºC)	Hot fluid flow rate (kg/s)
Input 1	25	0.051	60	0.5
Input 2	25	0.01	60	0.5
Input 3	25	0.2	60	0.5
Input 4	25	0.051	50	0.5
Input 5	25	0.01	50	0.5
Input 6	25	0.02	50	0.5
Input 7	25	0.051	40	0.5
Input 8	25	0.01	40	0.5
Input 9	25	0.02	40	0.5

Source: Author (2022).

5.2.2 Heat transfer rate

The following figures show a comparison between heat exchangers, nanofluids and volume flow, showing the heat transfer rate. The comparison between Figures 32, 33 and 34 show how heat transfer rate behaves with different nanofluids and different baffle configurations. Although the inner heat transfer area does not change, the difference comes mostly from the outside, shell area and baffle configuration, nanoparticles weight percentage made a significant difference which can be depicted in the figures.

Figure 32 – Heat Transfer Rate at 60^0C – graphene 0.0125% wt.

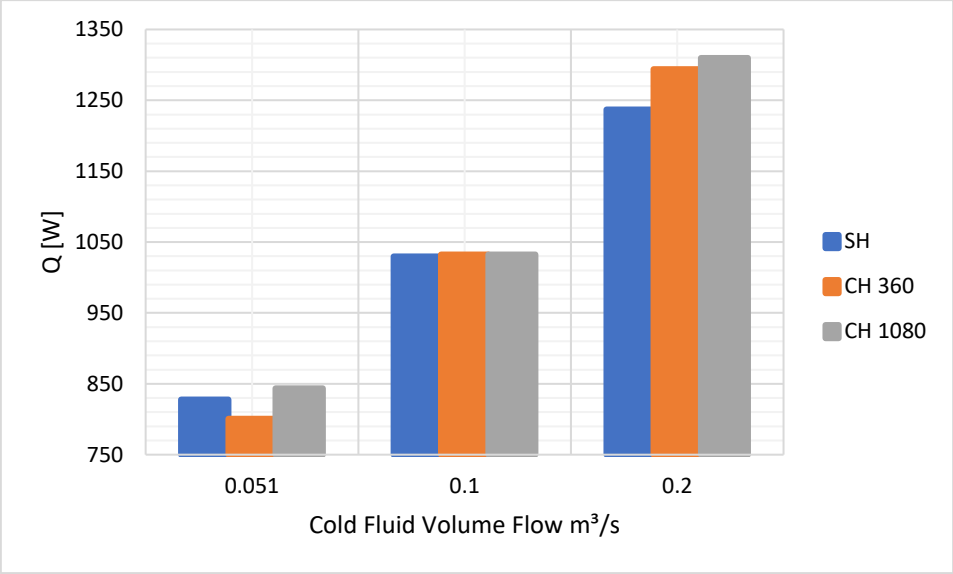

Source: Author (2022).

Figure 33 – Heat Transfer Rate at 60^0C - graphene 0.025% wt.

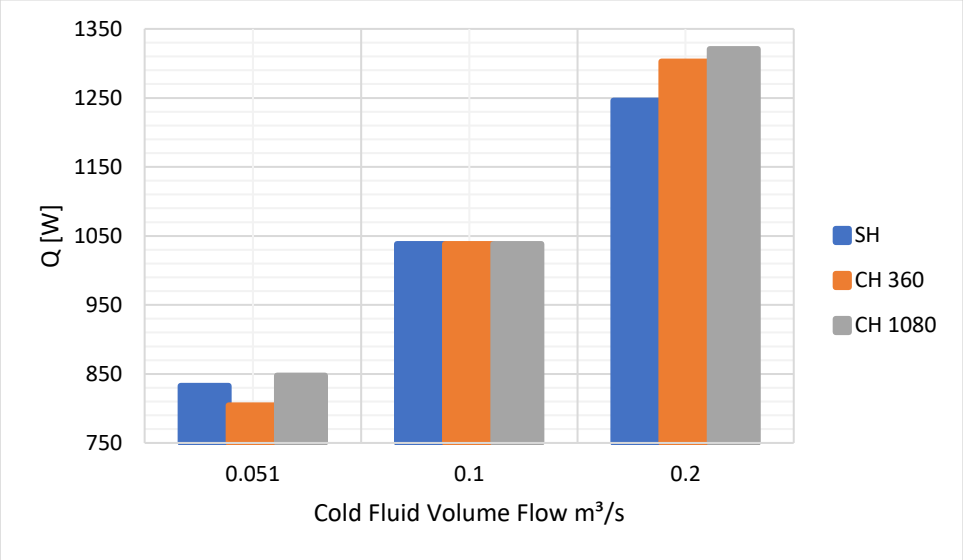

Source: Author (2022).

The 1080 CH configuration shows the highest heat transfer rate in any configuration. This scenario changes drastically when 360 CH and SH configurations are paired. The SH performs better in lower velocity cold fluid profiles, the claim is even more supported at Figure 32, running with a 0.05% wt. graphene as hot fluid.

Figure 34 –Heat Transfer Rate at 60^0C - graphene 0.05% wt.

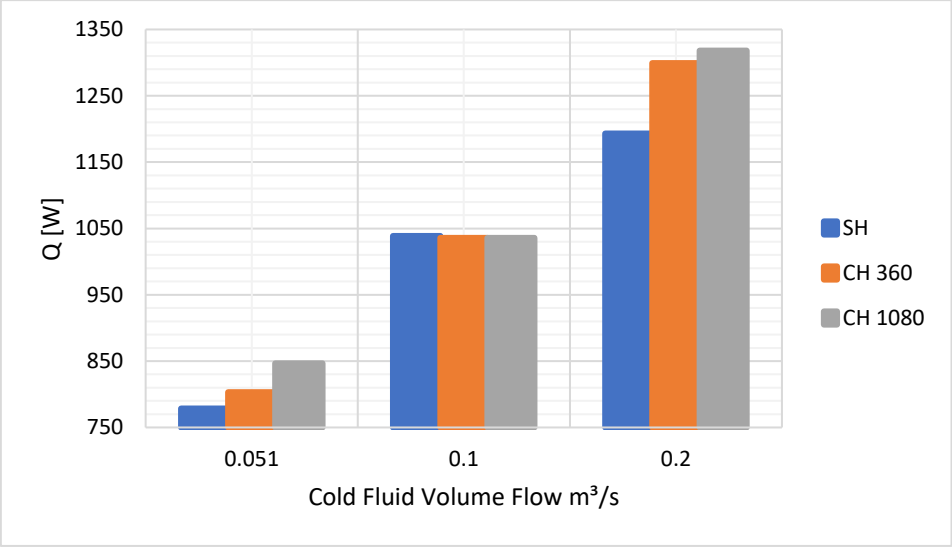

Source: Author (2022).

The highest heat transfer rate can be achieved in the 1080 CH configuration with the addition of a 0.025% wt. graphene nanofluid and running at a 0.2kg/s volume flow as shown in Figure 33. At the same volume flow, the worst scenario was found in the SH with 0.05% wt. graphene nanofluid, this shows a tipping point for graphene addition in the solution. It can also be noticed that at 0.1kg/s cold fluid flow, there is no significant difference between heat transfer rate in the three different designs, showing a possible limitation for the design since the heat transfer rate difference starts to become negligible.

Figure 35 – Heat Transfer Rate at 50^0C - graphene 0.025% wt.

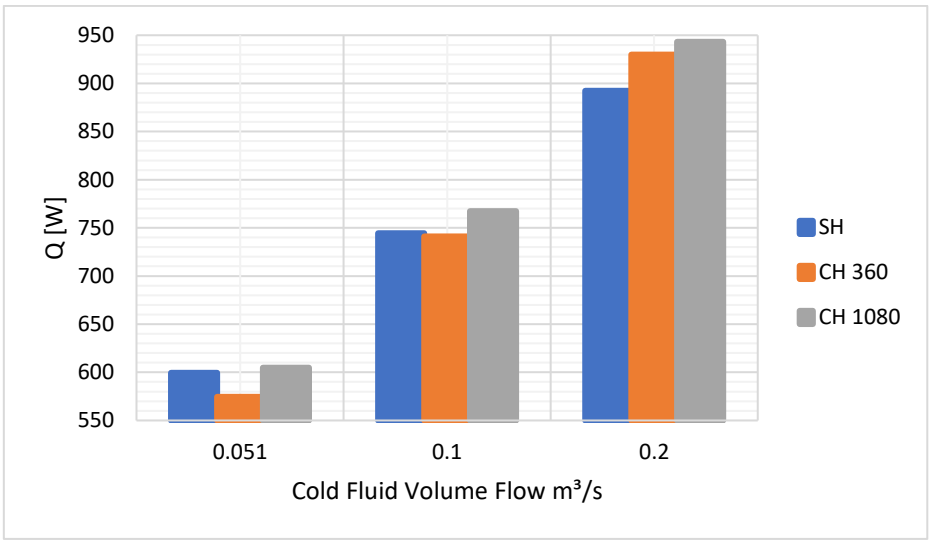

Source: Author (2022).

At lower temperatures (i.e., 50ºC and 40ºC) the small difference shown heat transfer rate at mid cold fluid flow, disappears and leaves place to a partly different behaviour. In Figure 35, it can be observed that the SH configuration performs better until it reaches mid-level cold fluid volume flow. On the other hand, CH 360 shows a very similar behaviour to the 1080CH at a more extreme volume flow. The SH configuration has shown an interesting performance at both lower cold fluid flow hot fluid's temperature. At 50ºC the SH is at its best performance, this is a very intriguing fact. It can lead to an optimized performance to determined applications at a very limited range of temperature and cold fluid flow.

Figure 36 – Heat Transfer Rate at 40^0C - graphene 0.025% wt.

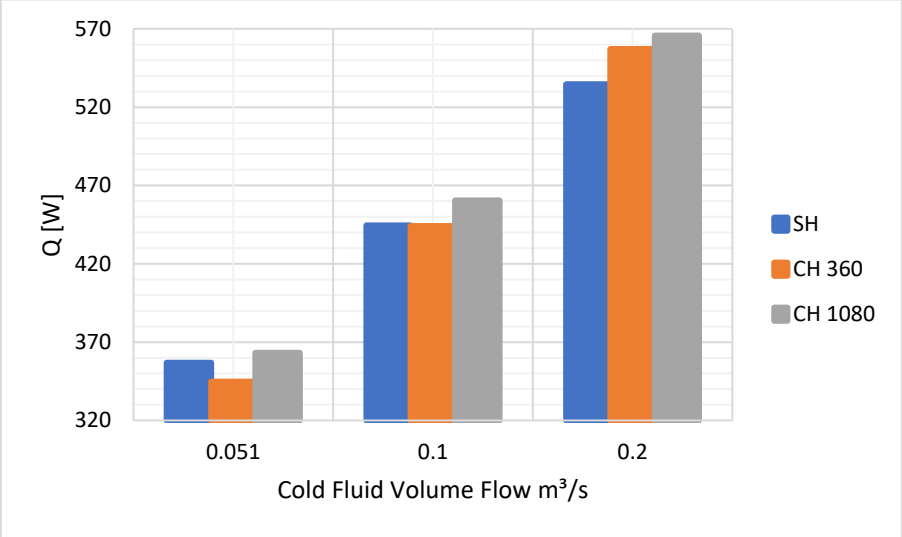

Source: Author (2022).

At 40ºC, all three different baffle configurations show the worst performance scenario due to the lowest temperature intake at the hot inlet. In terms of heat exchanger and nanofluid comparison, the patter does not change much. The pattern does not change much from a higher temperature scenario from what was seen at 50ºC and 60ºC.

5.2.3 Heat transfer coefficient, overall heat transfer coefficient and temperature distribution

Heat transfer coefficient is one of the most important parameters of a heat exchanger. It is crucial to evaluate performance requirements and shows how energy is being transferred in format of heat through tubes and shell.

Figure 37 depicts overall heat transfer coefficient for the Input 3. The results follow the same pattern shown in Figures 33-35. The best heat exchanger performance for this particular coefficient is the 1080CH configuration with 0.025%wt graphene nanofluid. The worst-case scenario is the SH with 0.05%wt graphene nanofluid. This confirms the findings from previous topics that the nanofluid at higher weight percentage than 0.025% does not contribute to achieve a higher overall heat transfer coefficient.

Figure 37 – Overall Heat Transfer coefficient – Input 3

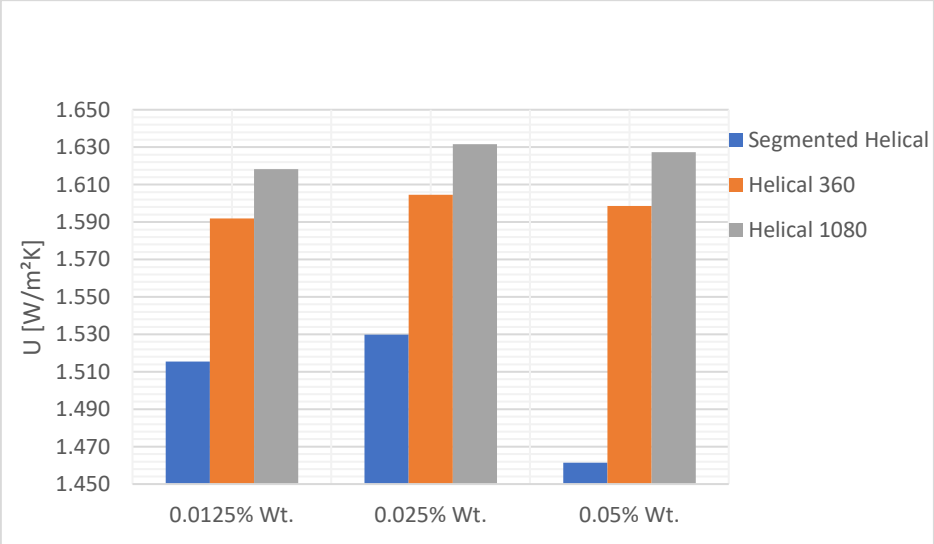

Source: Author (2022).

On the other hand, when only the heat transfer coefficient is seen, the heat exchanger with the highest coefficient is the 1080CH, as it was expected by the results seen above. But the individual behaviour of the heat transfer coefficient differs from the overall heat transfer coefficient. It can show the individual behaviour of the fluid flow

and how baffles can make a difference in flow properties and energy transfer, being discussed in the heat transfer coefficient section.

According to [32], for an amount of flow rate and temperature difference between the wall and the flow, the wall heat flux increases with the decrease of the intersection angle between velocity and temperature gradient. This can lead to drastic change in heat transfer coefficient, the Equation 40 show its dimensionless form, this is widely used as an alternative resource in addition to a higher Prandtl and Reynolds number, another two critical factors to achieve higher heat transfer coefficient.

$$N_u = R_e P_r \int_0^1 (\bar{U} \nabla\bar{T}) d\bar{y} \tag{40}$$

$$\bar{U} \nabla\bar{T} = \overline{|U|} |\nabla\bar{T}| \cos\theta_T \tag{41}$$

The intersection angle measured by Equation 40 and 41 when reduced, will increase heat transfer coefficient, being at its maximum rate at a cross-flow situation, when the intersection angle is equal to zero. A similarity to this situation is one of the goals of the geometries presented in this work, for instance, the 360CH configuration has a low helix angle, which leads to a smaller intersection angle, resulting in a higher heat transfer coefficient, which can be confirmed in Figure 38.

It is clear the intersection angle is one more parameter to explain heat transfer coefficient, but it does not respond for everything. From Figure 38, it can be seen a huge difference in heat transfer coefficient caused by the continuous helical design, allowing a much higher value, it also shows that adding baffles also causes a higher coefficient, which is the 1080CH case.

The heat transfer coefficient from Input 3 confirms what [32] presented about the intersection angle, but at the same time, the heat transfer coefficient only from the shell side is not enough to guarantee a better performance in the heat exchanger.

Figure 38 – Heat Transfer coefficient (Shell side) – Input 3

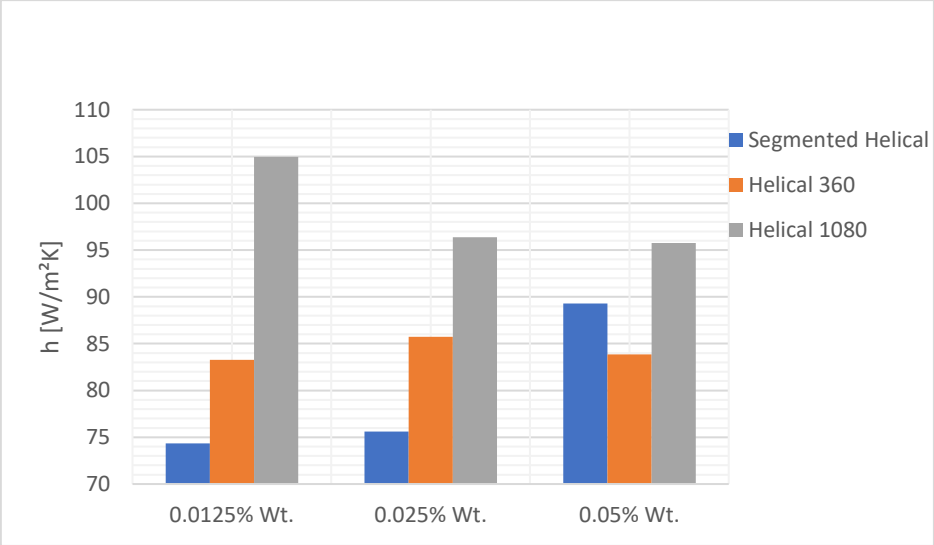

Source: Author (2022).

Although the 1080CH shows a better performance for any input inserted in this setup, the SH shows a significant advantage for some particular applications, such as lower hot fluid's temperature and cold fluid flow. In Figure 39, the overall heat transfer coefficient for the SH performs better than both 1080CH and 360CH for any working fluid. The tipping point which was evidenced in previous sections of this work is at 0.205% wt. graphene

It is clear now that the concentration and the working fluid's temperature is very sensitive to this heat transfer design. Inputs 2 and 3 follow the same pattern from Input 1. The SH configuration starts to have a much lower overall heat transfer coefficient as cold fluid flow is increased; the results can be seen in the Appendix.

Input 5 shows the tipping point where SH configuration has an advantage over 360CH. It must be remembered that this is at 0.1kg/s flow at 50ºC temperature, indicating a different behaviour at lower temperatures for this specific geometry, this can be an advantage for specific heat exchanger applications. Following the same temperature pattern, Inputs 4 and 6 behaves quite differently. What can be seen from the coefficient behaviour is that at higher fluid flow, 1080CH and 360CH have the highest coefficient respectively.

Figure 39 – Overall Heat Transfer coefficient – Input 5

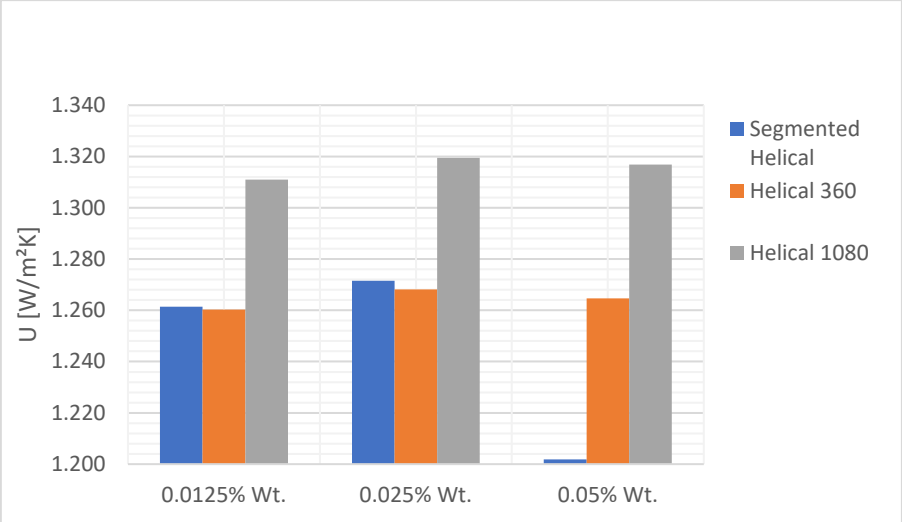

Source: Author (2022).

For the heat transfer coefficient, input 5 shows a similar behaviour from what was seen from Input 3, being only different at higher nanofluid concentration. The 1080CH continues to have the highest heat transfer coefficient (from a shell side perspective), the 360CH configuration performed slightly better with nanofluid at 0.0125% wt. At higher nanofluid concentration, the SH baffle design shows very similar pattern to what can be seen at higher hot fluid's temperature (Inputs 1-3).

Figure 40 – Heat Transfer coefficient (shell side) – Input 5

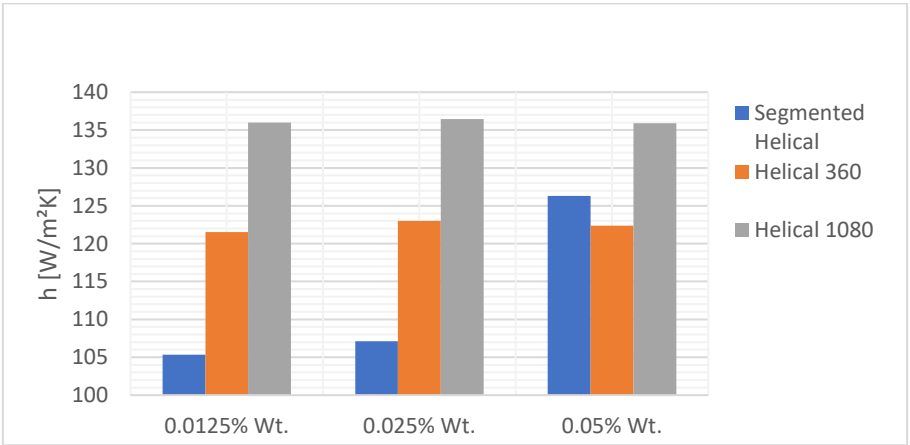

Source: Author (2022).

Moreover, when hot fluid temperature drops significantly, the SH heat exchanger shows a considerable advantage compared to both 1080CH and 360CH configurations.

Figure 40 correlates a higher thermal efficiency heat exchanger to a lower temperature hot fluid flow and lower cold fluid flow. The result is also very clear from the heat transfer coefficient perspective. The findings also pointed for an advantage for the SH for higher nanofluid concentration. Both 1080CH and 360CH followed the same pattern for nanofluid concentration at this lower temperature (50ºC).

Figure 41 – Overall Heat Transfer coefficient – Input 7

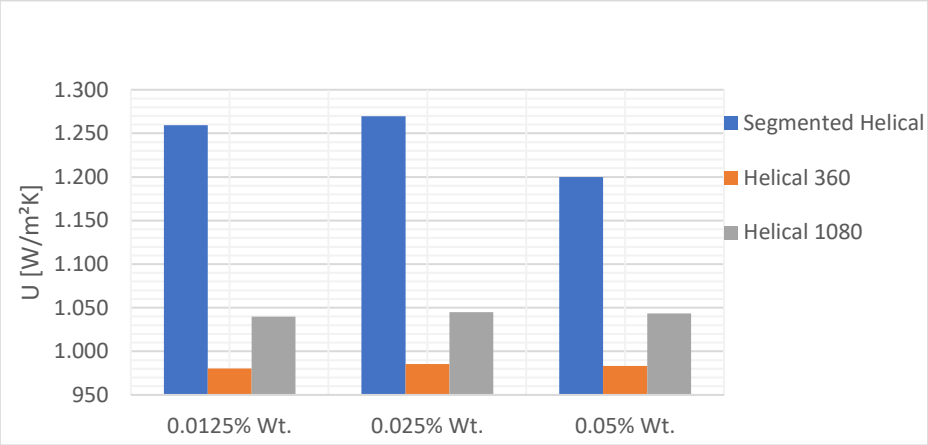

Source: Author (2022).

From Figure 41, it is important to mention that the 360CH has shown a poor performance in the overall heat transfer coefficient for a lower hot fluid's temperature (40ºC), from a point of view of the shell side, the heat transfer coefficient also keeps the lowest at this configuration, showing a particularly different result for higher hot fluid's temperature. It must be mentioned that at lower temperatures the difference in heat transfer coefficient starts to become almost uniform.

Figure 42 –Heat Transfer coefficient (shell side) – Input 7

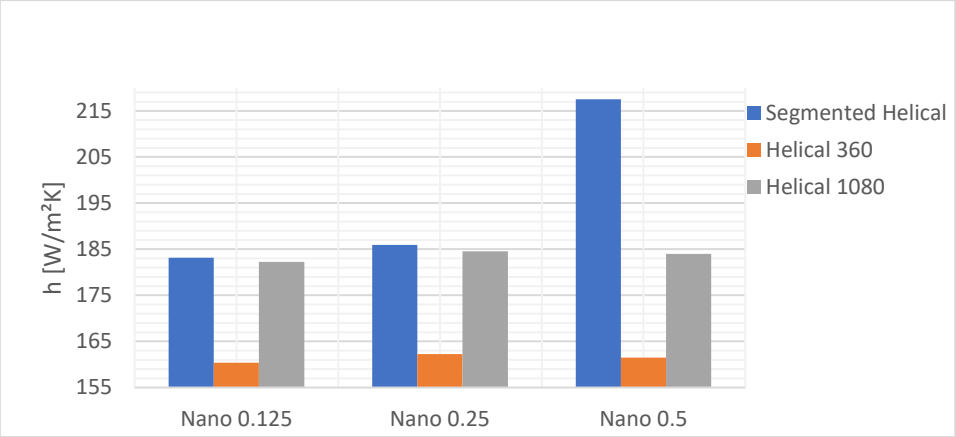

Source: Author (2022).

For Figure 42, it can be seen a particular value for the heat transfer coefficient for the higher concentration nanofluid. This result is interpreted as a probable numerical error, since the comparative results do not show this profile.

When it comes to temperature distribution, an analysis for each different input and nanofluid will show us a different temperature gradient. This is one of the most important outputs for each heat exchanger, since it is the main objective of the equipment. Figure 43 explains how temperature gradient behaves in both tubes and shell.

Figure 43 – Temperature distribution for 0.0125% wt. nanofluid for Input 3

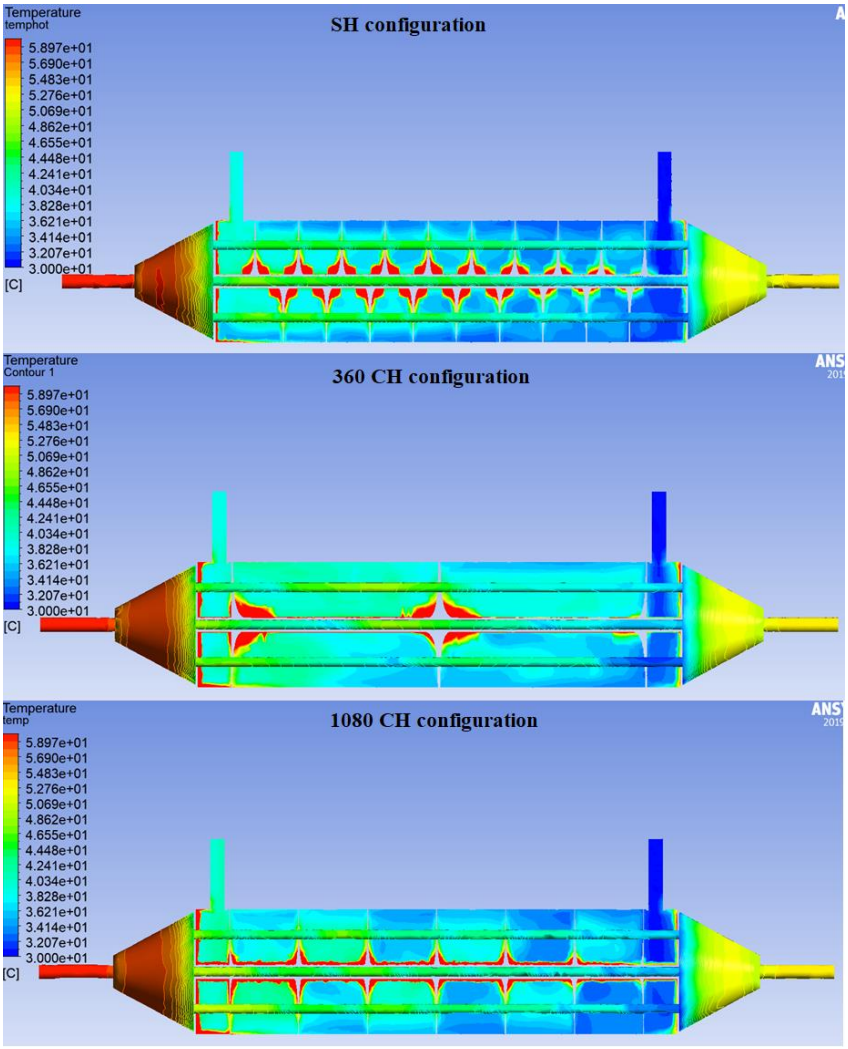

Source: Author (2022).

The Image was taken independently and then joined together to show each part's behaviour. The temperature gradient is very clear. In the SH configuration the high number of baffles creates an environment with reduced dead-zones, in other words, the turbulence created by the overlapping, high number of baffles, and aggressive helix angle (lower compared to the others) distributed the flow, causing the gradient to appear linearly. A similarity to cross-flow can be noticed for this configuration. Although the results seem interesting, it can still be seen "red regions", showing a possibility for improvement.

For the 360CH, there are two major dead-zones: at the half and at the end of the baffle. This happens by poor fluid distribution, causing a lower performance in this

region. For the 1080CH, although the fluid distribution at the beginning of the heat exchanger did not happen uniformly (which is seen by the “green spots” happening in an alternate pattern, evidencing that one side of the baffle have most of the flow) the dead-zones are small. Particularly in the 360CH the thermal gradient follows a very similar path to what was seen in the velocity vectors cold fluid behaviour. In all three configurations, a higher temperature gradient can be seen near the baffles. This was expected due to its greater surface, working similarly as a fin in addition to the dead-zones caused by the lack of fluid flow distribution.

Although is difficult to see for this temperature scale, which the outlet temperatures are similar, the 1080CH the exit cold flow has a subtle greener colour compared to the other configurations, meaning it has absorbed more heat and for this reason, the fluid has a higher temperature. For hot outlet, there cannot be seen a significant temperature difference, since the values are also similar, on the other hand, for the understanding of how temperature changed and how heat was transferred through the heat exchanger and its baffles, the figure shows the evidence needed to draw conclusions. To depict the difference from temperature inlet to outlet, which is one of the most important outputs from the entire analysis, Figures 44-46 shows every input correlation to each studied nanofluid for all three different baffle configurations.

Figure 44 - 0.0125% wt. Nanofluid Temperature Difference

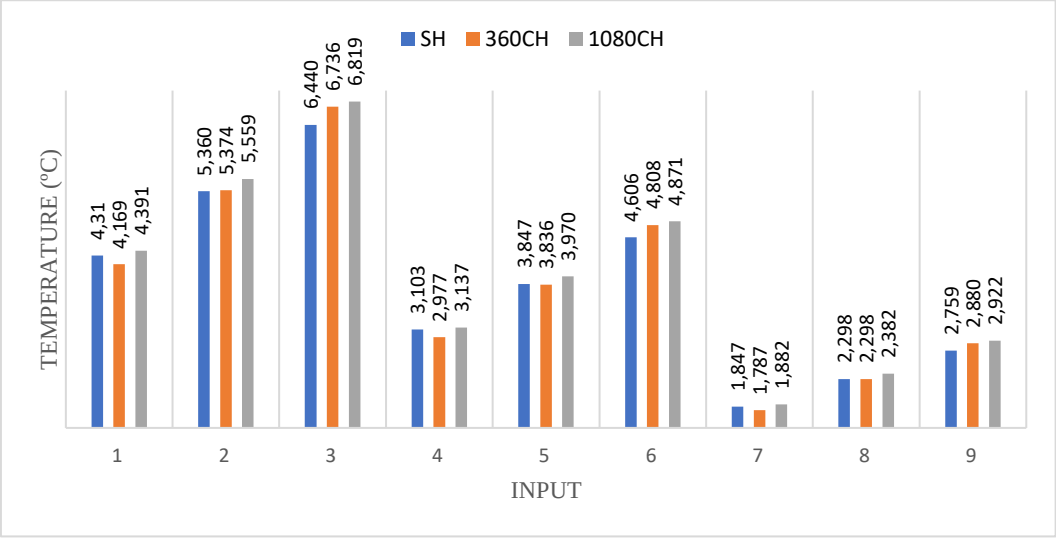

Source: Author (2022).

From figure 44, the 1080CH shows the highest temperature difference for all cases, having the highest thermal efficiency. It must be remembered that this outlet temperature is taken as an average of the hot fluid outlet, the difference from the average outlet temperature from the inlet temperature, both in hot domains is what the figure shows.

Figure 45 - 0.025% wt. Nanofluid Temperature Difference

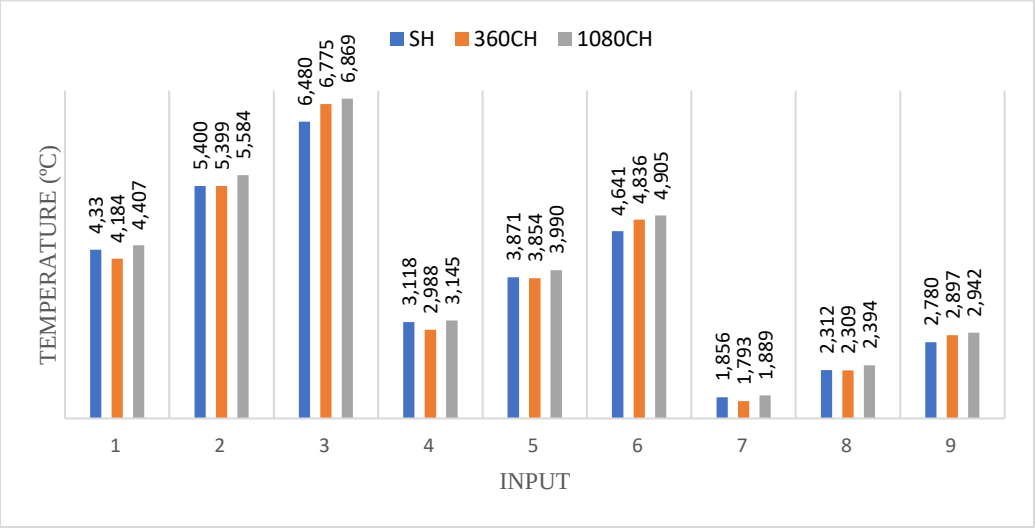

Source: Author (2022).

From Figure 45 the same result pattern from the 0.0125% wt. was achieved. Temperature difference is higher for Inputs 3, 6 and 9, which have the highest fluid flow. For the 0.025% wt. nanofluid, there is a subtle difference in temperature outlet values from the 0.0125% wt. showing a small advantage for this higher concentration. For the last nanofluid simulation, the 0.05% wt. is shown in Figure 46. In general, the results are slightly lower than what was seen for the 0.025% wt., but this is amplified for inputs 7, 8 and 9, where the higher nanofluid concentration shows the worst performance.

Figure 46 - 0.05% wt. Nanofluid Temperature Difference

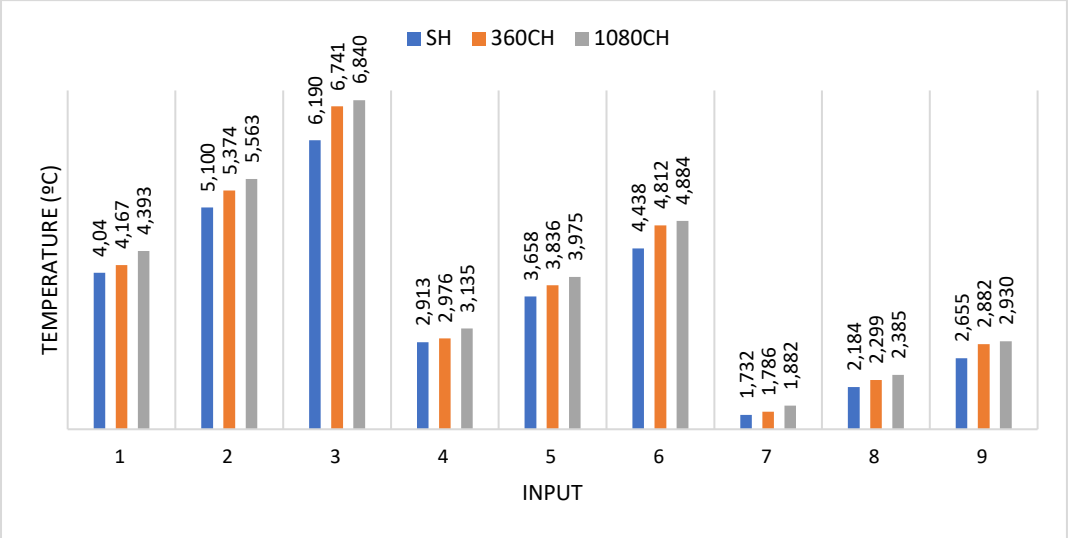

Source: Author (2022).

For general results, it is seen that most of the temperature difference is caused by the baffle configuration and the cold fluid flow, being the major factor of influence for hot outlet temperature.

5.2.4 Global thermal-hydraulic efficiency

As it was depicted explained in the last section, heat transfer coefficient is crucial to determine heat exchanger characteristics and performance. Whereas its importance, alone the coefficient does not show the complete thermo-hydraulic analysis in the heat exchanger.

The pressure drop also responds for global efficiency, being a very important part in the operation of the heat exchanger. The pressure drop can increase operating costs, making the decision to choose for a configuration reasonable or not. For the complete analysis, both overall heat transfer coefficient and pressure drop were related in a ratio for different scenarios represented by Inputs 1 to 9.

Figure 47 –Heat transfer rate per unit pressure drop versus volume flow rate at 60ºC

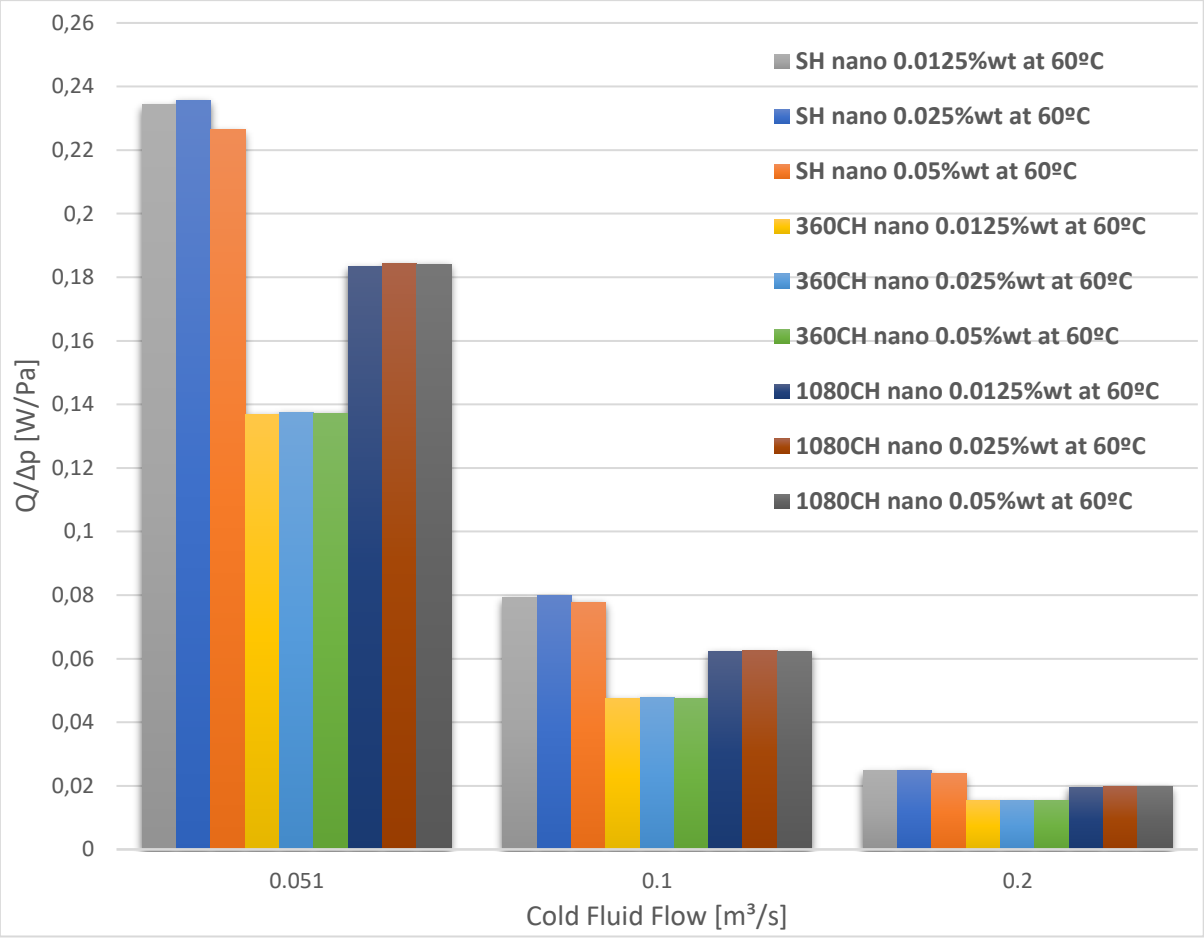

Source: Author (2022).

From Figure 47, the ratio between Q/Δp explains the relation of heat transfer rate and pressure drop. From the left to the right, the cold fluid flow is augmented to explain behaviour in different environment. It can be understood that heat exchangers with the lowest helix angles (around 40º helix angle) have the highest heat transfer rate per unit pressure drop for higher temperatures, confirming the previous findings from many authors discussed in the literature review, that nanofluids performs better at higher temperatures when acting as working fluid. It is also understandable that at higher flows, the ratio turns smaller, meaning the pressure drop is significantly dominant over the heat transfer rate. On the other hand, Figure 48 shows the ratio between heat transfer coefficient and pressure drop.

The ration shown in Figure 48 can be understood as the convective heat transfer behaviour, which increases with nanofluid concentration, and baffle design. It is clear that

the SH configuration has the best results for any nanofluid. The results is also converging with heat transfer rate, showing the pressure drop effect as dominant over heat transfer. The best scenario is seen with the 0.05% wt. nanofluid. This could be inferred as the highest thermal conductivity is achieved for this fluid. Both continuous helical geometries (1080CH and 360CH) had almost no difference for any working fluid; the worst performance was achieved by the 360CH followed by the 1080CH.

Figure 48 –Heat transfer coefficient per unit pressure drop versus volume flow rate at 60ºC

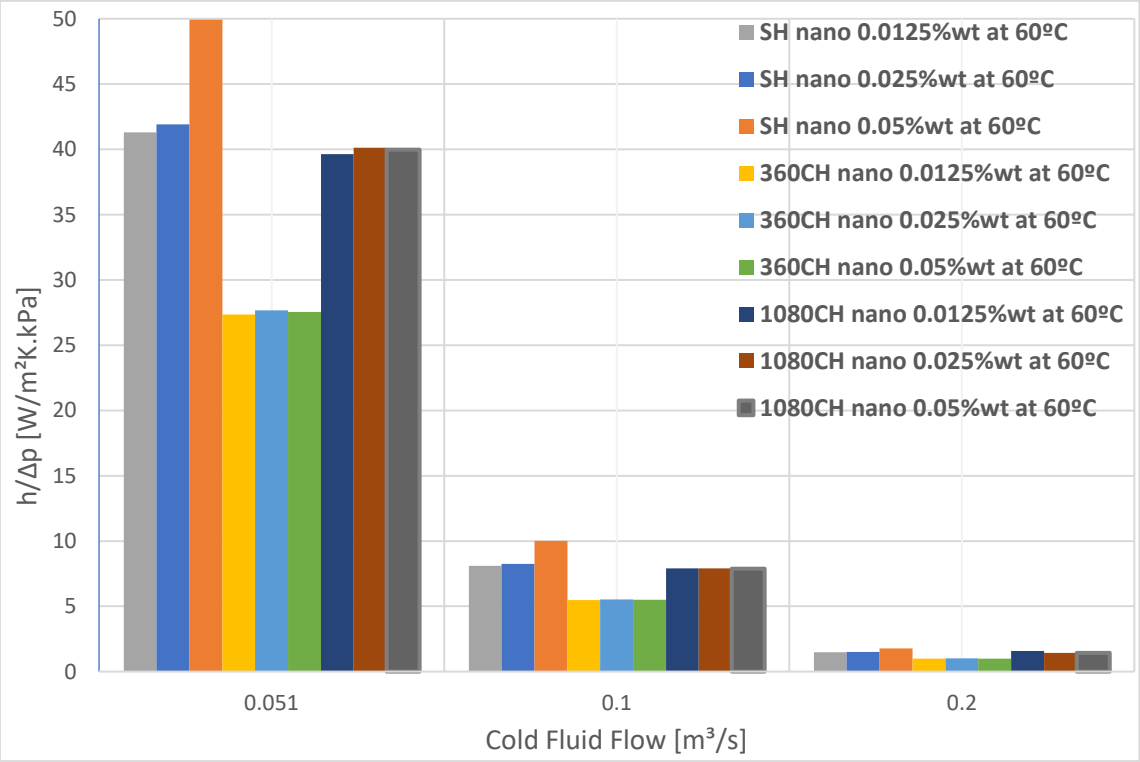

Source: Author (2022).

It is significant the difference that is created by the SH configuration, from both ratios explained in Figures 47 and 48, it is clear the higher efficiency. On the other hand, the continuous configurations have shown a lower performance at lower cold fluid flow. The 360CH has the worst performance as it was expected from fluid flow analysis. The 1080CH stayed close to the SH, but only for some configurations, for a higher nanofluid concentration, the SH has shown a better result. What can be observed from the analysis

is that all three different configurations shown almost the same result at a higher fluid flow, converging to a standard.

At 50ºC temperature (Inputs 4-6), the scenario does not change. The SH configuration keeps showing a very close performance to the 1080CH for almost all nanofluids and cold fluid flow, as can be seen in Figure 49.

Figure 49 – Heat transfer rate per unit pressure drop versus volume flow rate at 50ºC

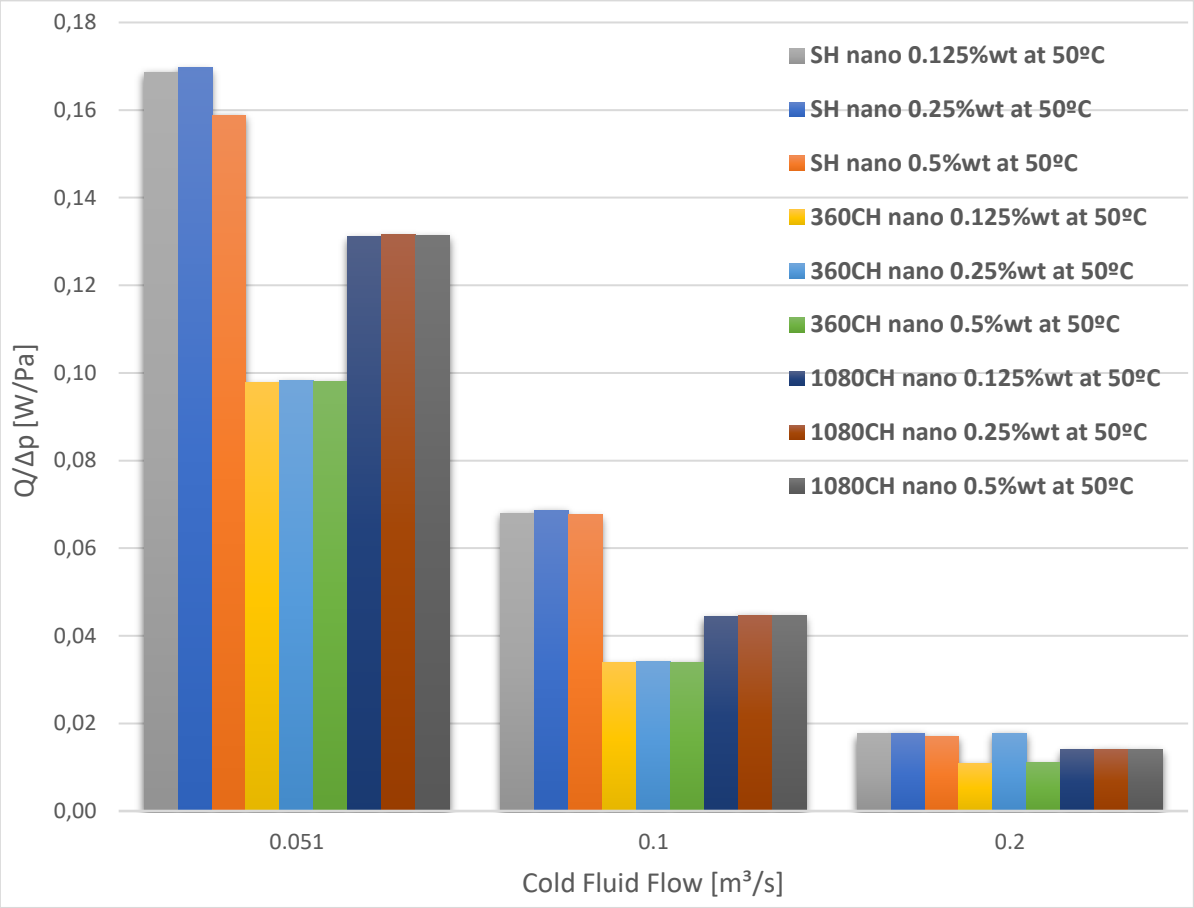

Source: Author.

For the 360CH the lower performance keeps the same for a lower input temperature. For the heat transfer rate per pressure drop, the SH keeps being the best option for any nanofluid, but for this time, as the hot inlet temperature dropped from 60º to 50º, the ratio is smaller than what was presented in Figure 47. The performance of all three configurations starts to stagnate and cannot be significantly different when the cold fluid flow starts to become higher, showing a very similar behaviour compared to Inputs 1-3. From what can be predicted, the curve for both continuous designs are showing a

lower performance ratio for lower fluid flow, while the tendency for SH is to stagnate performance when the flow increases.

In Figure 50, the scenario described for the overall heat transfer coefficient follows the same for the heat transfer coefficient per pressure drop ratio. From a fluid flow point of view, Figure 50 tells us the 1080CH configuration behaves nearly the SH at lower hot fluid temperature and lower cold fluid flow. At higher cold fluid flow, the path is almost the same, but with a tendency to a lower performance. With this finding, a pattern can be understood for heat transfer and overall heat transfer ratio with pressure drop. At 0.2 kg/s performance variations are negligible. Another important observation is to the ratio final value, it does not change much even at a lower inlet temperature (50ºC). In the next figures, the scenario of lower temperature will be depicted and if a pattern is achieved it is to be known.

Figure 50 – Heat transfer coefficient per unit pressure drop versus volume flow rate at 50ºC

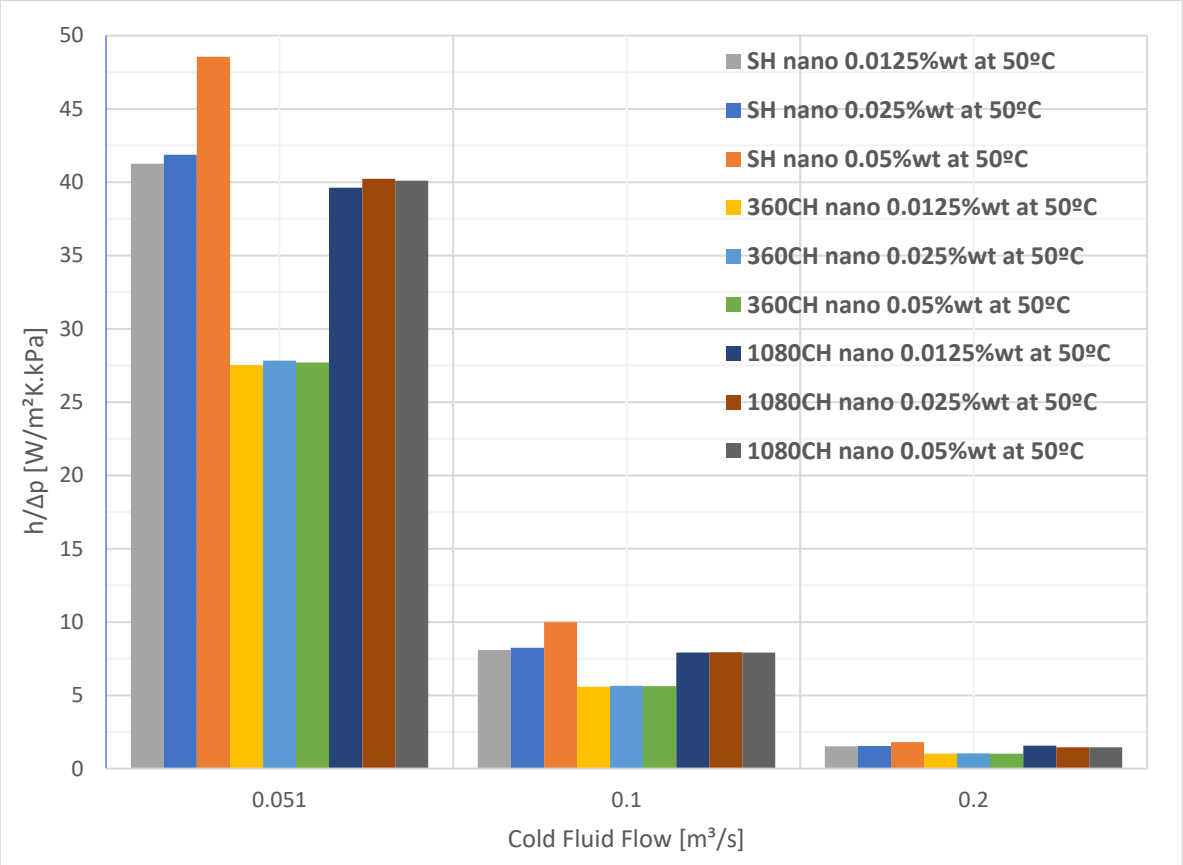

Source: Author (2022).

Figures 51 and 52 illustrates the last inputs comparison (Inputs 7-9). The difference between heat exchangers at this low inlet hot temperature makes a really difference to the heat exchanger performance. It is clear that the SH performs better than any other heat exchanger, specially at lower cold fluid flow, where the difference really takes place. As it was observed for higher inlet temperature Inputs, the ratio is significantly small due to the lower temperature and consequently smaller heat transfer rate. The most significant difference is SH's performance at 0.051 kg/s, indicating the advantage for the geometry at lower temperatures and lower cold fluid flow.

Figure 51 –Heat transfer rate per unit pressure drop versus volume flow rate at 40ºC

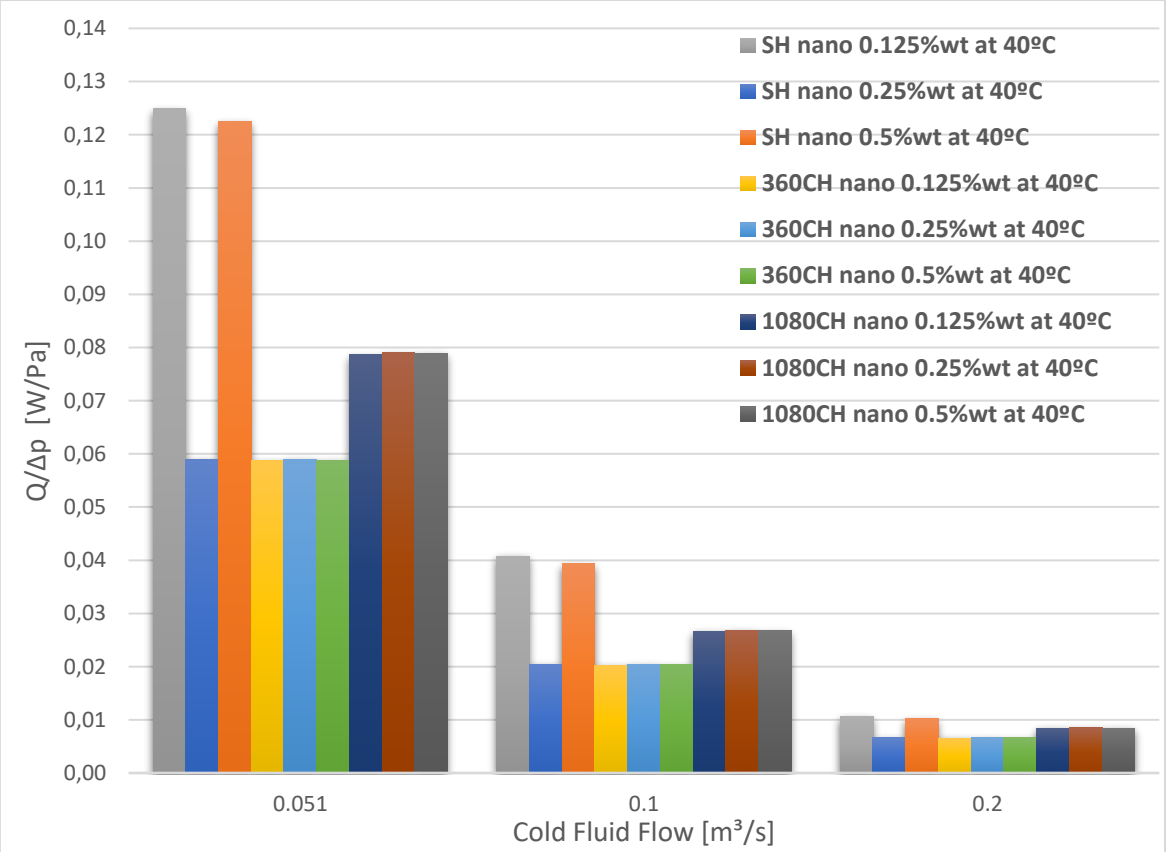

Source: Author (2022).

For the 0.025% wt. nanofluid, an unusual result has shown for this temperature. It can both indicate a propagated error from the simulation or a tipping point which only the 0.0125% wt. and 0.05% wt. are worth for lower input temperatures, but from the previous results, it must be interpreted as a propagated error. For higher values in fluid flow, there is still an advantage for the SH geometry at 0.1 kg/s, but for the highest fluid

flow, there can be seen almost no significant difference in performance for any heat exchanger, exacerbating the limitation shown in the last figures.

Figure 52 – Heat transfer rate per unit pressure drop versus volume flow rate at 40ºC

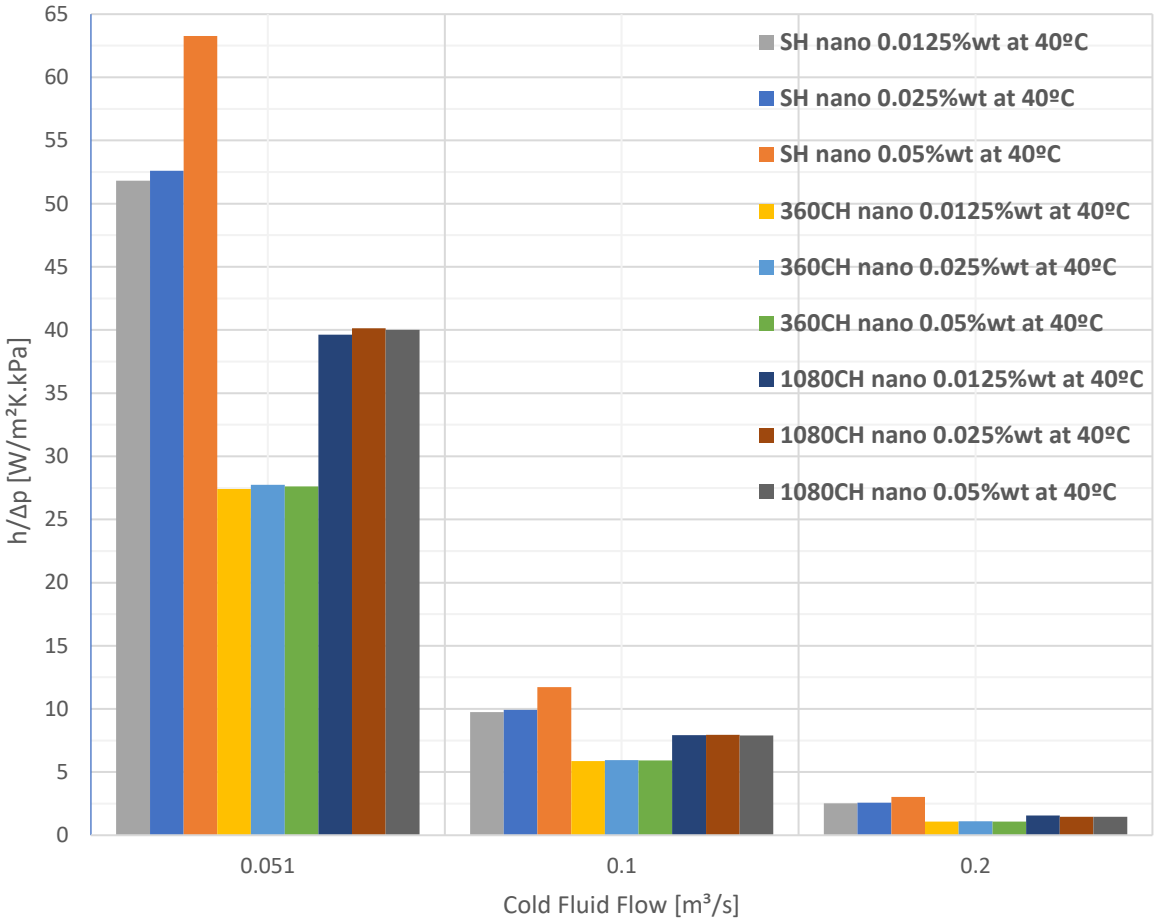

Source: Author (2022).

For the continuous helical configurations, both 360CH and 1080CH performed poorly until cold fluid flow reaches a higher level, which can be seen almost no difference from nanofluid inputs. It must be remembered that this ratio allows to understand both heat transfer characteristics and fluid flow losses, being a crucial point to heat exchanger design and financial suitability.

A clear finding which is clear in all configurations is that at highest fluid flow, there is no significant difference in thermohydraulic efficiency for any of the heat exchangers explored in this study.

This can be understood as a limitation to the cold fluid flow in this geometry, since it cannot absorb more without the side-effect of higher pressure drop. As can also be noticed, the pressure drop does not change between nanofluid switching, since they are only allocated in the heat pipes, the only difference is geometrical. This was noticed in all input comparison, especially in the heat transfer coefficient per pressure drop ratio, which demonstrated a thermo-hydraulic analysis from the cask of the heat exchanger.

For the heat transfer coefficient per unit pressure drop ratio, the advantage for the SH follows the same path, but for this scenario, the ratio is the biggest from all inputs. This can be understood as a better performance of the nanofluids for the lower temperature input.

6 CONCLUSION

In this work, shell and tube heat exchangers with different helix baffles were simulated though ANSYS CFX software for heat transfer and flow characteristics in a parametric analysis with a variety of graphene nanofluids. A comparison of geometry complexity, baffle characteristics, heat transfer, fluid flow, nanofluid influence and performance were made to investigate the outcome of nine simulation. The investigation aimed to understand the association of baffle geometry and nanofluids in the overall performance of a shell and tube heat exchanger with helical baffles. Three different geometries were created in Solidworks CAD software, each one with a different baffle profile: 360º Continuous Helical, 1080º Continuous Helical and Segmented Helical. Three different graphene based nanofluids were used as hot fluid: 0.0125% wt. graphene, 0.025% wt. graphene and 0.05% wt. graphene. The conclusions are as follows:

For the pressure drop, the SH heat exchanger configuration has shown the least pressure drop even at higher volume flows. The 1080CH comes after and for the last the 360CH. The shell side pressure drop is significantly reduced when baffle helix angle is also small. The SH configuration has shown the smallest helix angle, the 360CH the second smaller and the last the 1080CH. The findings shown in flow analysis explain that not only the helix angle has an influence, but also fluid flow distribution inside the shell. From the velocity vectors, it can be seen that eddy motion is presented for both all three baffle designs. These findings suggests that the number of baffles are crucial to flow guidance and to reduce dead-zones. The baffles have also an effect on reflux and fluid distribution, which was mostly seen in the 360CH configuration, which flow was not well distributed, causing a significant amount of pressure drop without the benefit of higher heat transfer. From this perspective, it can be concluded that the best configuration to reduce friction between fluid and surface is the SH. For heat transfer rate, results have shown the superiority of the 1080CH configuration for almost any input, which translated in a lower hot fluid's outlet temperature. The outlet temperature was observed and the evidence confirms that the best heat exchanger configuration to achieve the lowest hot fluid's outlet temperature is the 1080CH. The SH configuration has shown advantages when temperature and flow is lower, being better than the 360CH but not outperforming the 1080CH. In a perspective of overall heat transfer, it can be concluded that the best-

case scenario is achieve at 1080CH configuration running a 0.025% wt. graphene nanofluid. This finding also confirmed what was concluded from the previous chapters: 0.025% wt. nanofluid is the tipping point for heat transfer performance for the geometries studied in this paper. The highest heat transfer coefficient is achieved at higher fluid flow, which is 0.2 kg/s. At this rate, the Reynolds number shows a mixed scenario depending on the baffle configuration: for the SH and 360CH there is turbulence, for the 1080CH the flow is laminar and the highest heat transfer coefficient is explained by the best achieved fluid flow. The highest heat transfer for Inputs 1-3, was achieved by the 0.0125% wt. nanofluid. All inputs for higher inlet temperature show the same behaviour, with the 1080CH being the highest heat transfer coefficient, followed by the 360CH and for the last the SH. For the temperature distribution, a slightly difference is seen for the 1080CH, but what really can be seen is the reduced dead zones caused by 1080CH and SH baffle geometries. For the ratio between fluidic and thermal properties, the 60ºC degree input for the SH configuration has shown the best ratio both for the heat transfer rate and for the heat transfer coefficient. Smaller helix angle from the SH helps to lower friction between wall and fluid. In addition to that, the lower fluid flow has shown the best performance results, as it was expected due to lower turbulence, resulting in less friction between fluid and internal tubes, but on the other hand, consequently it causes a lower heat transfer. For 50ºC inputs, the behaviour of the SH configuration follows the same path from the 60ºC input. For 40ºC inputs, the SH baffle configuration performance is superior than any other configuration. The difference occurs in both ratios, confirming the best scenario for the configuration. The 360CH has the worst performance of all three configurations for any input. From a thermodynamic point of view, there is no concrete advantage to choose for the 360CH, unless it can be more viable for fabrication or other limitation which is beyond this presented work. The SH has shown a very interesting behaviour for all inputs, but at the same time if the main goal is to achieve a higher thermal exchange, the best choice is the 1080CH, on the other hand, the SH configuration is the best choice for a good thermal exchange and considerably lower pumping costs. The nanofluids presented in this work has shown subtle advantages for the application in the hot fluid's inlet. The 0.025% wt. graphene nanofluid has shown the best performance.

This study has contributed to knowledge augmentation in the field of heat exchanger and baffle design, with the focus on nanofluids usage. It is suggested that in

further studies, a variation in the baffle angle geometry for the SH and the CH should be made with the addition of higher fluid flow to understand its superior limit and the effects in both heat transfer and energy losses. In addition to that, the pressure drop caused by the inlet geometry, and its relation with the internal heat exchanger diameter must be considered and should also be an interesting topic for further discussions. It was also clear that the nanofluid field is promising, but still unknown. The search for better graphene based nanofluids must continue. Different surfactants and concentrations must be tested experimentally for the next steps.

REFERENCES

[1] Somasekhar, K., Malleswara Rao, K. N. D., Sankararao, V., Mohammed, R., Veerendra, M., & Venkateswararao, T. (2018). A CFD Investigation of Heat Transfer Enhancement of Shell and Tube Heat Exchanger Using Al 2 o 3 -Water Nanofluid. Materials Today: Proceedings, 5(1), 1057–1062.

[2] Bichkar, P., Dandgaval, O., Dalvi, P., Godase, R., & Dey, T. (2018). *Study of Shell and Tube Heat Exchanger with the Effect of Types of Baffles. Procedia Manufacturing, 20, 195–200.*

[3] El-Said, E. M. S., & Abou Al-Sood, M. M. (2019). *Shell and Tube Heat Exchanger with New Segmental Baffles Configurations: A comparative experimental investigation. Applied Thermal Engineering.*

[4] L. He, P. Li, Numerical investigation on double tube-pass shell-and-tube heat exchangers with different baffle configurations, Applied Thermal Engineering (2018)

[5] Said, Z., Rahman, S. M. A., El Haj Assad, M., & Alami, A. H. (2019). Heat transfer enhancement and life cycle analysis of a Shell-and-Tube Heat Exchanger using stable CuO/water nanofluid. Sustainable Energy Technologies and Assessments, 31, 306–317.

[6] Kazemi, I., Sefid, M., & Afrand, M. (2020). *A novel comparative experimental study on rheological behavior of mono & hybrid nanofluids concerned graphene and silica nano-powders: Characterization, stability and viscosity measurements. Powder Technology.*

[7] Pendyala, R., Ilyas, S. U., Lim, L. R., & Marneni, N. (2016). CFD Analysis of Heat Transfer Performance of Nanofluids in Distributor Transformer. Procedia Engineering, 148, 1162–1169.

[8] M.U. Sajid, H.M. Ali, Recent advances in application of nanofluids in heat transfer devices : a critical review, Renew. Sustain. Energy Rev. 103 (2019) 556–592,

[9] Wang, Z., Wu, Z., Han, F., Wadsö, L., & Sundén, B. (2018). *Experimental comparative evaluation of a graphene nanofluid coolant in miniature plate heat exchanger. International Journal of Thermal Sciences, 130, 148–156.*

[10] Kamyar, A., Saidur, R., & Hasanuzzaman, M. (2012). Application of Computational Fluid Dynamics (CFD) for nanofluids. International Journal of Heat and Mass Transfer, 55(15-16), 4104–4115.

[11] Sadri, R., Mallah, A. R., Hosseini, M., Ahmadi, G., Kazi, S. N., Dabbagh, A., … Yaakup, N. A. (2018). CFD modeling of turbulent convection heat transfer of nanofluids containing green functionalized graphene nanoplatelets flowing in a horizontal tube: Comparison with experimental data. Journal of Molecular Liquids, 269, 152–159.

[12] Çengel, Yunus A. Transferência de calor e massa: uma abordagem prática. 4ed. Porto Alegre: AMGH, 2012.

[13] Frank Kreith, Raj M. Manglik, Mark S. Bohn. Principles of heat transfer. 7th edition. USA. Cengage Learning, 2011.

[14] Choi SUS, Eastman JA. Enhancing thermal conductivity of fluids with nanoparticles. ASME; 1995.

[15] K. V. Wong and M. J. Castillo, "Heat transfer mechanisms and clustering in Nanofluids," *Advances in Mechanical Engineering*, vol. 2, Article ID 795478, 2010.

[16] Ambreen, T., & Kim, M.-H. (2020). *Influence of particle size on the effective thermal conductivity of nanofluids: A critical review. Applied Energy, 264, 114684.*

[17] Bai, M., Liu, J., He, J., Li, W., Wei, J., Chen, L., … Li, C. (2020). *Heat transfer and mechanical friction reduction properties of graphene oxide nanofluids. Diamond and Related Materials, 107982.*

[18] A. Naghash, et al., Experimental assessment of convective heat transfer coefficient enhancement of nanofluids prepared from high surface area nanoporous, Int. Commun. Heat Mass Transf. (2016).

[19] Fares, M., AL-Mayyahi, M., & AL-Saad, M. (2020). *Heat transfer analysis of a shell and tube heat exchanger operated with graphene nanofluids. Case Studies in Thermal Engineering, 18, 100584.*

[20] Bahiraei, M., & Heshmatian, S. (2019). *Graphene family nanofluids: A critical review and future research directions. Energy Conversion and Management, 196, 1222–1256.*

[21] Selvam, C., Solaimalai Raja, R., Mohan Lal, D., & Harish, S. (2017). *Overall heat transfer coefficient improvement of an automobile radiator with graphene based suspensions. International Journal of Heat and Mass Transfer, 115, 580–588.*

[22] Arzani, H. K., Amiri, A., Kazi, S. N., Chew, B. T., & Badarudin, A. (2015). *Experimental and numerical investigation of thermophysical properties, heat transfer and pressure drop of covalent and noncovalent functionalized graphene nanoplatelet-based water nanofluids in an annular heat exchanger. International Communications in Heat and Mass Transfer, 68, 267–275.*

[23] Sarafraz, M. M., Yang, B., Pourmehran, O., Arjomandi, M., & Ghomashchi, R. (2019). *Fluid and heat transfer characteristics of aqueous graphene nanoplatelet (GNP) nanofluid in a microchannel. International Communications in Heat and Mass Transfer, 107, 24–33.*

[24] Bahiraei, M., Hangi, M., & Saeedan, M. (2015). *A novel application for energy efficiency improvement using nanofluid in shell and tube heat exchanger equipped with helical baffles. Energy, 93, 2229–2240.*

[25] Lei, Y.-G., He, Y.-L., Chu, P., & Li, R. (2008). *Design and optimization of heat exchangers with helical baffles. Chemical Engineering Science, 63(17), 4386–4395.*

[26] Dong, C., Chen, Y.-P., & Wu, J.-F. (2015). *Flow and heat transfer performances of helical baffle heat exchangers with different baffle configurations. Applied Thermal Engineering, 80, 328–338.*

[27] Duan, Z., Shen, F., Cao, X., & Zhang, J. (2016). *Comprehensive effects of baffle configuration on the performance of heat exchanger with helical baffles. Nuclear Engineering and Design, 300, 349–357.*

[28] Cao, X., Chen, D., Du, T., Liu, Z., & Ji, S. (2020). *Numerical investigation and experimental validation of thermo-hydraulic and thermodynamic performances of helical baffle heat exchangers with different baffle configurations. International Journal of Heat and Mass Transfer, 160, 120181.*

[29] Gao, B., Bi, Q., Nie, Z., & Wu, J. (2015). *Experimental study of effects of baffle helix angle on shell-side performance of shell-and-tube heat exchangers with discontinuous helical baffles. Experimental Thermal and Fluid Science, 68, 48–57.*

[30] LIMA, C. C. X. S (2020) ESTUDO TEÓRICO E EXPERIMENTAL DA TRANSFERÊNCIA DE CALOR UTILIZANDO NANOFLUIDOS EM TROCADORES DE CALOR. UFPE.

[31] Simscale Thermal Simulations 2021, accessed 29th May 2021, <https://www.simscale.com/docs/simulation-setup/global-settings/k-epsilon/>

[32] Guo, Z. Y., Tao, W. Q., & Shah, R. K. (2005). *The field synergy (coordination) principle and its applications in enhancing single phase convective heat transfer. International Journal of Heat and Mass Transfer.*

[33] Alperen, M. A., Kayabaşi, E., & Kurt, H. (2019). *Detailed comparison of the methods used in the heat transfer coefficient and pressure loss calculation of shell side of shell and tube heat exchangers with the experimental results. Energy Sources, Part A: Recovery, Utilization, and Environmental Effects, 1–20.*

[34] U. Ur-Rehman, Heat transfer optimization of shell–and–tube heat exchanger through CFD studies, M.Sc. Thesis, Chalmers University of Technology, Göteborg, Sweden, 2011.

APPENDIX A – NUMERICAL RESULTS

Heat Transfer Rate Characteristics

Figure 55 – Heat Transfer Rate at 50^0C – graphene 0.0125% wt

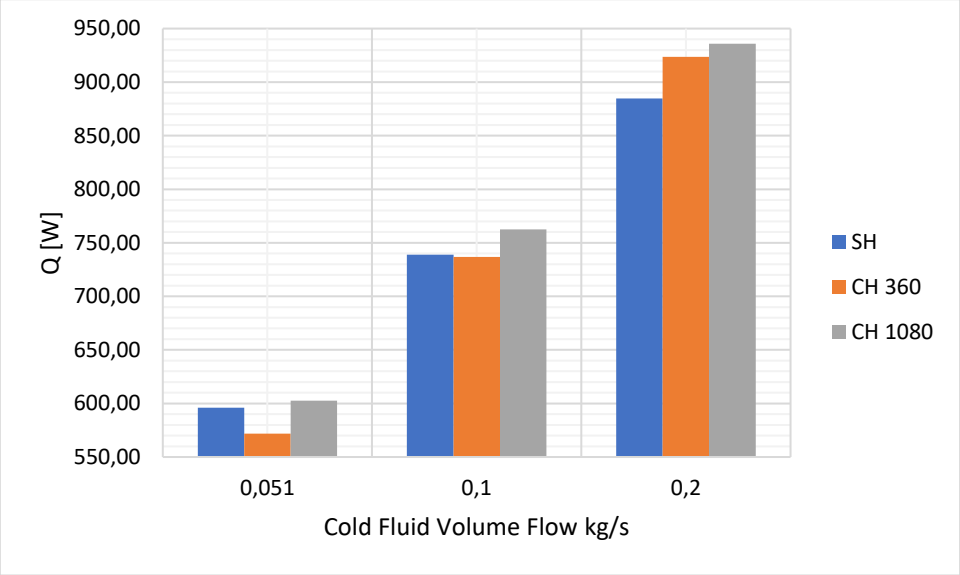

Source: Author (2022).

Figure 56 – Heat Transfer Rate at 50^0C – graphene 0.05% wt

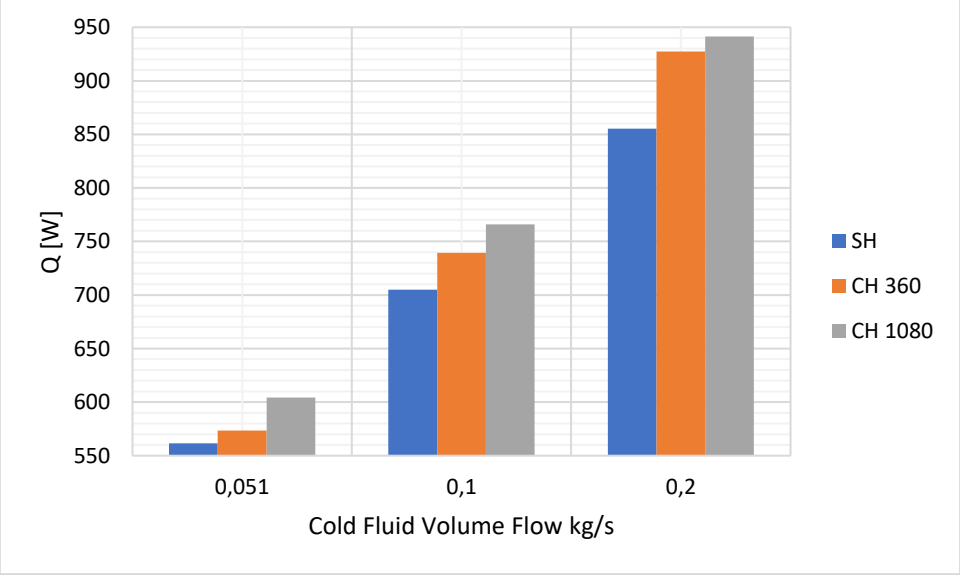

Source: Author (2022).

Figure 57 – Heat Transfer Rate at 40^0C – graphene 0.0125% wt

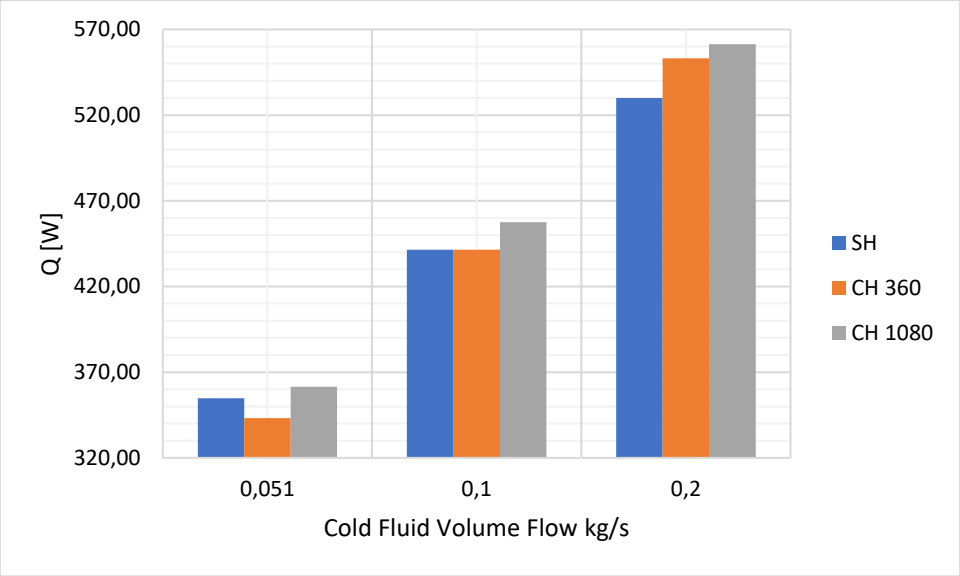

Source: Author (2022).

Figure 58 – SH Heat Transfer Rate at 40^0C – graphene 0.05% wt

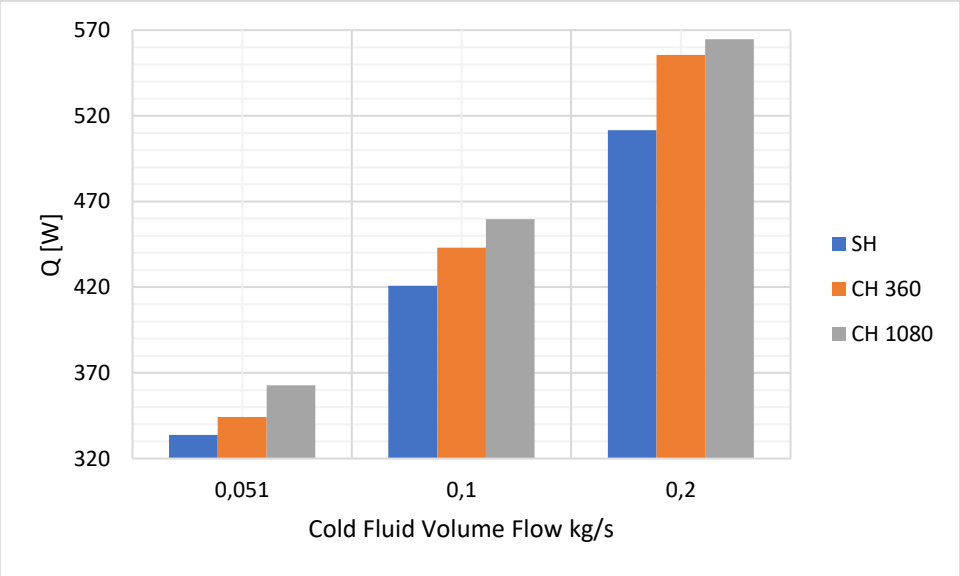

Source: Author (2022).

Figure 59 - Overall heat transfer coefficient – Input 1

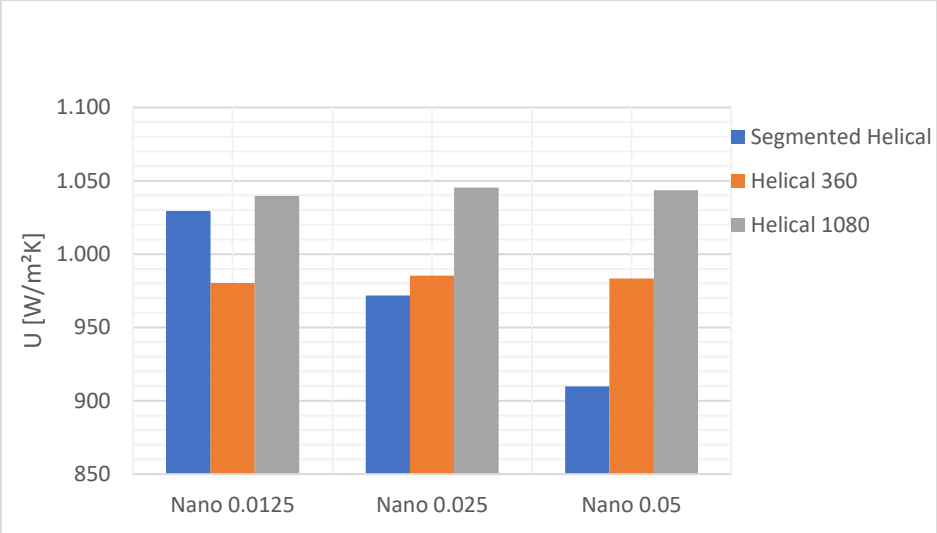

Source: Author (2022).

Figure 60 - Overall heat transfer coefficient – Input 2

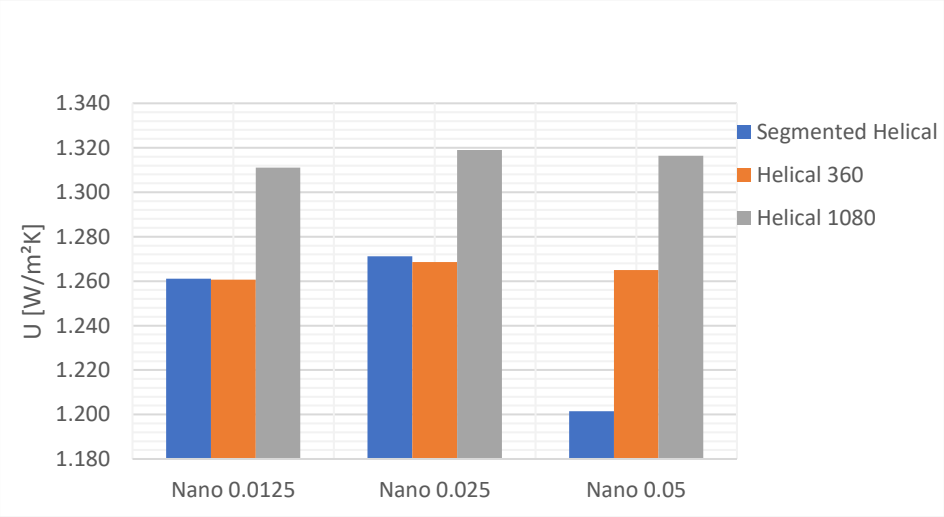

Source: Author (2022).

Figure 61 - Overall heat transfer coefficient – Input 4

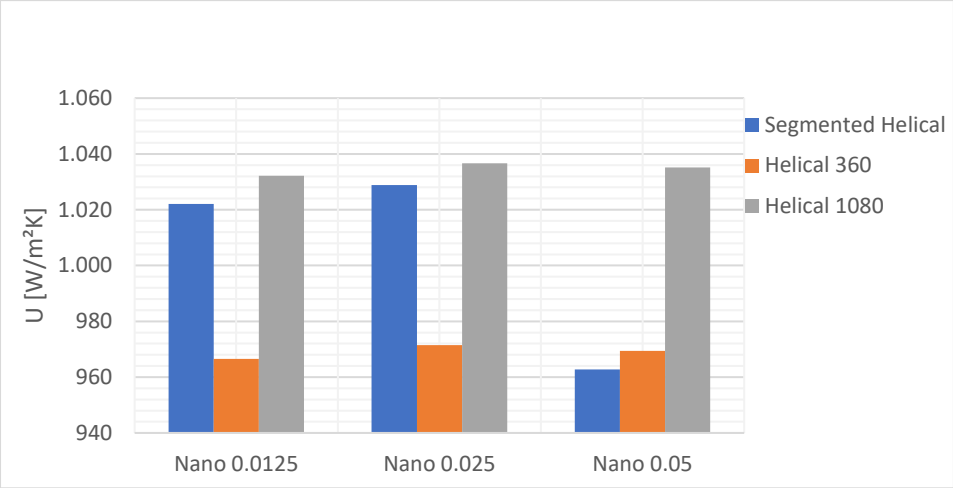

Source: Author (2022).

Figure 62 - Overall heat transfer coefficient – Input 6

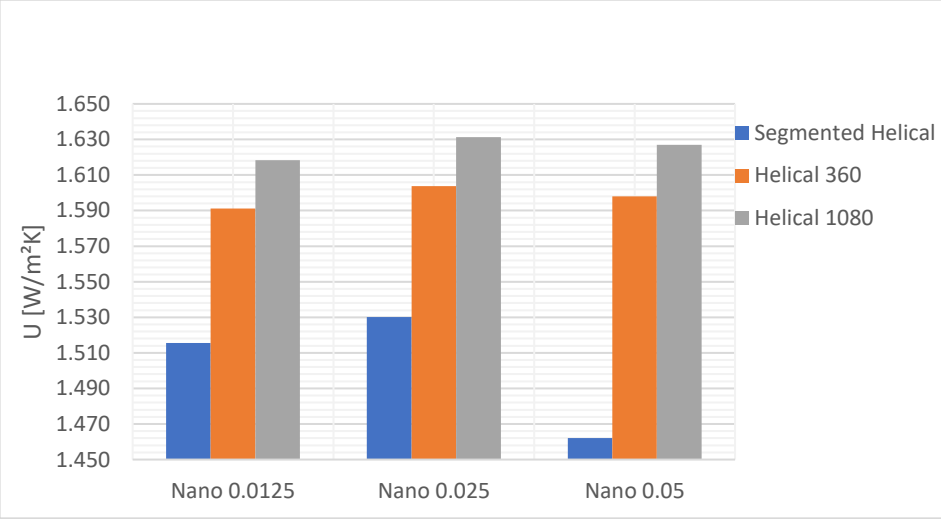

Source: Author (2022).

Figure 63 - Overall heat transfer coefficient – Input 7

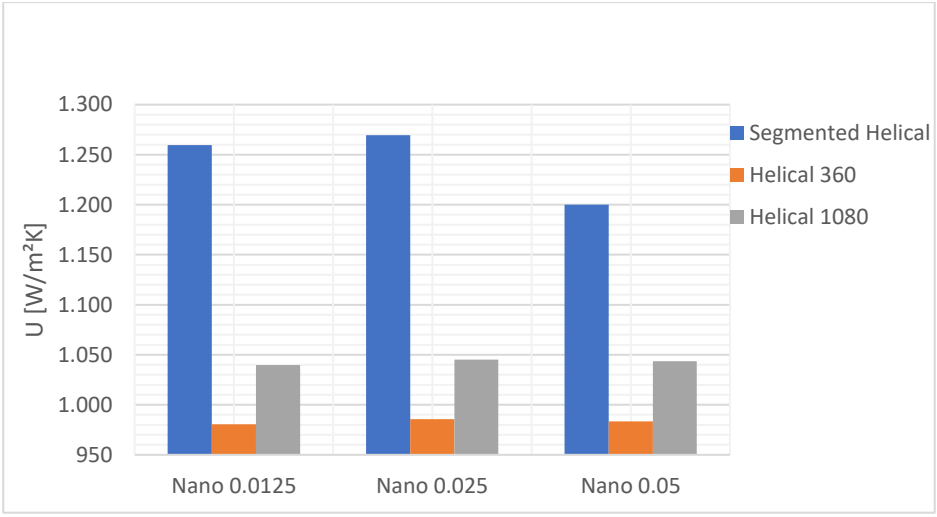

Source: Author (2022).

Figure 64 - Overall heat transfer coefficient – Input 8

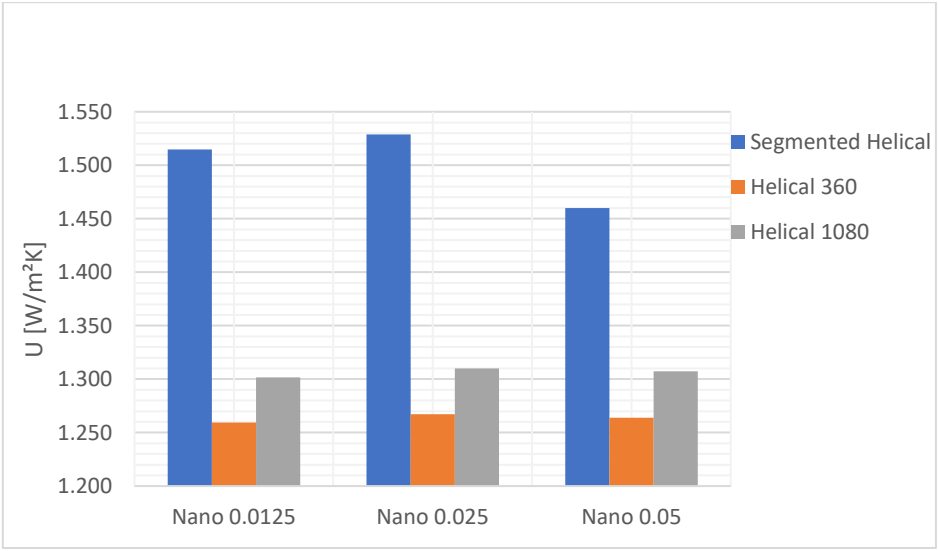

Source: Author (2022).

Figure 65 - Overall heat transfer coefficient – Input 9

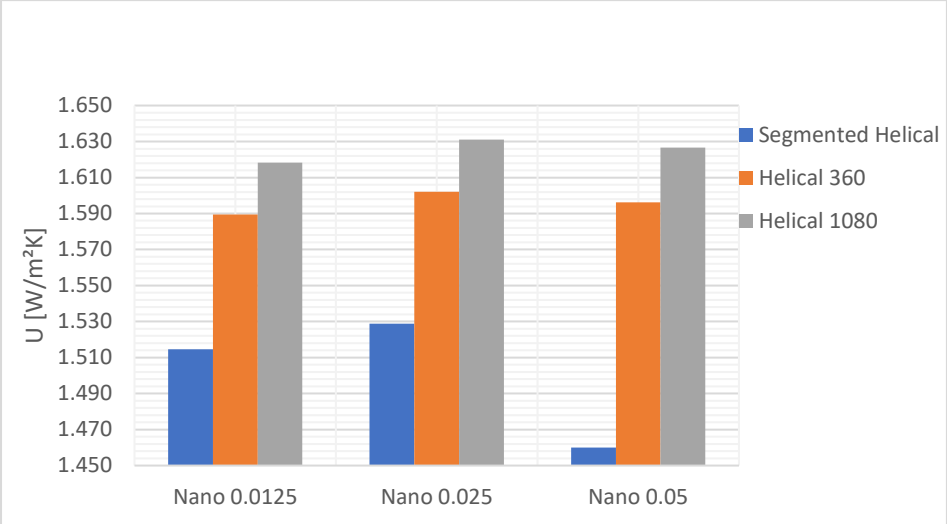

Source: Author (2022).

Figure 66 - Heat transfer coefficient – Input 1

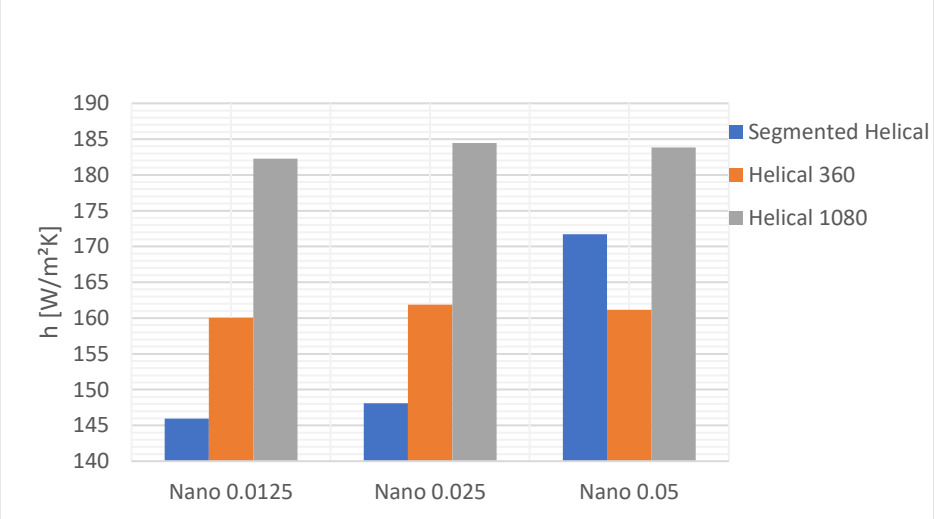

Source: Author (2022).

Figure 67 - Heat transfer coefficient – Input 2

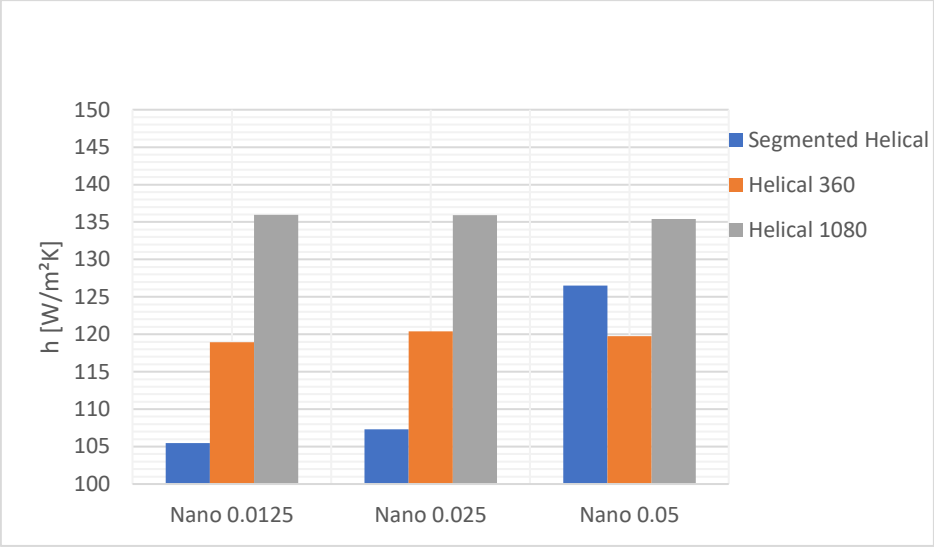

Source: Author (2022).

Figure 68 - Heat transfer coefficient – Input 3

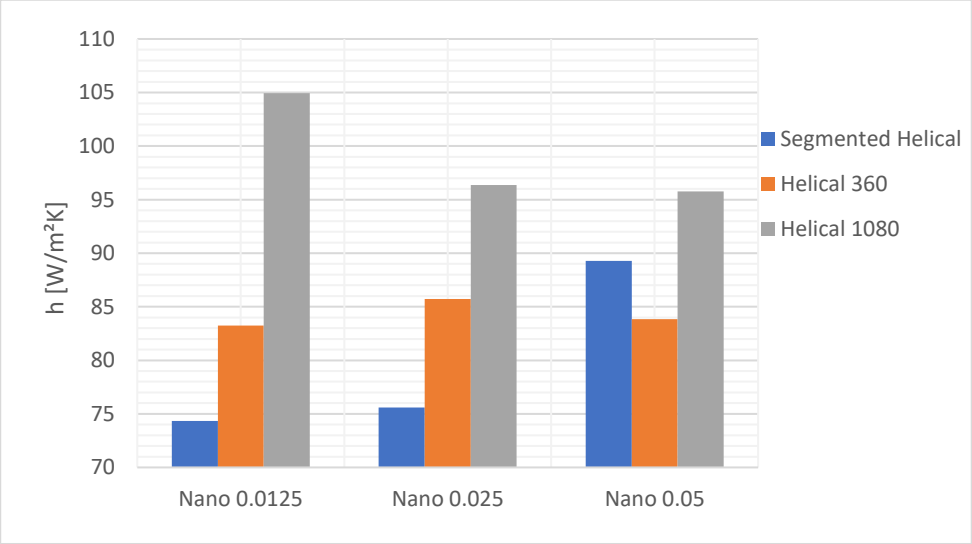

Source: Author (2022).

Figure 69 - Heat transfer coefficient – Input 4

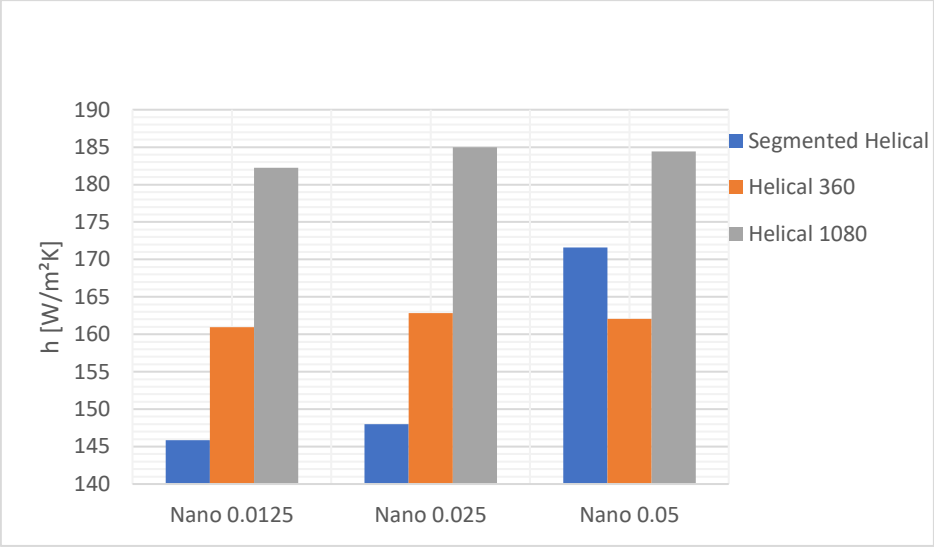

Source: Author (2022).

Figure 70 - Heat transfer coefficient – Input 5

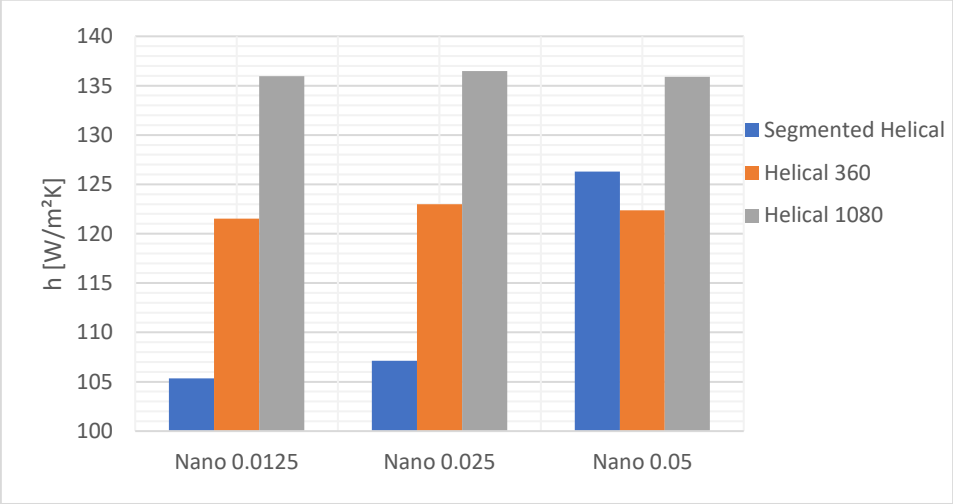

Source: Author (2022).

Figure 71 - Heat transfer coefficient – Input 6

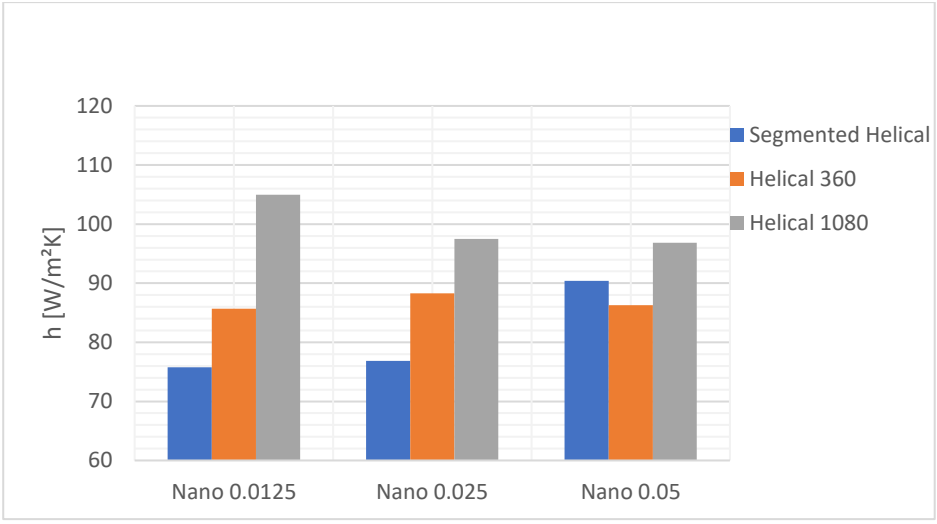

Source: Author (2022).

Figure 72 - Heat transfer coefficient – Input 7

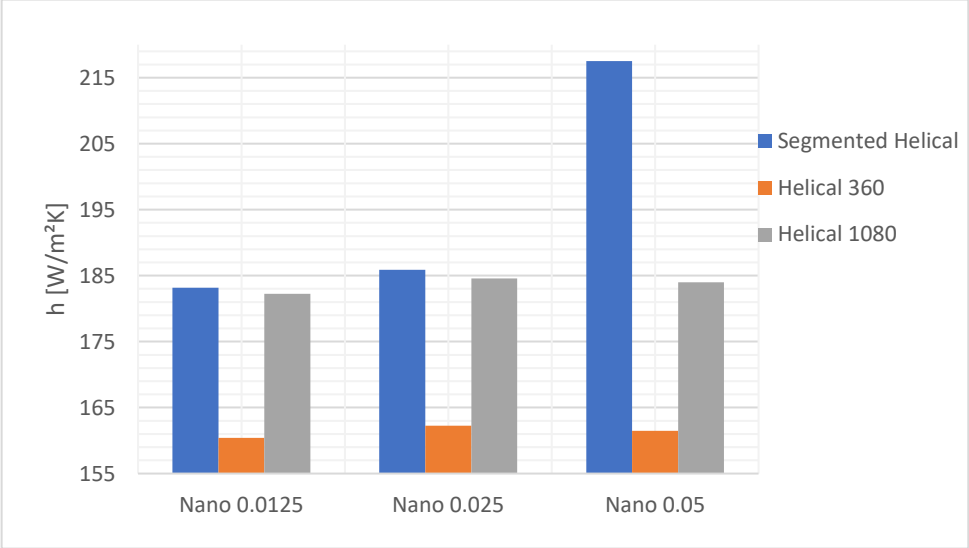

Source: Author (2022).

Figure 73 - Heat transfer coefficient – Input 8

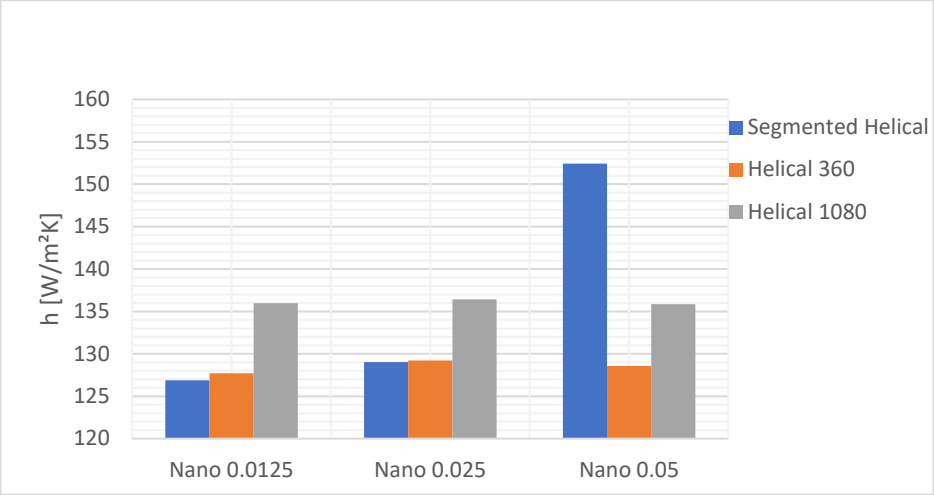

Source: Author (2022).

Figure 74 - Heat transfer coefficient – Input 9

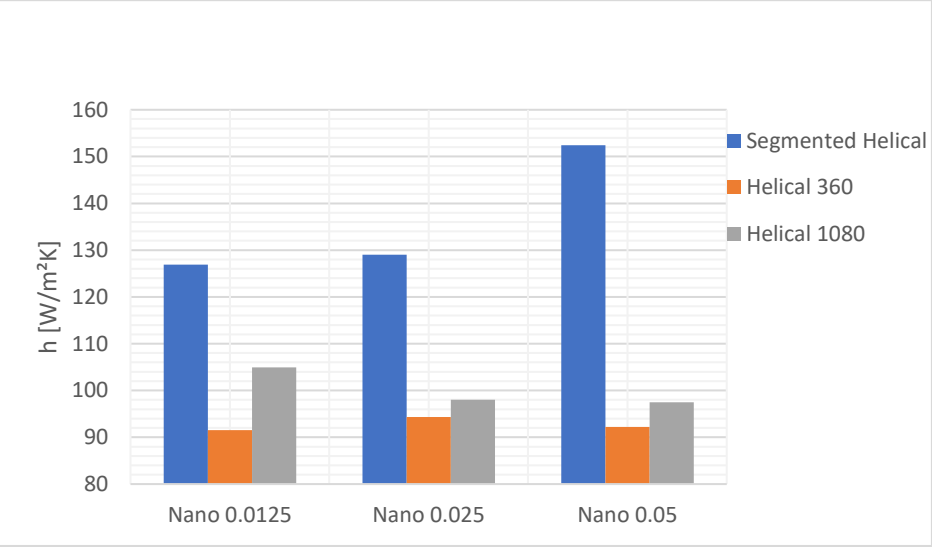

Source: Author (2022).

ATTACHMENT A – EXPERIMENTAL SETUP

Physical Model

The Figure 53 shows the original shell and tube heat exchanger. The equipment is originally established at IFPE campus Recife, in the fluid mechanics laboratory. Its designed for experiments and general teaching of heat transfer, but it is also used to research.

Figure 53 – Experimental heat exchanger

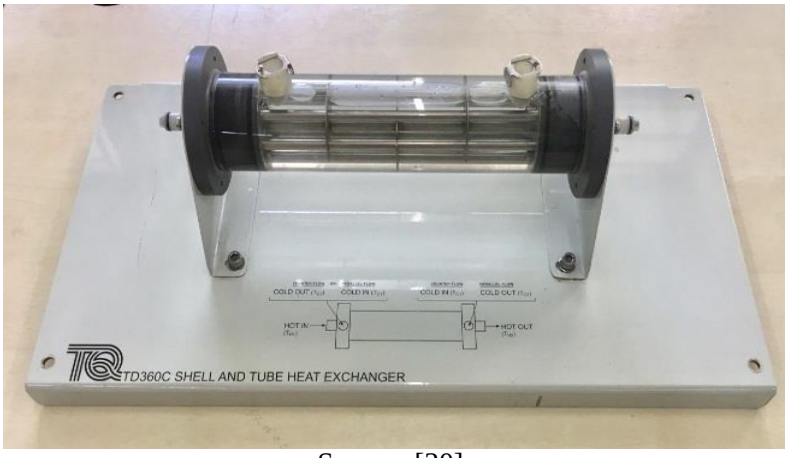

Source: [30].

The heat exchanger is connected to a control bench which shows fluid behaviour and temperature. The system is both closed loop and open loop. The cold water works on a open loop system, tap water flows through the heat exchanger and it discharges in sewer. Hot water, which is heated by a resistor inside the hot water tank (which level varies and is controlled by a floater and can be seen in a digital display) with a maximum capacity of 7L, passes through a centrifugal pump to be conducted to the heat exchanger tubes.

The PID (Proportional integral derivative) controller is the brain of the operation. Thermocouples send a signal of cold and hot water (inlet and outlet) to the PID, with the support of flow meters. The thermocouples (Type K – Nickel-Chromium/Nickel-Alumel) have a precision of 0,1°C, and temperature range between -200°C to 1260°C. The flow meter is a turbine type needle valves with high precision to adjust fluid flow.

A picture of the schematics can be seen in Figure 54, and the technical parameters of the heat exchanger is depicted in Table 1[30].

Figure 54 – Control bench

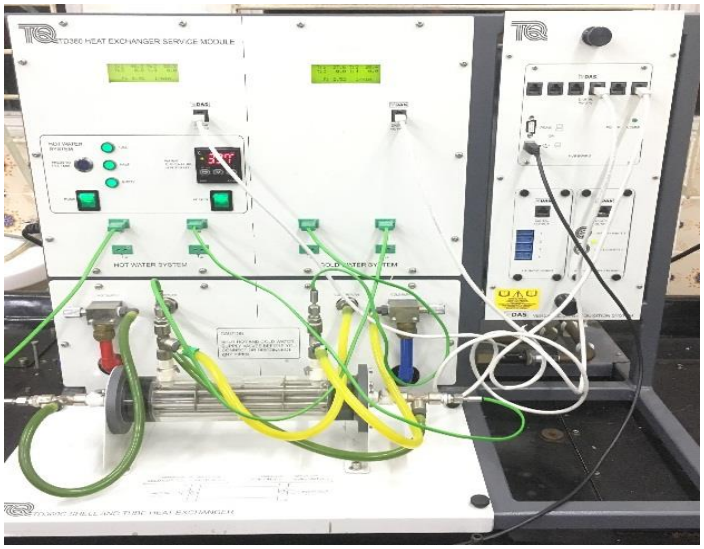

Source: [30].

Table 5 – Parameters of the original heat exchanger

PARAMETERS	CHARACTERISTICS
Shell	Poly methyl methacrylate (Acrylic)
Tubes	Stainless steel
Shell Diameter	150mm
Total Weight	2,7kg
Total Heat Transfer Area	0,02m^2
Baffles	3 units
Baffle Diameter	10mm
Baffle Width	1mm
Tubes Internal Diameter	4mm
Tubes External Diameter	6mm
Complementary Parts	Steel

Source: Adapted from Lima [30].